

AN ABSTRACT OF THE THESIS OF


George Joseph Vierra, Jr. for the Doctor of Philosophy
(Name) (Degree)

in Chemical Engineering presented on July 2, 1971
(Major) (Date)

Title: A STUDY OF CLIMBING-FILM FLOW CHARACTERISTICS OF
VARIOUS LIQUIDS AND AIR IN AN ANNULAR DUCT

Abstract approved:

Redacted for Privacy

 James G. Knudsen

Momentum transfer in climbing-film flow in an annular duct was investigated. Air and various liquids, with a wide range of viscosities and surface tensions, were investigated. The two phases flowed co-currently upward, the liquid climbing as a thin film on the inner wall while the outer wall remained dry.

The annulus was constructed of a three inch I. D. acrylic plastic tube and a one inch O. D. stainless steel rod. The dry, clear plastic outer wall made determination of pressure losses in the gas phase, radii of the point of maximum velocity, and outer wall shear stresses straightforward. High-speed motion picture photography of the liquid film was used to study the liquid film thickness and the wave character of the liquid surface.

It was attempted to determine the effect of the liquid properties on the character of the liquid film and on the hydrodynamics of the

air-liquid flow. The liquids used were water, Shellsolv, iso-octyl alcohol and light oil (viscosity ranging from 6.75×10^{-4} to 1.22×10^{-2} $\text{lb}_m/\text{ft sec}$ and surface tension ranging from 24.4 to 72.75 dyne/cm at 68°F). The experimental investigation covered an air flow range of $7 \times 10^4 < \text{Re} < 2 \times 10^5$ and a liquid flow range of 0.10 to 0.755 lb_m/min .

The results of this investigation are subsequently presented.

1. Friction factors for air flowing alone in the annulus were 2% to 13% larger than smooth tube values. The radius at the point of maximum velocity was in agreement with the values predicted by existing empirical correlations.

2. The two-phase pressure losses increased with increases in air and liquid flow rates. At the same liquid flow rate, the pressure losses were larger for the more viscous liquids.

3. The presence of the liquid film flowing on the inner wall caused only small changes in the outer wall shear stress from the single-phase values. Correlations were found for friction factor and Reynolds number using the region between the point of maximum velocity and the outer wall as the hydraulic flow region. In the region of low liquid entrainment the following empirical correlation was found

$$f_2 = .201 \text{Re}_2^{-.326}$$

4. The radius of the point of maximum velocity increased as the liquid flow rate increased and was larger for the more viscous

liquids. The following empirical correlation was found

$$y^* = .01 \text{Re}_L^{.246} \mu^{*.48}$$

5. The two-phase pressure losses were predicted well by the Lockhart and Martinelli correlation over the entire range of the data and for all liquids.

6. The laminar film model gives a reasonable approximation of the liquid film thickness for all the liquids investigated. The data indicate that the film thickness is proportional to the liquid viscosity to the .3 power.

7. Shear stresses at the air-liquid interface were 33% to 52% larger than the outer wall shear stresses and 7% to 130% larger than the inner wall shear stresses. The interfacial and the inner wall shear stresses approach each other at the high air flow rates, indicating the velocity profile in the liquid film is approaching linearity.

8. The frequency of the waves on the liquid surface increase as the air and liquid flow rates increase. The frequency was larger for the less viscous liquids and also for the liquids with the lower surface tensions. The wave celerity increases with increases in air and liquid flow rate and was 3% to 6% of the average air velocity. This compares well with the 5% to 10% reported for a liquid film climbing on a tube wall.

A Study of Climbing-Film Flow Characteristics
of Various Liquids and Air in
an Annular Duct

by

George Joseph Vierra, Jr.

A THESIS

submitted to

Oregon State University

in partial fulfillment of
the requirements for the
degree of

Doctor of Philosophy

June 1972

APPROVED:

Redacted for Privacy

Professor of Chemical Engineering

in charge of major

Redacted for Privacy

Head of Department of Chemical Engineering

Redacted for Privacy

Dean of Graduate School

Date thesis is presented July 2, 1971

Typed by Barbara Eby for George Joseph Vierra, Jr.

ACKNOWLEDGMENTS

I wish to extend my grateful appreciation to the following:

To Dr. James G. Knudsen, professor of Chemical Engineering, for his very generous assistance throughout the duration of this investigation.

To the National Science Foundation for its financial assistance.

To the Department of Chemical Engineering, Charles E. Wicks, head, for the use of its facilities.

To Mr. William B. Johnson for his helpful suggestions and aid in construction of the equipment.

And finally to Bobbie, who deserves no less than half of the credit for completion of this work.

TABLE OF CONTENTS

| | <u>Page</u> |
|---|-------------|
| INTRODUCTION | 1 |
| PREVIOUS WORK | 4 |
| Single-Phase Flow in an Annulus | 4 |
| Two-Phase Gas-Liquid Flow | 13 |
| Pressure Drop | 15 |
| Rough Wall Effects Caused by Annular Flow | 22 |
| Thin Liquid Films | 24 |
| THEORETICAL ANALYSIS | 36 |
| Analysis of Liquid Film | 36 |
| Estimation of Shear Stresses | 44 |
| EXPERIMENTAL PROGRAM | 50 |
| DESCRIPTION OF EXPERIMENT: APPARATUS | 52 |
| The Air Source and Peripheral Equipment | 54 |
| The Annular Duct | 55 |
| The Liquid Source and Injector | 55 |
| The Air-Liquid Separator and Liquid Recycling Tank | 56 |
| DESCRIPTION OF EXPERIMENT: MEASUREMENTS | 59 |
| Measurement of Inlet Air Density | 59 |
| Measurement of Air Flow Rate | 59 |
| Measurement of Column Temperature and Pressure | 59 |
| Measurement of Pressure Gradient | 60 |
| Measurement of Shear Stresses at the Outer Wall | 60 |
| Measurement of Velocity | 61 |
| Purge System and Manometers | 61 |
| Measurement of Liquid Flow Rate | 63 |
| Measurement of Liquid Films | 63 |
| DISCUSSION OF RESULTS | 68 |
| Single-Phase Flow | 68 |
| Two-Phase Flow Pressure Drop | 73 |
| Shear Stresses at the Outer Wall | 79 |
| Radius at the Point of Maximum Velocity | 93 |
| Two-Phase Pressure Drop Correlations | 98 |
| Liquid Film Thickness and Shear Stress Distribution | 105 |
| Wave Characteristics of the Liquid Film | 118 |

| | <u>Page</u> |
|--|-------------|
| CONCLUSIONS | 123 |
| RECOMMENDATIONS FOR FURTHER WORK | 127 |
| BIBLIOGRAPHY | 128 |
| APPENDIX I: Physical Property Determination | 137 |
| APPENDIX II: Calibration of the Air Flow Orifice | 146 |
| APPENDIX III: Shear Stress at the Outer Wall | 150 |
| APPENDIX IV: Photographic Methods and Data | 154 |
| APPENDIX V: Entrainment | 160 |
| APPENDIX VI: Freely Falling Liquid Film | 170 |
| APPENDIX VII: Tables of Data | 177 |
| APPENDIX VIII: Nomenclature | 182 |

LIST OF FIGURES

| <u>Figure</u> | | <u>Page</u> |
|---------------|---|-------------|
| 1 | Film flowing on a plane surface. | 37 |
| 2 | Annular duct cross-section. | 48 |
| 3 | Experimental system. | 53 |
| 4 | Liquid injection system. | 57 |
| 5 | Liquid separator. | 58 |
| 6 | Purging system and manometer connections. | 62 |
| 7a | Friction factor - Reynolds number for air data. | 69 |
| 7b | Friction factor - Reynolds number for air data. | 70 |
| 8 | Pressure drop vs. air flow rate - water. | 74 |
| 9 | Pressure drop vs. air flow rate - Shellsolv. | 75 |
| 10 | Pressure drop vs. air flow rate - light oil. | 76 |
| 11 | Pressure drop vs. air flow rate - iso-octyl alcohol. | 77 |
| 12 | Friction factor vs. Reynolds number - water. | 80 |
| 13 | Friction factor vs. Reynolds number - Shellsolv. | 81 |
| 14 | Friction factor vs. Reynolds number - light oil. | 82 |
| 15 | Friction factor vs. Reynolds number - iso-octyl alcohol. | 83 |
| 16 | Shear stress at outer wall vs. air flow rate - water. | 84 |
| 17 | Shear stress at outer wall vs. air flow rate - Shellsolv. | 85 |

| <u>Figure</u> | | <u>Page</u> |
|---------------|--|-------------|
| 18 | Shear stress at outer wall vs. air flow rate - light oil. | 86 |
| 19 | Shear stress at outer wall vs. air flow rate - iso-octyl alcohol. | 87 |
| 20 | Two-phase friction factor, f_2 , vs. Reynolds number, Re_2 . | 91 |
| 21 | Radius of maximum velocity vs. liquid flow rate. | 95 |
| 22 | Correlation for radius of maximum velocity. | 97 |
| 23 | Orkiszewski pressure drop correlation - water. | 100 |
| 24 | Lockhart-Martinelli pressure drop correlation - water. | 101 |
| 25 | Lockhart-Martinelli pressure drop correlation - Shellsolv. | 102 |
| 26 | Lockhart-Martinelli pressure drop correlation - light oil and iso-octyl alcohol. | 103 |
| 27 | Film thickness vs. average air velocity: liquid flow rate $.10 \text{ lb}_m/\text{min}$. | 106 |
| 28 | Film thickness vs. average air velocity: liquid flow rate $.305 \text{ lb}_m/\text{min}$. | 107 |
| 29 | Film thickness vs. average air velocity: liquid flow rate $.59 \text{ lb}_m/\text{min}$. | 108 |
| 30 | Lockhart-Martinelli void fraction correlation. | 112 |
| 31 | Comparison of Martinelli correlation with experimental values of R_L . | 114 |
| 32 | Comparison of laminar film model with experimental values of R_L . | 116 |
| I-1 | Density vs. temperature - water. | 140 |

| <u>Figure</u> | | <u>Page</u> |
|---------------|--|-------------|
| I-2 | Density vs. temperature - Shellsolv. | 140 |
| I-3 | Density vs. temperature - light oil. | 141 |
| I-4 | Density vs. temperature - iso-octyl alcohol. | 141 |
| I-5 | Viscosity vs. temperature - water. | 142 |
| I-6 | Viscosity vs. temperature - Shellsolv. | 142 |
| I-7 | Viscosity vs. temperature - light oil. | 143 |
| I-8 | Viscosity vs. temperature - iso-octyl alcohol. | 143 |
| I-9 | Surface tension vs. temperature - water. | 144 |
| I-10 | Surface tension vs. temperature - Shellsolv. | 144 |
| I-11 | Surface tension vs. temperature - light oil. | 145 |
| I-12 | Surface tension vs. temperature - iso-octyl alcohol. | 145 |
| II-1 | Air flow orifice calibration curve. | 149 |
| III-1 | Preston tube calibration. | 153 |
| VI-1 | We vs. α - falling film. | 174 |

LIST OF TABLES

| <u>Table</u> | | <u>Page</u> |
|--------------|--|-------------|
| 1 | Predicted values of the radius of maximum velocity. | 72 |
| 2 | Comparison of single- and two-phase pressure drop and friction factor. | 78 |
| 3 | Comparison of single- and two-phase outer wall shear stress. | 89 |
| 4 | Prediction of liquid film thickness. | 110 |
| 5 | Distribution of shear stresses. | 117 |
| 6 | Wave characteristics. | 119 |
| IV-1 | Photographic settings. | 159 |
| V-1 | Prediction of V_{CR} . | 169 |
| VII-1 | Air data. | 178 |
| VII-2 | Air - water data. | 179 |
| VII-3 | Air - Shellsolv data. | 180 |
| VII-4 | Air - light oil data. | 181 |
| VII-5 | Air - iso-octyl alcohol data. | 181 |

A STUDY OF CLIMBING-FILM FLOW CHARACTERISTICS OF VARIOUS LIQUIDS AND AIR IN AN ANNULAR DUCT

INTRODUCTION

Annular flow is one of several flow regimes of gas-liquid two-phase flow. In the annular regime the liquid flows as a film on a duct wall while the gas flows in the core of the duct. Annular flow is characterized by a single, wavy gas-liquid interface.

If the liquid and gas flow vertically upward, the phenomenon is known as climbing film flow. In climbing film flow, the gas flowing in the duct transfers momentum to the liquid and causes the liquid to climb as a film on the duct wall. The momentum transfer to the liquid will result in a pressure loss in the duct, and drag at the gas-liquid interface will cause the liquid surface to become wavy.

It has been suggested that the wavy character of the surface of the climbing film is the reason for the high heat transfer and mass transfer coefficients accompanying the flow. Collier (1961) reports heat transfer coefficients in the two-phase forced convection region of $10,000 \text{ Btu/hr ft}^2 \text{ }^\circ\text{F}$ for steam-water systems at atmospheric pressure.

It is believed that the heat transfer through the liquid film is entirely governed by the hydrodynamic conditions of the film. In turn,

the film hydrodynamics are largely governed by conditions in the gas phase which exerts the shearing force at the gas-liquid interface.

Because of the very high heat and mass transfer accompanying film flow, two-phase flow finds application in a large number of fields. Of particular importance are the petroleum industry, the nuclear industry (where film flow is used for heat removal in reactors), and the food industry (where film flow is used for cleaning purposes).

In the present investigation, the liquid film was made to climb on the inner tube of an annulus while the outer tube remained dry. This flow arrangement allowed for unobstructed visual observation of the film and made determination of pressure losses, points of maximum velocity in the gas phase, and outer wall shear stresses relatively straightforward. High-speed motion picture photography was used to investigate the liquid film. The film was analyzed to determine the liquid film thicknesses and the characteristics of the wavy surface.

This investigation is concerned only with the momentum transfer taking place as air and a liquid film flow co-currently upward. Of particular interest is the effect of the liquid properties on the hydrodynamics of the liquid film and the air stream. Water, Shellsolv, iso-octyl alcohol, and light oil were studied.

The pressure loss and film thickness values were compared with several of the more widely used empirical correlations. In addition,

the film thickness and wave character were compared with a theoretical laminar film model patterned after the work of Kapitza.

The present investigation is a continuation of the work done by Kim (1965), Sutey (1967), and Scott (1969). It is hoped that the findings of this study will contribute to a better understanding of a very complex flow phenomenon.

PREVIOUS WORK

Single-Phase Flow in an Annulus

Annular flow studies are of interest because they have direct engineering application and also because they provide a useful system in which to investigate fluid flow. Unlike the case in both tube flow and flow between parallel planes, changes in wall shear stresses in annular flow are manifested quite clearly by shifted and deformed velocity profiles. It should also be noted that pipe flow and parallel plane flow are symmetrical limiting cases of annular flow (the diameter ratio r^* ($= d_1/d_2$) $\rightarrow 0$ and $r^* \rightarrow 1$, respectively).

If one assumes wall roughness to be negligible, dimensional analysis will show that the friction factor is a function of Reynolds number and the diameter ratio r^* . Lorenz (1932), in a much overlooked experimental work, showed friction factor to increase with r^* . Extremely accurate data are necessary to observe this trend; consequently, most investigators have found only small changes, or none at all. In the same work, the point of maximum velocity was shown to be different for laminar and turbulent flow.

Several investigators have reported experimental velocity profiles, pressure drops, and points of maximum velocity in turbulent annular flow. Determination of the latter is very difficult because of the flatness of the velocity profile. Nevertheless, it is an extremely

important quantity which, once determined, allows for calculation of the wall shear stress.

Rothfus, Monrad, and Senecal (1950) found that, for fully turbulent flow, the pressure drop in annuli can be correlated with pipe data by applying the hydraulic radius concept to that portion of the fluid which lies outside the radius of maximum local velocity. That is, the friction factor at the outside surface

$$f_2 = \frac{r_2^2 - r_m^2}{r_2} \frac{g_c}{\rho U^2} \frac{-dP_f}{dx} \quad (1)$$

is related to the Reynolds number

$$Re_2 = \frac{2(r_2^2 - r_m^2)}{r_2} \frac{U\rho}{\mu} \quad (2)$$

in the same manner that the friction factor in a tube is related to the bulk Reynolds number.

Rothfus and colleagues (1955) also defined an inner and outer wall friction factor as

$$f_1 = \frac{2\tau_1 g_c}{\rho U^2} \quad (3)$$

$$f_2 = \frac{2\tau_2 g_c}{\rho U^2} \quad (4)$$

and used the latter to correlate Re_2 by $(10,000 < Re_2 < 45,000)$

$$\frac{1}{\sqrt{f_2}} = 4.0 \log_{10} (\text{Re}_2 \sqrt{f_2}) - 0.40 \quad (5)$$

This correlation is identical in form to the one used to predict the friction factor in turbulent flow in smooth tubes. These investigators deduced that, within experimental accuracy, r_m was the same for laminar and turbulent flow.

Knudsen (1962) reported a friction factor-Reynolds number relation approximated by

$$f_2 = .079 \text{Re}_2^{-.25} \quad (6)$$

Knudsen and Katz (1958) stated that most experimental results can be represented by

$$f = .079 \text{Re}^{-.25} \quad (7)$$

with deviations being as large as 35%, where Re and f are defined in the usual manner, as follows:

$$\text{Re} = \frac{d_2 - d_1}{\mu} U \rho \quad (8)$$

$$f = \frac{d_2 - d_1}{\rho U^2} g_c \frac{-dP_f}{dx} \quad (9)$$

Prengle and Rothfus (1955) also showed that pressure drop data in annuli can be correlated with pipe data, again by applying the hydraulic radius concept to that portion of the fluid lying outside the radius

of maximum velocity. For pipe flow, where the maximum velocity is at the center line, the hydraulic diameter reduces to the tube diameter. These investigators demonstrated experimentally that transition to turbulent flow begins at the point of maximum velocity, and they concluded that at Re_2 between 700 and 2300, the point of maximum velocity in an annulus appears to shift inward from its position in fully viscous and turbulent flow.

Meter and Bird (1961) examined data from many sources and found that the friction factor in annuli with small values of r^* is about 10% greater than that for tubes. They also reported that, as r^* decreases, f decreases slightly.

A Reynolds number was further defined by Meter and Bird as

$$Re_B = \frac{d_2 - d_1}{\mu} \rho U \phi_* \quad (10)$$

where ϕ_* is a correction factor allowing for variation in r^* defined by

$$\phi_* = \frac{1}{(1-r^*)^2} \left[(1+r^*)^2 - \frac{(1-r^*)^2}{\ln(1/r^*)} \right] \quad (11)$$

Using the Prandtl mixing length theory, they arrived at the expression

$$\frac{1}{\sqrt{f}} = G \log_{10} (Re_B \sqrt{f}) - H \quad (12)$$

where G and H are functions of r^* alone. However, in their analysis they assume that the point of maximum velocity is the same for both turbulent and laminar flow. In their study, curves of friction factor vs. Re_B are presented with a different curve for each value of r^* . Their model is compared to the available data with an average absolute deviation of 2.7%.

Kays and Leung (1963) postulated an expression for the location of the maximum velocity based upon previously available data. Over a range of $10^4 < Re_2 < 7 \times 10^5$ they found that

$$\frac{r_m - r_1}{r_2 - r_m} = r^* . 343 \quad (13)$$

The scatter about the correlation curve appears to be less than $\pm 10\%$. Considering that this correlation is based upon data gathered from several investigations, each with varying degrees of uncertainty, it predicts r_m remarkably well.

Brighton and Jones (1964), using some very precise measurements, demonstrated that r_m for turbulent flow is definitely less than for laminar flow. They studied both air and water over a range $4000 < Re < 3 \times 10^5$ and investigated several annuli with a range of $.0625 < r^* < .562$. From their data they concluded that f is not a function of r^* and is dependent upon Re .

The friction factors for air flow were found to be 1% to 10% higher than pipe flow values and had little dependence upon r^* .

These investigators proposed as an upper limit to their data the relation for $Re < 10^6$

$$f = 0.087 Re^{-.25} \quad (14)$$

The velocity gradients in the region of maximum velocity were determined by using two pitot tubes and were found to be linear when plotted vs. distance from the tube wall. The radius of maximum velocity was the point at which the velocity gradient became zero.

They also found a slight dependence of r^* on Re , which became more important at values of r^* less than .0625. In this region, r_m decreases as Re increases.

Hewitt (1964) derived equations from which it is possible to determine the flow parameters in an annulus if the pressure drop is known. The flow is divided into two regions, bounded by the plane of zero shear or maximum velocity, and the Reynolds number, friction factor, and other parameters are defined for each region. This technique serves as a first approximation when measurement of velocity profiles is not possible. The model has been used to analyze air-water, climbing film flow data.

For a smooth outer and a rough inner surface, the Koo equation was used to predict the friction factor as follows:

$$f_k = .00070 + .0625 \text{Re}_k^{-.32} \quad (15)$$

where

$$\text{Re}_k = \frac{U_2 \rho}{\mu} \frac{2(r_2^2 - r_m^2)}{r_2} \quad (16)$$

$$f_k = \frac{(r_2^2 - r_m^2)}{2r_2} \frac{g_c}{\rho U_2^2} \frac{-dP_f}{dx} \quad (17)$$

and U_2 is the average velocity between r_m and r_2 .

Nicol and Medwell (1964) experimented with an inner pipe that was artificially roughened while the outer pipe was always kept smooth. The variation of r_m with Re was too small to be detected; however, r_m did vary with the degree of roughness. As the wall roughness increased, the point of maximum velocity shifted toward the outer wall. Knudsen (1949) in an earlier study showed that the point of maximum velocity moves toward the outer wall when the inner wall is roughened.

Macagno and McDougall (1966) calculated the friction factor for uniform annular flow by assuming that the logarithmic velocity distribution laws apply to the inner and outer regions of flow, these regions being separated by the point of maximum velocity. Their determination of the location of the point of maximum velocity was based upon

turbulent flow characteristics. Their analysis also shows that f should vary with r^* .

Rothfus, Sartory, and Kermode (1966), working in the highly turbulent range, arrived at the following relation to relate r_m to r^* :

$$\frac{r_m - r_1}{r_2 - r_1} = \frac{1}{2} r^{*.2} \quad (18)$$

This relation fits the data of Brighton and Jones very well.

Quarmby (1967) carried out an experimental study in several annuli with r^* varying from .1065 to .348. He found that the hydrodynamic entrance length was much the same as for rough walled tubes, i. e., 30 to 40 equivalent diameters. His studies showed that f is independent of r^* but that r_m is dependent upon both Re and r^* .

Clump and Kwasnoski (1968) determined the point of maximum velocity by applying standard polynomial curve-fitting techniques to the data of Brighton and Jones. Although the Brighton and Jones data indicated a slight Re dependence at small values of r^* , this dependence was excluded from the work of Clump and Kwasnoski. They arrived at the following relations:

$$\frac{r_m - r_1}{r_2 - r_1} = \frac{1}{2} (1.08 r^{*3} - 2.20 r^{*2} + 1.65 r^* + .48) \quad (19)$$

$$(0.0625 < r^* < 1)$$

and

$$\frac{r_m - r_1}{r_2 - r_1} = 18.1 r^* \quad (20)$$

$$(r^* < 0.0625)$$

Hanks and Bonner (1971), while studying transition phenomena in annuli, observed that during transition the value of r_m first increases to a maximum value and then decreases sharply to a value less than r_m for laminar flow.

Thus, past work indicates that r_m for turbulent flow is definitely less than for laminar flow. It seems evident that the transition region needs more study before conclusions can be drawn concerning r_m . A rough inner wall appears to shift the velocity profile toward the outer wall. In the turbulent region, it appears that r_m is a slight function of Re , with the role of Re becoming more important at low values of r^* where r_m decreases as Re increases. Friction factors in annuli appear to be on the order of 10% larger than for tubes. The dependence of the friction factor upon r^* appears to be slight. For correlation purposes, using the region from the point of maximum velocity to the outer tube wall as an equivalent diameter yields the best results.

Two-Phase Gas-Liquid Flow

The simultaneous flow of a gas and a liquid or of two immiscible liquids is commonly defined in the literature as two phase flow, although gas-solid and liquid-solid flow also fit this definition. Several possible configurations can be assumed by a gas and a liquid flowing simultaneously in a duct. However, the classification of flow patterns in gas-liquid flow is at present not highly standardized; many investigators have defined different regimes and transition lines between regimes.

Vohr (1960) surveyed the literature on flow patterns occurring in two-phase gas-liquid flow through ducts. In an attempt to unify the reported observed regimes and to bring some order to the myriad of names given to each regime by many investigators, he listed the following basic vertical flow patterns (they are presented in the direction of increasing gas flow rate):

1. bubble flow, in which gas in the form of bubbles flows along with the liquid;
2. piston flow, in which the gas flows up through the liquid in quasi-periodic bullet-shaped plugs;
3. churn flow (also designated by different researchers as dispersed flow, emulsion flow, turbulent flow, and semi-annular flow), a regime lying in a wide range between piston flow (2) and annular flow (4) in which definition of the complex flow patterns is difficult;

4. annular flow, in which the liquid flows in an annulus around the walls of the flow duct and the gas flows in a central core; and
5. spray flow, in which the liquid flows as a homogeneous mist carried by the gas.

Many attempts have been made to illustrate the various flow regimes. The reader is referred to the studies of Calvert and Williams (1955), Anderson and Russell (1965), Collier (1961), Brodkey (1967), and Vohr, which are all fairly representative.

It is necessary to consider the flow regimes separately when studying the hydrodynamics of the phenomena taking place in two-phase flow. The past few years have witnessed the publication of several books, monographs, and review articles dealing, in whole or in part, with distinct flow regimes or with all regimes. Tong (1965) discussed the significance of two-phase flow as applied to boiling heat transfer. D. S. Scott (1963) dealt with all regimes of gas-liquid co-current two-phase flow. Fulford (1964) discussed the flow of liquid in thin films. Brodkey recently published a fluid dynamics text in which two chapters dealt exclusively with two-phase flow. This appears to be the first attempt to present two-phase flow as a separate and distinct field of fluid dynamics, a position presently enjoyed by the study of rheology, flow through porous media, and others. Wallis (1969) wrote a monograph on one-dimensional two-phase flow with the hope that it would

be used as an introductory textbook in a graduate course on the subject. Considering the rate at which two-phase flow literature is expanding, any attempts to bring order to the subject in the form of a book or review article is certainly a welcome event.

Pressure Drop

The pressure drop in a gas-liquid co-current flow pipeline is always greater than it would be if either of the two phases was flowing alone in the pipe. Irreversible work done by the gas on the liquid as the liquid is dragged along causes some of the greater energy loss, and further losses are a consequence of the reduction of flow areas resulting from the presence of two phases.

Two general procedures are used to predict the pressure drop in gas-liquid co-current flow. In the first method, one attempts to correlate pressure drop in terms of dimensionless groups and other parameters, as in single-phase flow. In the second method, one attempts to analyze the hydrodynamics of individual flow patterns. Both approaches have their disadvantages: the former suffers because the mechanisms of energy losses differ over the range of flow conditions, the second because an approximate knowledge of the flow pattern is necessary before the prediction of pressure drop can be made.

Lockhart and Martinelli (1949) presented correlations which do not require knowledge of the flow regime. Orkiszewski's method (1967),

on the other hand, requires determination of the flow regime prior to applying the correlational equations. Anderson and Russell have reviewed several pressure drop correlations, and claim that if one knows the flow pattern and all the physical and geometrical properties of the system the best correlations will predict the pressure drop with an accuracy of 25%.

The simplest technique for analyzing two-phase flow involves the use of a homogeneous model. Using this method, suitable average properties are determined and the mixture is treated as a pseudofluid which will obey the usual equations of single-component flow. Pressure drop in annular flow will be adequately predicted with a homogeneous model at entrainment levels greater than 20%.

A modified homogeneous model which takes surface tension into account is the CISE (Casagrande, 1963) model. These workers found that the surface tension, σ , was far more significant a variable than the viscosity of either of the two phases or any form of homogeneous average viscosity. The correlation presented for frictional pressure drop takes the form

$$-\left(\frac{dP}{dx}\right)_f = C \frac{G^{1.4} \bar{v}^{-0.86} \sigma^{.4}}{D^{1.2}} \quad (21)$$

where C is a constant, G is the total mass flux, \bar{v} the average homogeneous mixture specific volume, and D an equivalent diameter.

Although this model is of little use in predicting pressure drop in pure annular flow, it is of interest because it demonstrates the strong dependence of surface tension on pressure drop under appropriate flow conditions.

Semi-empirical approaches to pressure drop correlations have been utilized by a number of investigators. Lockhart and Martinelli have set forth a pressure drop correlation which seems to be the most widely used. Their approach is based on the idea that the pressure drop in two-phase flow can be calculated from single-phase flow equations and graphs if the individual phase velocities are known. If the phases are assumed to be completely separated, phase velocities are easily defined in terms of hydraulic diameters. Their correlation is based upon two assumptions: (1) the static pressure drop in the gas phase is the same as in the liquid phase regardless of flow pattern (provided that an appreciable radial static pressure difference does not exist), and (2) the volume occupied by the liquid plus the volume occupied by the gas at any instant equals the total pipe volume.

For given flow rates of gas and liquid, Lockhart and Martinelli calculated the pressure gradient which would occur if either fluid was flowing alone in the pipe, expressed as $(dP/dx)_G$ and $(dP/dx)_L$. Variables were defined in terms of the ratio between the observed friction pressure gradient $(dP/dx)_{TP}$ and the values for each phase alone. It was assumed that phase changes, surface tension of the

liquid, and acceleration could be neglected. Since these investigators were carrying out their work in horizontal flow, they also chose to disregard the effect of body forces. In essence, the Martinelli correlation balances frictional shear stresses vs. static pressure drop. Thus, the variables take the form

$$\Phi_G^2 = \frac{(dP/dx)_{TP}}{(dP/dx)_G} \quad (22)$$

$$\Phi_L^2 = \frac{(dP/dx)_{TP}}{(dp/dx)_L} \quad (23)$$

and, in order to avoid having $(dP/dx)_{TP}$ in both correlating parameters, they defined

$$\chi^2 = \frac{\Phi_G^2}{\Phi_L^2} \quad (24)$$

where χ^2 gives a measure of the degree to which the two-phase mixture behaves as a liquid, rather than as a gas. Four different correlations for χ vs. Φ_G and Φ_L are obtained, depending upon whether the individual phases are in laminar or turbulent flow.

Schneider, White and Huntington (1954) experimented with horizontal gas-liquid flow using water and kerosene as the liquids. These researchers found that increasing either the gas or liquid flow rate would increase the pressure drop. Their data showed that the pressure drop was more a function of the gas than of the liquid flow rate. In

addition, the physical properties of the liquid were shown to have a questionable effect; all else being equal, the kerosene exhibited a higher pressure drop than the water.

Hoogendoorn (1959), in a horizontal gas-liquid flow study using oils as the liquid, found that the Martinelli correlation was invalid for both mist-annular and wavy flow (in wavy flow the liquid flows entirely on the bottom of the tube and the surface is characterized by an irregular wave shape). The correlation over-predicted pressure drop. In both of the regimes he studied, a large amount of the liquid was atomized. He found that the effect of liquid viscosity on the location of the lines of transition between the various flow regimes is small.

Martinelli and co-workers (1944), investigating several liquids in two-phase horizontal flow, found that the liquid surface tension had no apparent effect on the pressure drop. They also reported that as the liquid viscosity increased the pressure drop increased.

Collier and Hewitt (1961) conducted an experimental study of air-water climbing film flow in which the water flow rate varied from .15 to 1.5 lb_m/min. The predicted pressure drops using Martinelli's correlation are in good agreement with experimental values ($\pm 25\%$). At low pressure drops, however, the predicted values were above experimental values.

Gill, Hewitt and Lacy (1963), investigating a system similar to that of Collier and Hewitt (1961), also found that Martinelli's correlation

predicted pressure drops with an accuracy of 30% to -3%. They found that a homogeneous model did an extremely poor job of predicting experimental values.

Kim (1965), while studying air-water climbing film flow in an annular duct, found that the Martinelli correlation predicted the two-phase pressure drop quite accurately.

In a recent six part series, DeGance and Atherton (1970) attempted to critically review the models presently available for predicting pressure drop and found Orkiszewski's to be the best vertical flow correlation. Orkiszewski presented a model for predicting two-phase pressure drop in vertical flow which, he claimed, had a precision of about 10%. In this study, a tremendous amount of data was obtained for pipe flow, and correlations of several investigators were compared.

Orkiszewski divided vertical two-phase flow into four regimes and gave the best correlations for each. Defined were bubble, slug, annular-slug transition, and annular-mist flows. As defined, the annular-mist region includes pure annular flows. It was assumed by the investigator that in the annular-mist region the majority of the liquid is entrained and that there is virtually no slip between the phases; therefore, he concluded that the effect of the liquid film is secondary. A major effect in the resulting pressure drop expression is an acceleration term which would be negligible in pure annular flow.

It is pointed out in the paper that the method should be used with discretion in ducts other than circular tubes.

In an attempt to put two-phase flow on a unified basis, Wallis (1966) introduced dimensionless volumetric fluxes for liquid and gas, defined respectively as

$$j_L^* = \frac{j_L \rho_L^{\frac{1}{2}}}{(gD(\rho_L - \rho_G))^{\frac{1}{2}}} \quad (25)$$

$$j_G^* = \frac{j_G \rho_G^{\frac{1}{2}}}{(gD(\rho_L - \rho_G))^{\frac{1}{2}}} \quad (26)$$

where j_L and j_G are the superficial liquid and gas velocities. He found that if gas velocities are high enough ($j_G^* \gg 2$) for shear stresses to dominate the flow, then the Martinelli correlation can be applied to vertical flow. When gas velocities are not high, the gravity force must be compensated for and, making a force balance on vertical annular flow, the following can be derived:

$$\phi_G^2 \Delta P_G^* - \phi_L^2 \Delta P_L^* = R_L \quad (27)$$

where R_L is the liquid volumetric fraction and

$$\Delta P_G^* = \frac{-(dP/dx)_G}{g(\rho_L - \rho_G)} \quad (28)$$

$$\Delta P_L^* = \frac{-(dP/dx)_L}{g(\rho_L - \rho_G)} \quad (29)$$

Wallis (1966) further defined a dimensionless two-phase pressure drop as

$$\Delta P^* = \frac{-(dP/dx)_{TP} - \rho_G g}{g(\rho_L - \rho_G)} \quad (30)$$

leading to the relations

$$\Delta P^* = \Phi_G^2 \Delta P_G^* \quad (31)$$

$$\Delta P^* = \Phi_L^2 \Delta P_L^* + R_L \quad (32)$$

Using correlations to relate Φ_L and Φ_G to R_L , he generated curves that allow for direct prediction of vertical two-phase pressure drop.

Rough Wall Effects Caused by Annular Flow

Experimental studies have demonstrated that in single-phase flow the existence of a rough boundary causes a change in the dimensionless velocity distribution curve. Flow in an annular duct in which one wall is roughened will cause the point of maximum velocity to shift away from the roughened wall. Annular film flow gives rise to a similar rough wall effect and causes a shift in the velocity profile.

Hanratty and Engen (1957), Ellis and Gay (1959), Lilleleht and Hanratty (1961), Hewitt, King and Lovegrove (1962), Shearer and Nedderman (1965), Kim, and Hewitt and Nicholls (1969) have all shown

experimentally that a liquid film flowing on one wall of a duct will cause a shift in the velocity profile similar to that occurring when a single phase flows near a roughened wall. Several attempts have been made to relate the annular flow velocity shift to one-phase flow correlations.

Hanratty and Engen attempted to relate the liquid film thickness to an equivalent sand roughness. Their experiments in horizontal flow showed that the velocity shift seemed to be determined by the liquid Reynolds number, with the variation of gas rate having little effect.

Lilleleht and Hanratty also related the shifting velocity profile to an equivalent sand roughness. They correlated the increase in the interfacial shear stress to the displacement of the point of maximum velocity of the liquid from its average height. They offered no theoretical basis for their correlation.

Ellis and Gay studied annular flow on one wall of a channel. They concluded that the part of the velocity profile near the smooth wall is unaffected by the presence of the liquid film on the other wall and vice versa.

Kim measured the velocity profiles in an annulus in which a liquid film was climbing on the inner wall while the outer wall remained dry. He too found that the velocity profile near the dry wall was unchanged from that of air flowing alone in the annulus. He also reported that the shear stress at the outer wall was essentially unchanged.

Hartley and Roberts (1961) presented a correlation for friction factor taking the liquid film thickness into account. The reasoning behind their correlation was that if the liquid film is thinner than the gas boundary layer thickness, then there is no change in the pressure gradient from that of gas flowing alone. Their correlation is only applicable at low liquid and high gas flow rates where the liquid film is fairly thin and flat.

Hewitt and Nicholls found that the ratio of the wave height for disturbance or roll waves to the mean film thickness was approximately constant. They noted that the relative roughness (apparent roughness height divided by the equivalent diameter) is a unique function of the relative film thickness (film thickness divided by the equivalent diameter). If the heights of the disturbance waves on the liquid surface are about the same for a given mean film thickness, it follows that the distance between waves must also be about the same for a similar roughness to occur. The results of Hewitt and Nicholls suggest that there is some geometrical similarity for disturbance waves at a given film thickness.

Thin Liquid Films

Steam condensing on a vertical wall gives rise to a falling liquid film. Nusselt (1916) was one of the first to attempt to analyze this

phenomenon. Neglecting inertial forces in the film, he furnished the following expression for the liquid film thickness:

$$h_o = \left(\frac{3\nu u_o}{g} \right)^{\frac{1}{2}} \quad (33)$$

where u_o is the average velocity in the liquid film. Although his solution only applies when the free liquid surface is wave free, it serves as a good first approximation in any case of film flow.

It was noticed quite early that flowing surfaces are characterized by waves. Jeffreys (1925) appears to have been the first to attempt a prediction of the initiation of these roll (or disturbance) waves. For flow down a vertical plane, he found that the motion of the film is laminar when the liquid Reynolds number is less than 300. Jeffreys introduced the theory of sheltering. According to this theory, air flowing over a deformed water surface is unable to follow the surface, thus, it separates at each crest. As a result, regions of low velocity and pressure are formed on the leeward side. This situation causes a difference in normal pressure between the windward and leeward sides of each crest and, if the wind velocity exceeds the wave velocity, energy is transferred from the air to the liquid.

Hanratty and Hershmann (1961) applied the theories of Jeffreys to explain the initiation of roll waves on a liquid surface in a system consisting of the co-current flow of a gas and a liquid. In their model, they assumed that the leading edge of each roll wave rises sharply

from the thin film while the trailing edge gradually tapers back off into it. Data were presented which indicate that surface disturbances are damped more with a higher viscosity liquid.

Lighthill and Whitham (1955) also concerned themselves with roll waves. They demonstrated that, in a flowing liquid, the crests of disturbances with a long wavelength move faster than the troughs, thus causing the downstream end of the wave to steepen and roll over upon itself. It is this action which causes increases in mass transfer rates in wetted wall columns and large heat transfer rates in film cooling.

The principal work dealing with the mathematical interpretation of surface waves on a flowing film is that of Kapitza (1948); however, the reader is also referred to Levich (1962) for extensions and corrections of his work. Kapitza's was the first attempt to describe wavy flow by postulating an oscillatory steady state solution of the equations of motion. A relative deviation of the instantaneous film thickness, h , from the average film thickness, h_o , was defined as

$$\phi = \frac{h - h_o}{h_o} \quad (34)$$

where ϕ takes the form

$$\phi = A \sin k(x - ct) \quad (35)$$

and where k is the wave number, c is the celerity, and A the wave amplitude. Kapitza employed an integral approach; he assumed a

parabolic velocity profile, integrated the equation of motion over the entire film, and solved the resulting equation after linearizing. Surface tension was introduced into his analysis through the pressure gradient term in the equation of motion.

Kapitza's solution predicts that the dimensionless wave celerity, α (the wave celerity divided by the average velocity in the liquid film), is constant and is equal to three. It is also predicted that the wavelength decreases with increasing liquid flow rate. Both of these conclusions have been shown to be correct only at low liquid Reynolds numbers (see Tailby and Portalski (1962) and Appendix VI).

To find the wave amplitude, Kapitza assumed that the correct value is that which provides the least viscous dissipation of mechanical energy. A proof has never been set forth for this assumption. Kim and B. Scott (1969) have both applied this technique to climbing film flow. Massot, Irani, and Lightfoot (1966) extended Kapitza's method by taking the higher order terms of viscous dissipation; unfortunately, their prediction of wave amplitude is poor.

Semenov (1950) applied a theoretical approach to a smooth laminar film acted upon by interfacial stress resulting from co-current and counter-current gas flows. He extended his smooth film flow solution to wavy film flow by simplifying Kapitza's theory. He argued that for very thin films the viscous forces in the film predominate and hence solved the equation of motion neglecting the inertia terms.

Kasimov and Zigmond (as cited by Fulford, 1964) presented a general solution to the equations of wavy films which was patterned after the work of Kapitza and Semenov. They found that the wavelength should be proportional to surface tension to the $1/3$ power and proportional to kinematic viscosity to the $1/9$ power.

Kapitza's theory was applied to climbing film flow in an annulus by both Kim and B. Scott. As did Kapitza, both neglected the variation of the film thickness with time and the flow direction. Kim's predictions of film thickness are fairly accurate; however, he underpredicted wavelength by as much as 500% for the high liquid flow rate regime. Scott attempted to improve Kim's correlation, but in fact arrived at an impossible solution. His final expression does not reduce to the correct limit when interfacial shear stress is set to zero. Scott also used a gas density in his expression for film thickness where a liquid density should have been used.

In studying climbing film flow, Willis (1965) assumed a smooth interface and a film of constant thickness. He arrived at an expression relating film thickness to liquid flow rates. The Willis model was compared with experimental values by B. Scott, who found that the variance in the predicted liquid flow rate ranged from 60% to 250% of the actual values.

Massot, Irani and Lightfoot, in a theoretical study of a viscous falling film with a wavy surface, followed Kapitza's method in linearizing

the equations of motion. Some basic inconsistencies in their analysis have been pointed out by Levich and Krylov (1969). Unlike Kapitza, they did not neglect the term $\partial^2 u / \partial x^2$ in the x-directed motion equation. However, they disregarded terms in their boundary conditions that are of the same order of magnitude as this term.

Berbente and Ruckenstein (1968) used a solution for a falling liquid film in wave motion which included a triple series expansion. They asserted that the parabolic velocity profile assumption in the liquid film is not satisfactory and, instead, proposed a polynomial of at least degree four to describe the velocity in the film. This requires that the point of maximum velocity in the liquid film lie below the interface.

There are several investigators who have taken the position that the flowing liquid film more accurately fits a turbulent model. Dukler and Berglin (1952) were among the first to consider the films as turbulent. They examined the hydrodynamic relationships in a system in which a turbulent flowing core of gas is exerting a shear stress on the liquid film flow on the tube wall. They assumed that this interfacial shear stress set up a turbulent velocity profile in the liquid film, and, for their analysis, used the von Karman universal velocity profile.

Equations for climbing film flow in a circular pipe were developed by Calvert and Williams. Their basic goal was to relate the liquid film flow rate, the film thickness, and the interfacial shear. They

accomplished this by postulating a velocity profile in the film in terms of the interfacial shear stress, and by subsequently integrating to give the film flow rate. They divided the liquid film into two regions: a laminar sublayer and a turbulent region.

Dukler (1960) also divided a downward flowing film into two regions and applied the Deissler and von Karman eddy viscosity equations to the film in order to generate a velocity profile in the film. He presented numerical solutions for the parallel flow of both a liquid film with interfacial shear due to the action of a co-current gas stream and a freely falling film. His equations represent an equilibrium between the shear and the gravity forces on the film.

A mathematically more rigorous approach to the study of thin films is that of stability analysis. Investigations using linear stability analysis are based on the assumption that infinitesimally small disturbances are superimposed upon the laminar film flow, and they deal with the examination of the growth of these small disturbances.

Stability analysis of the liquid film surface, as used by Benjamin (1957), has shown theoretically that the film surface becomes unstable at a very small Reynolds number for horizontal flow and that vertical film flow is always unstable. Benjamin studied the stability of a uniform laminar stream of viscous liquid (with a free surface influenced by surface tension) which was running down an inclined plane under the influence of gravity. He found that a class of undamped waves exist

for all finite Reynolds numbers. Prior to Benjamin's study, it was widely believed that there existed a critical Reynolds number at which wavy motion would commence. Because they were unaware of the fact that at low Reynolds numbers the surface instabilities are very small and may not manifest themselves physically, many experimenters erroneously claimed that waves first appear on the film surface at approximately a liquid Reynolds number of 10.

Yih (1963) showed that the stability characteristics of a falling film at small Reynolds numbers are governed by the velocity of the surface waves. Using Yih's idea that surface waves govern the film stability, Anshus and Goren (1966) presented an approximate solution to the flow of a liquid film down a vertical wall. Their method consisted of replacing the velocity (normally a function of distance from the wall) by its value at the free surface while keeping the second derivative of the velocity at its true value. The model predicts a minimum in the wavelength vs. Reynolds number curve and fits the data taken by Tailby and Portalski quite well.

Krantz and Goren (1970, 1971a, 1971b) have also used stability analysis for predicting the wave forms of finite-amplitude, long wave disturbances found on liquid films flowing down a plane. Their solutions are in very good agreement with their experimental data. Unfortunately, numerical stability analysis yields a separate wave solution (and a separate curve when plotted) for each Reynolds number. On

the other hand, classical film analysis, be it for a turbulent or a laminar model, produces a solution valid for all liquid Reynolds numbers.

Gollan and Sideman (1969), utilizing Yih's conclusion, have assumed that the interfacial velocity, and not the distribution of the velocity through the film, controls the hydrodynamics of film flow. Extending the analysis of Massot, Irani, and Lightfoot, they improved it by including the normal stress induced by velocity in the film in the boundary condition. They also solved the equation of motion by utilizing the controlling interfacial velocities rather than by averaging the equation.

A literature survey dealing, however remotely, with waves on a liquid surface must certainly recognize the tremendous amount of pertinent work done in Oceanography. Kinsman's (1965) tome on wind waves enumerated all the important models of wave generation and propagation on the ocean surface. Since almost all oceanographic work deals with wave formation in deep water, it does not apply to wave formation on thin films. However, Oceanography has contributed peripherally to the study of waves on thin films by establishing that ocean waves constitute a stochastic process; accordingly, the problems of ocean wave analysis must be formulated in terms of statistically meaningful quantities, such as probability distributions and spectra.

Telles (1968) explored the structure of the gas-liquid interface by analyzing the time-varying film thickness obtained from electrical

conductivity measurements. He presented power spectra plots and used the peaks to describe the most probable wave frequencies. The mean film thickness and wave variance of film thickness was obtained by making probability statements about the distribution of the film thickness.

Using another approach (which is specifically designed for use in the annular flow regime), the film thickness can be immediately obtained if one first predicts the liquid holdup, R_L (the volumetric fraction of liquid). Three holdup correlations are of interest. The first was introduced by Lockhart and Martinelli, who used their variable, χ , to correlate liquid holdup data. Kim has found that this correlation overpredicts R_L in the low liquid flow rate region. The second was described by Hughmark and Pressburg (1961), who used the data of several investigators to find a correlation for liquid holdup in vertical flow. The third, termed the Dartmouth Correlation and presented by Wallis, Steen, and Turner (1964), was specifically designed for annular flow. All three of these correlations will be discussed more fully later.

There have been many experimental studies of annular flow. Principally concerned with air-water or steam-water systems, few have investigated the effects of the physical properties of other liquids on the annular film structure. Some of the more important experimental investigations are presented below.

Van Rossum (1959) confirmed experimentally that, over a wide range of flow conditions, the mean actual film thickness is about 60% of that predicted by laminar film theory. He found that for shallow water waves, the wavelength is much shorter than predicted by Jeffreys and concluded that surface tension must have some effect in this range.

Collier and Hewitt (1961) analyzed the data presented by Bennett (1958) using the methods of both Calvert and Williams and Anderson and Mantzouranis (1960). It should be pointed out here that several investigators have shown the analysis of Anderson and Mantzouranis to be in error. They assumed a constant shear stress within the liquid and assumed it to be equal to the shear stress at the wall. Unfortunately, at low gas flow rates, this assumption introduces large errors. Collier and Hewitt (1961) found that the film thickness became enlarged with increasing liquid rate (the rate of increase fell rapidly). The Calvert and Williams model was found to predict film thickness better than the others.

An extensive experimental study of wave patterns in the climbing film flow of air-water mixtures was carried out by Hall-Taylor and Hewitt (1962). They found that roll waves are nearly always observed in this type of a system. The waves, which have a "milky" appearance because light is scattered by their irregular surfaces, travel rapidly along the surface of the liquid film. The mean celerity of the roll waves was found to be 5% to 10% of the air velocity; dimensionless

celerity was always around three. The average celerity increased rapidly with an increase in air flow rate but was insensitive to changes in water flow rate. Conversely, the wave frequency was insensitive to the air flow rate but increased proportionately with the liquid flow rate. The latter effect suggests that the waves are transporting the liquid. As the liquid rate is increased at constant air rate, the wavelength is considerably reduced.

Woodmansee and Hanratty (1969), while conducting experimental studies in a rectangular horizontal channel, found that the film consisted of roll waves moving over a thin liquid base film. They proposed that increasing the liquid flow rate does not change the thickness of this base film thickness, but that the liquid becomes transformed into roll waves. They also found that the roll wave height is much greater than the base film height.

Lacey, Hewitt, and Collier (1962), in a survey article on climbing film flow, stressed the importance of learning more about the hydrodynamics of the climbing film. They pointed out that climbing film heat transfer is entirely controlled by hydrodynamics and that the only effect of the heat transfer is to alter the physical properties. They reported that roll wave celerity is entirely controlled by the gas flow rate and that the average wavelength is inversely proportional to the liquid flow rate.

THEORETICAL ANALYSIS

Analysis of Liquid Film

A general theoretical solution for a thin film flowing on a plane and influenced by a parallel flowing gas stream is presented in this section. The technique of Kapitza is the basis for the solution; however, the assumption will be made that the hydrodynamics of the film structure is controlled by the velocity of the liquid surface. A solution is obtained by setting the velocity related terms in the motion equation equal to the values at the surface $y = h(x, t)$, rather than by averaging the motion equation by integrating over the thickness of the film. In Figure 1 some of the terms to be used are defined.

The equations of motion in two dimensions for the liquid film flowing on a wall and the incompressible fluid continuity equation are the beginning relationships

$$\frac{\partial u}{\partial t} + u \frac{\partial u}{\partial x} + v \frac{\partial u}{\partial y} = \nu \frac{\partial^2 u}{\partial x^2} + \nu \frac{\partial^2 u}{\partial y^2} \pm g \sin \theta - \frac{1}{\rho} \frac{\partial P}{\partial x} \quad (36)$$

$$\frac{\partial v}{\partial t} + u \frac{\partial v}{\partial x} + v \frac{\partial v}{\partial y} = \nu \frac{\partial^2 v}{\partial x^2} + \nu \frac{\partial^2 v}{\partial y^2} \pm g \cos \theta - \frac{1}{\rho} \frac{\partial P}{\partial y} \quad (37)$$

$$\frac{\partial u}{\partial x} + \frac{\partial v}{\partial y} = 0 \quad (38)$$

In Equations (36) and (37), the \pm gravity terms correspond to the

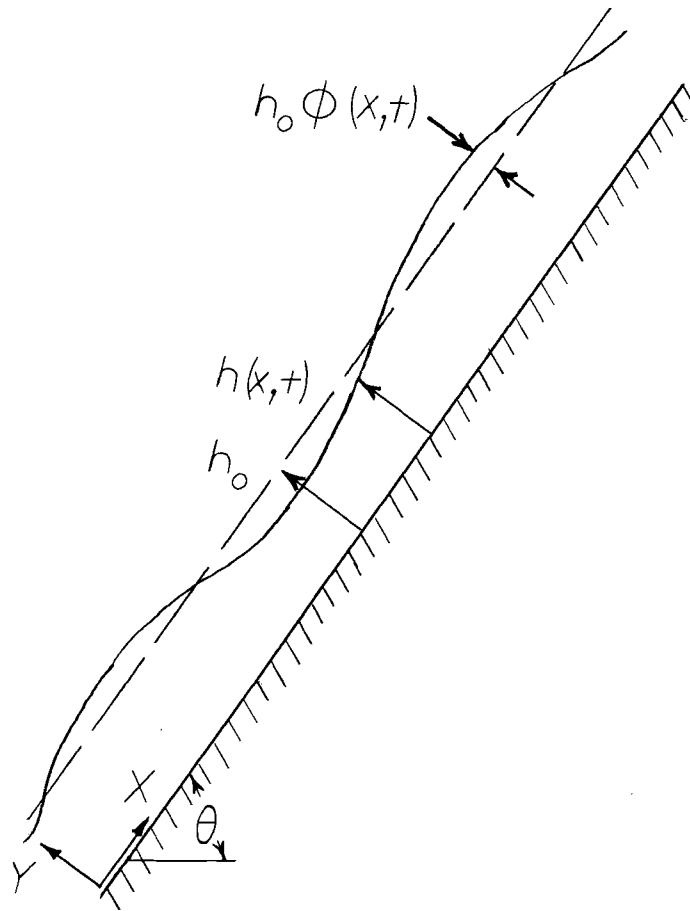


Figure 1. Film flowing on a plane surface.

falling and climbing film, respectively. The boundary conditions are:

$$\text{at } y = 0 \quad u = v = 0 \quad (39)$$

$$\text{at } y = h(x, t) \quad P = P_G + P_\sigma + 2\mu \frac{\partial v}{\partial y} \quad (40)$$

$$\text{at } y = h(x, t) \quad \mu \left(\frac{\partial v}{\partial x} + \frac{\partial u}{\partial y} \right) = \pm \tau_1(x, t) \quad (41)$$

Zero slip at the wall is assumed in Equation (39). Equation (40) balances the normal stresses at the liquid surface $y = h(x, t)$. The pressure in the liquid film P , is balanced by the pressure in the gas stream P_G , a pressure resulting from the capillary forces at the curved interface and the viscosity-induced normal stress in the liquid. The tangential stresses are balanced at the interface in Equation (41). The term $\pm \tau_1(x, t)$ is the interfacial shear stress due to the drag of the gas on the liquid, the \pm referring to the co- and counter-current gas-liquid flow, respectively. For convenience in writing, the \pm will be dropped at this point from the gravity and shear stress terms and the co-current climbing film solution will be pursued.

Assuming the amplitude of the surface disturbances to be small compared to their wavelength, it can be shown that when these displacements are in one direction only (Levich, p. 375)

$$P_\sigma = - \sigma \frac{\partial^2 h}{\partial x^2} \quad (42)$$

With Equations (38) and (42), (40) becomes

$$P = P_G - \sigma \frac{\partial^2 h}{\partial x^2} - 2\mu \frac{\partial u}{\partial x} \quad (43)$$

For very thin films, the terms in the y -directed motion equation, in comparison to those in the x -directed equation, can be neglected by order of magnitude arguments. Equation (37) reduces to

$$\frac{dP}{dy} = 0 \quad (44)$$

which allows the substitution of Equation (43) directly into Equation (36) since $P = P(x, t)$. Hence,

$$\frac{\partial u}{\partial t} + u \frac{\partial u}{\partial x} + v \frac{\partial u}{\partial y} = \nu \frac{\partial^2 u}{\partial y^2} + 3\nu \frac{\partial^2 u}{\partial x^2} - \frac{1}{\rho} \frac{\partial P_G}{\partial x} + \gamma \frac{\partial^3 h}{\partial x^3} - g \quad (45)$$

where $\gamma = \sigma/\rho$ is the kinematic surface tension. We can further reduce Equation (45) by making the boundary layer assumption that $\partial^2 u/\partial y^2 \gg \partial^2 u/\partial x^2$, giving

$$\frac{\partial u}{\partial t} + u \frac{\partial u}{\partial x} + v \frac{\partial u}{\partial y} = \nu \frac{\partial^2 u}{\partial y^2} - \frac{1}{\rho} \frac{\partial P_G}{\partial x} + \gamma \frac{\partial^3 h}{\partial x^3} - g \quad (46)$$

with boundary conditions

$$\text{at } y = 0 \quad u = v = 0 \quad (39)$$

$$\text{at } y = h(x, t) \quad \frac{\partial u}{\partial y} = \frac{1}{\mu} \tau_i(x, t) \quad (47)$$

Equation (46) with boundary conditions (39) and (47) cannot be solved analytically. A simplified model is proposed which will yield

an approximate velocity profile. Then, using this velocity profile and the simplified boundary conditions, a solution can be found for Equation (46).

Assuming that the film has a fairly constant thickness, Equation (47) becomes

$$\text{at } y = h(x, t), \quad \frac{\partial u}{\partial y} = \frac{1}{\mu} \tau_i \quad . \quad (48)$$

It is also assumed that the velocity profile in the liquid film is approximately parabolic. Using boundary conditions (39) and (48),

$$u = \frac{3}{h} \frac{\tau_i}{2} \left(\frac{h}{2} \frac{\tau_i}{\mu} - \bar{u} \right) \left(\frac{y^2}{2} - hy \right) + \frac{\tau_i y}{2} \quad (49)$$

where the instantaneous average velocity $\bar{u} = \bar{u}(x, t)$ is defined as

$$\bar{u} = \frac{1}{h} \int_0^h u dy = \frac{\tau_i h}{2\mu} - \frac{1}{3} \left(\frac{1}{\mu} \frac{\partial P_G}{\partial x} - \frac{g}{\nu} \right) \quad . \quad (50)$$

It has been shown by Yih that the stability characteristics for a freely falling film are governed by the surface waves. It therefore can be assumed that, for a liquid film influenced by a parallel flowing gas stream, the surface phenomena govern the entire film structure.

Utilizing the interfacial velocities and their related derivatives,

$$u \approx u|_{y=h}, \quad v \approx v|_{y=h}, \quad \partial u / \partial t = \partial u / \partial t|_{y=h}, \quad u \partial u / \partial x \approx u \partial u / \partial x|_{y=h},$$

etc. are substituted in Equation (46). Substituting and employing

lengthy but straightforward algebra

$$\frac{3}{2} \frac{\partial \bar{u}}{\partial t} + \left(\frac{9}{4} \bar{u} + \frac{3}{8} \frac{\tau_i h}{\mu} \right) \frac{\partial \bar{u}}{\partial x} - \frac{\tau_i h}{\mu} \frac{\partial \bar{u}}{\partial x} = \nu \left(\frac{3}{2} \frac{\tau_i}{\mu h} - \frac{3\bar{u}}{h^2} \right) - \frac{1}{\rho} \frac{\partial P_G}{\partial x} + \gamma \frac{\partial^3 h}{\partial x^3} - g \quad (51)$$

Further, the continuity equation can be rewritten in the form

$$v(x, y, t) = - \frac{d}{dx} \int_0^y u dy \quad (52)$$

and at the surface

$$\frac{\partial h}{\partial t} \approx v \quad (53)$$

leading to

$$\frac{\partial h}{\partial t} = - \frac{d}{dx} \int_0^h u dy \quad (54)$$

Substituting Equation (49) into (54), and carrying out the indicated operations will yield

$$\frac{\partial h}{\partial t} = -\bar{u} \frac{\partial h}{\partial x} - h \frac{\partial \bar{u}}{\partial x} \quad (55)$$

Expressing the film thickness h in terms of the average film thickness h_o and the local amplitude $h_o \phi$,

$$h = h_o (1 + \phi) \quad (56)$$

For two dimensional waves, a possible solution is that of a rigid sinusoidal wave of amplitude A moving in the positive x -direction with celerity $c = 2\pi\tilde{f}/k$, where \tilde{f} is the wave frequency and k the wave number:

$$\phi = A \sin k z \quad (57)$$

where $z = x - ct$. Transforming variables in Equation (51),

$$-\frac{3}{2}c \frac{\partial \bar{u}}{\partial z} + \left(\frac{9}{4}\bar{u} + \frac{3}{8} \frac{h\tau_i}{\mu}\right) \frac{\partial \bar{u}}{\partial z} - \frac{\tau_i h}{\mu} \frac{\partial \bar{u}}{\partial z} = v \left(\frac{3}{2} \frac{\tau_i}{\mu h} - \frac{3\bar{u}}{h^2}\right) - \frac{1}{\rho} \frac{\partial P_G}{\partial x} + \gamma \frac{\partial^3 h}{\partial z^3} - g \quad (58)$$

Equations (57) and (56) are forced as a solution on Equation (58).

Transforming variables in Equation (55) and substituting Equation (56) gives an ordinary differential equation

$$-c h_o \frac{d\phi}{dz} = -\bar{u} h_o \frac{d\phi}{dz} - h_o (1 + \phi) \frac{d\bar{u}}{dz} \quad (59)$$

which becomes

$$\frac{d}{dz} [(1+\phi)(c-\bar{u})] = 0 \quad (60)$$

and integrating

$$(1+\phi)(c-\bar{u}) = C_1 \quad (61)$$

where C_1 is a constant which can be determined using the condition that when $h = h_o$, $\bar{u} = u_o$. Equation (61) therefore becomes

$$\bar{u} = c - \frac{c - u_o}{1 + \phi} \quad (62)$$

and for very small amplitude waves $\phi \ll 1$ and Equation (62) can be expanded using a binomial series

$$\bar{u} = c - (c - u_o)(1 - \phi + \dots) \quad (63)$$

where all terms of ϕ of second order and higher can be neglected.

Equation (63) can be rearranged

$$\bar{u} = u_o + (c - u_o)\phi \quad (64)$$

It is now possible to substitute Equations (56) and (64) into Equation (58) and, after rearranging and using a binomial series expansion,

$$\begin{aligned} & (c - u_o) \left[-\frac{3}{2}c + \frac{9}{4}u_o + \frac{3}{8} \frac{\tau_i h_o}{\mu} - \frac{\tau_i h_o}{\mu} \right] \frac{d\phi}{dz} \\ & = \frac{3\nu\tau_i}{2\mu h_o} - \frac{3\nu u_o}{h_o^2} - g - \frac{1}{\rho} \frac{dP_G}{dx} + \gamma h_o \frac{d^3\phi}{dz^3} + \phi \left[\frac{6\nu u_o}{h_o^2} - \frac{3\nu\tau_i}{2\mu h_o} - \frac{3\nu}{h_o^2}(c - u_o) \right]. \end{aligned} \quad (65)$$

Equation (65) can be changed to a more convenient form by using the following dimensionless variables: $\alpha = c/u_o$ (dimensionless celerity); $B_m = \tau_i h_o / \mu u_o$; and $We = u_o^2 h_o / \gamma$ (Weber number). Thus,

$$\begin{aligned}
& \frac{h_o^2}{We} \frac{d^3 \phi}{dz^3} + \left(\frac{3}{2} \alpha - \frac{9}{4} + \frac{5}{8} B_m \right) (\alpha - 1) \frac{d\phi}{dz} + \left(3 - \alpha - \frac{1}{2} B_m \right) \frac{3\nu}{h_o^2 u_o} \phi \\
& + \frac{3\nu \tau_i}{2\mu h_o u_o} - \frac{3\nu}{h_o^2 u_o} + \frac{1}{u_o} \left(-g - \frac{1}{\rho} \frac{dP_G}{dx} \right) = 0 \quad (66)
\end{aligned}$$

For Equation (66) to yield a periodic solution of the form of Equation (57), it is necessary that the constant term and the coefficient on the ϕ term both vanish; thus,

$$\left(3 - \alpha - \frac{1}{2} B_m \right) \frac{3\nu}{h_o^2 u_o} = 0 \quad (67)$$

$$\frac{3\nu \tau_i}{2\mu h_o u_o} - \frac{3\nu}{h_o^2 u_o} + \frac{1}{u_o} \left(-g - \frac{1}{\rho} \frac{dP_G}{dx} \right) = 0 \quad (68)$$

Rearranging (67) and (68)

$$\alpha = 3 - \frac{1}{2} B_m \quad (69)$$

and

$$h_o = \frac{\frac{3\nu \tau_i}{2\mu} \pm \sqrt{\frac{9\nu^2 \tau_i^2}{4\mu^2} - 12\nu u_o \left(g + \frac{1}{\rho} \frac{dP_G}{dx} \right)}}{2 \left(g + \frac{1}{\rho} \frac{dP_G}{dx} \right)} \quad (70)$$

The remainder of Equation (66) is of the form

$$\frac{h_o^2}{We} \frac{d^3 \phi}{dz^3} + (\alpha - 1) \left(\frac{3}{2} \alpha - \frac{9}{4} + \frac{5}{8} B_m \right) \frac{d\phi}{dz} = 0 \quad (71)$$

which satisfies Equation (57) when

$$k = \sqrt{\frac{We}{h_o^2} (\alpha-1) \left(\frac{3}{2} \alpha - \frac{9}{4} + \frac{5}{8} B_m \right)} . \quad (72)$$

Since the wavelength, $\lambda = 2\pi/k$,

$$\frac{\lambda}{h_o} = \frac{2\pi}{\sqrt{We(\alpha-1) \left(\frac{3}{2} \alpha - \frac{9}{4} + \frac{5}{8} B_m \right)}} \quad (73)$$

If τ_i , dP_G/dx and the liquid physical properties are known, Equations (69), (70), and (73) can be used to determine the film thickness, h_o , the wave celerity, c , and the wavelength, λ .

For the case of a freely falling liquid film, the effects of the gas can be neglected and Equation (70) becomes

$$h_o = \sqrt{\frac{3\nu u_o}{g}} \quad (74)$$

which is identical to the Nusselt film thickness, Equation (33), presented previously. Similarly, Equation (69) becomes

$$\alpha = 3 \quad (75)$$

which is Kapitza's falling film solution for small amplitude waves. An alternate falling film solution is presented in Appendix VI.

For a climbing film on the inner wall of an annulus, the film is very thin and the curvature of the inner core can be neglected.

Therefore, our expressions derived for a film climbing on a vertical plane can be used to predict the film characteristics in the present system.

It is necessary to predict the interfacial shear stress τ_i to be used in Equations (69), (70), and (73). An approximate value for τ_i can be obtained by making a simple momentum balance on the annular cross-section with the liquid film climbing on the inner wall.

Estimation of Shear Stresses

The equation of motion in cylindrical coordinates for upward flow in an annulus is:

$$\rho \left(\frac{\partial u}{\partial t} + u \frac{\partial u}{\partial r} + \frac{w}{r} \frac{\partial u}{\partial \theta} + u \frac{\partial u}{\partial x} \right) = - \frac{\partial P}{\partial x} + \left(\frac{1}{r} \frac{\partial}{\partial r} (r \tau_{rx}) + \frac{1}{r} \frac{\partial \tau_{\theta x}}{\partial \theta} + \frac{\partial \tau_{xx}}{\partial x} \right) - \rho g \quad (76)$$

Assuming one-dimensional, steady-state flow, with constant pressure gradient and no mass transfer between the gas and liquid phases (constant density), Equation (76) becomes

$$\rho u \frac{\partial u}{\partial x} = - \frac{dP}{dx} + \frac{1}{r} \frac{\partial}{\partial r} (r \tau_{rx}) - \rho g \quad (77)$$

If it is also assumed that the kinetic energy term is negligible compared to the others,

$$\frac{dP}{dx} + \rho g = \frac{1}{r} \frac{\partial}{\partial r} (r \tau_{rx}) \quad (78)$$

To solve for shear stress at any radius, this equation must be integrated with respect to r . Integrating between any two radii, signified by 1 and 2,

$$\frac{dP}{dx} \int_1^2 r dr + \rho g \int_1^2 r dr = \int_1^2 \frac{1}{r} \frac{\partial}{\partial r} (r\tau) r dr$$

$$\frac{dP}{dx} \left. \frac{r^2}{2} \right|_1^2 + \rho g \left. \frac{r^2}{2} \right|_1^2 = r\tau \Big|_1^2 \quad (79)$$

Referring to Figure 2, applying Equation (79) between any two radii yields the following:

1. For the liquid film between r_1 and r_i ($r_i = r_1 + h_o$),

$$\frac{dP}{dx} \frac{r_i^2 - r_1^2}{2} + \rho_L g \frac{r_i^2 - r_1^2}{2} = r_i \tau_i - r_1 \tau_1$$

$$\frac{dP}{dx} + \rho_L g = 2 \left(\frac{r_i \tau_i - r_1 \tau_1}{r_i^2 - r_1^2} \right) \quad (80)$$

2. For the gas phase from r_i to r_m ,

$$\frac{dP}{dx} \frac{r_m^2 - r_i^2}{2} + \rho_G g \frac{r_m^2 - r_i^2}{2} = r_m \tau_m - r_i \tau_i$$

$$\frac{dP}{dx} + \rho_G g = 2 \left(\frac{r_m \tau_m - r_i \tau_i}{r_m^2 - r_i^2} \right)$$

but the shear at r_m is zero, thus

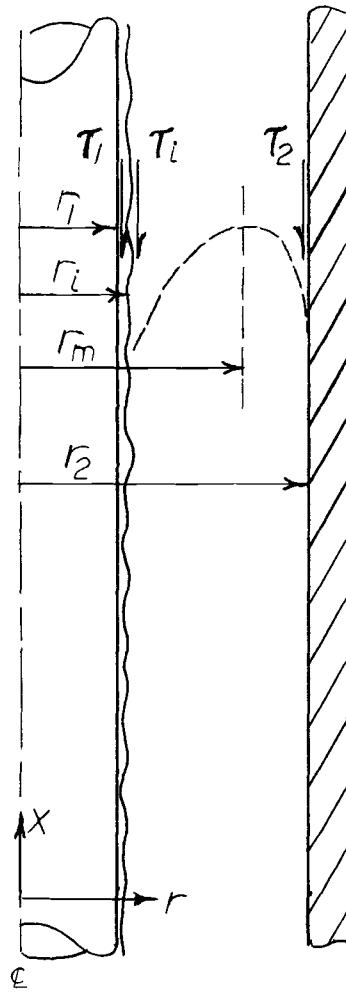


Figure 2. Annular duct cross section.

$$\frac{dP}{dx} + \rho_G g = \frac{-2r_i \tau_i}{r_m^2 - r_i^2} \quad (81)$$

3. For the gas phase from r_m to r_2 (note that the limits are reversed when $r > r_m$),

$$\frac{dP}{dx} \frac{r_2^2 - r_m^2}{2} + \rho_G g \frac{r_2^2 - r_m^2}{2} = r_m \tau_m - r_2 \tau_2$$

$$\frac{dP}{dx} + \rho_G g = \frac{-2r_2 \tau_2}{r_2^2 - r_m^2} \quad (82)$$

The shear stress at the outer wall can be calculated using Equation (82); that is,

$$\tau_2 = \frac{r_2^2 - r_m^2}{2r_2} \left(-\frac{dP}{dx} - \rho_G g \right) \quad (82)$$

Equations (81) and (82) can be solved for τ_i as follows:

$$\tau_i = \tau_2 \frac{r_2}{r_i} \frac{r_m^2 - r_i^2}{r_2^2 - r_m^2} \quad (83)$$

and Equation (80) can be rearranged to solve for τ_1 as

$$\tau_1 = \frac{l}{r_1} \left[r_i \tau_i - \frac{r_i^2 - r_1^2}{2} \left(\frac{dP}{dx} + g \rho_L \right) \right] \quad (80)$$

Therefore, an approximate value for τ_i is determined from Equation (83) and this value is used in solving for the film characteristics previously derived.

EXPERIMENTAL PROGRAM

The purpose of this investigation was to study momentum transfer in climbing film flow. In particular, it was hoped to determine the effect of variations in the liquid properties of four different liquids (water, Shellsolv, light oil, and iso-octyl alcohol) on momentum transfer.

For this investigation, the liquid film was made to climb on the inner wall of an annulus while the outer wall remained dry. Measurements were taken in both the gas phase and at the outer wall, and high-speed motion picture photography was utilized to analyze the liquid film. The following experimental program was carried out:

1. The momentum transfer of single-phase air flow in the annulus was initially investigated. Pressure losses, shear stresses at the outer wall, and radii of maximum velocity were determined over a range of air Reynolds numbers from 7×10^4 to 2×10^5 .
2. Static pressure taps on the outer wall were used to measure two-phase pressure loss. Air flow rates were in the same range as the air flow rates used in the single-phase investigation, and the liquid flow rates ranged from 0.10 to 0.755 lb_m/min.

3. A Preston tube placed on the outer wall was used to measure the shear stress at the outer wall. Data were taken for each liquid at all combinations of air and liquid flow rates.
4. The radius of the point of maximum velocity was determined with the aid of a traversing pitot tube.
5. High-speed motion picture photography was used to photograph the liquid film climbing on the inner wall. The liquid film thickness, wave celerity, and wavelength were determined by analyzing the photographic film.

DESCRIPTION OF EXPERIMENT: APPARATUS

The majority of two-phase gas-liquid flow studies are conducted in circular tubes. If photographic analysis is utilized in studying the flow, the tube can present some very special problems. Light reflection and refraction through the liquid is one of these (it is discussed, along with other problems relating to photography through liquid film, by Cooper, Hewitt and Pinchin (1963)). In addition, pressure taps mounted on the tube walls with liquid and gas flowing over them create a situation in which two phases may be existing in the pressure lines, thus rendering the measured pressure reading questionable.

However, if an annular test section is used, and the liquid film is made to flow on the central core, neither of the above two problems occur. Because of the fact that the outer wall remains dry, photography through the outer wall yields pictures that are easily analyzed, and the pressure taps in the outer wall only come into contact with the gas.

The experimental system can be described most clearly by dividing it into the following four sections: (a) the air source and peripheral equipment, (b) the annular duct, (c) the liquid source and injector, and (d) the air-liquid separator and liquid recycling tank. A drawing of the entire system is presented in Figure 3.

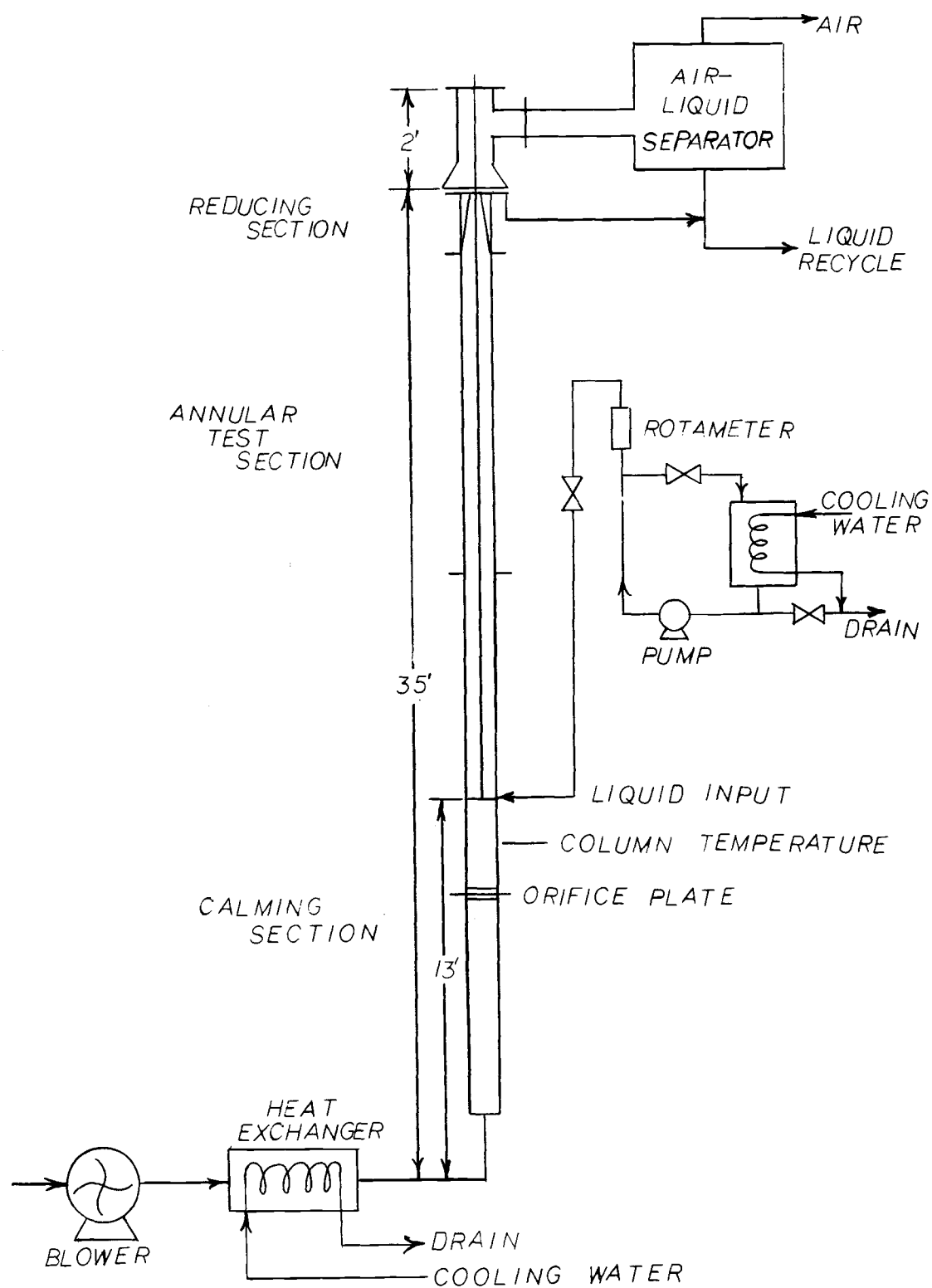


Figure 3. Experimental system.

The Air Source and Peripheral Equipment

Air for the system was supplied by a Sutorbilt 8HB rotary blower which was rated at 550 cfm (1 atm and 68°F) at 9 psi outlet pressure and which was driven by a 30 hp, 1760 rpm General Electric a-c induction motor. At the blower intake, the air was filtered with a fine cloth screen to insure freedom from dust. The exhaust of the blower was fitted with a gate valve which would divert the air through a baffled bypass, thus allowing for air flow rate regulation.

Air passed from the blower through a copper, water-cooled, finned heat exchanger which was connected to the blower with a flexible rubber hose to prevent the blower vibrations from being transferred to the column. The air temperature was regulated by varying the water flow rate through the exchanger.

The heat exchanger was in turn connected to a three inch (I. D.) galvanized pipe by the above mentioned flexible hose. This pipe extended 11 feet above the blower and was connected to the first of five acrylic plastic flanged tubes (the outer wall of the annular duct described below). Mounted in the pipe approximately 8 feet above the blower was an orifice plate for measuring air flow rate, and a few feet above this orifice a thermometer was inserted into the air stream.

The Annular Duct

The annulus was approximately 20 feet long and consisted of an acrylic plastic outer tube and a one-inch (O. D.) stainless steel inner core. The outer tube was composed of five, four foot long tubes, each with a three-inch inside diameter. It was supported laterally at two positions and was made vertical with the aid of a plumb bob and transit. The inner tube was aligned and made concentric with the aid of a transit, adjustment being accomplished with stainless steel centering screws.

In previous work the centering screws were tapered to reduce the amount of liquid entrainment caused by the screws in the test section. This design left much to be desired because the screws were the major cause of liquid entrainment. In the present system, no screws were used in the annular test section; rather, the screws used for centering were not tapered and were only used at the test section extremities. When the untapered screws were used in large numbers, the column was made concentric, no noticeable gain in the minor core vibration occurred, and a total reduction of centering screw-induced entrainment was realized.

The Liquid Source and Injector

The liquid was stored in a 20 gallon, stainless steel, jacketed kettle, and supplied by a Tuthill gear-type rotary pump which was

driven by a $\frac{1}{4}$ -hp a-c induction motor. When liquid entered the column (at a point where the galvanized pipe and acrylic plastic tube met), it flowed 2 feet up inside the inner core and escaped through a porous injection section onto the annular core. The injection system consisted of a two-inch long cylinder of $\frac{3}{16}$ -inch porous stainless steel connected to a six-inch section of Bendix-Poroloy rolled wire mesh tubing, and was designed so that the liquid was injected in a uniform ring around the core. It should be mentioned, in addition, that no entrainment was observed at the injector. This system is diagramed in Figure 4.

The Air-Liquid Separator and Liquid Recycling Tank

At the top of the annular section the outside tube converged to two inches (I. D.), causing the air to increase in velocity and entrain the liquid. Thus, the liquid was carried out of the top of the column totally entrained, at which point the mist was blown tangentially into a 55 gallon barrel. The barrel, coated on the interior surface with an inert marine paint, was fitted with a liquid withdrawal tube at the bottom and a large air exhaust pipe at the top. When the liquid was withdrawn from the barrel, it flowed into a recycle tank where it could be stored until ready to be re-used.

The air-liquid separator is shown in Figure 5.

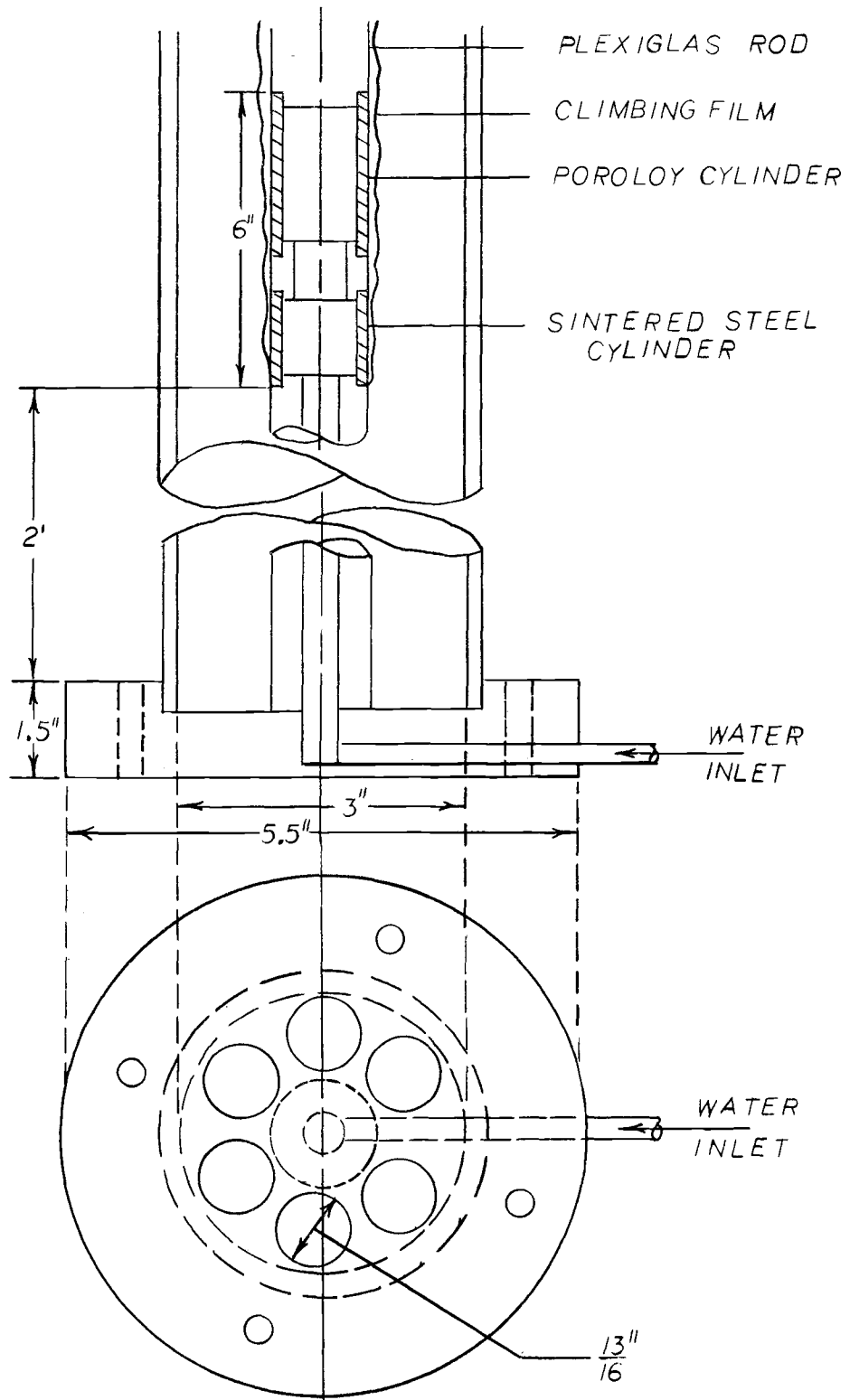


Figure 4. Liquid injection system.

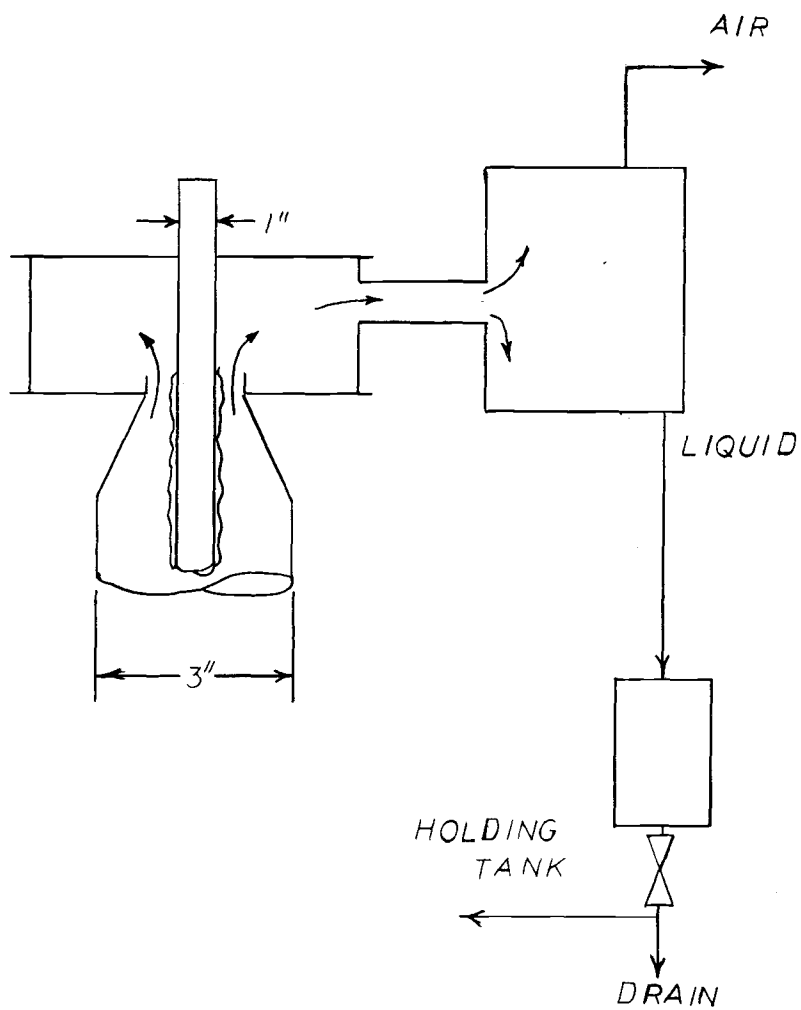


Figure 5. Liquid separator.

DESCRIPTION OF EXPERIMENT; MEASUREMENTS

Measurement of Inlet Air Density

Wet and dry bulb temperatures at the blower inlet were observed prior to each run; the density of the inlet air was obtained from a psychrometric chart. Using ideal gas assumptions and the measured column temperature and pressure, the density of air in the column was determined.

Measurement of Air Flow Rate

The air flow rate was measured with a two-inch, sharp-edged, brass orifice plate which was 1/16-inch thick and was mounted in the three-inch galvanized pipe. Radius taps, located one pipe diameter upstream and $\frac{1}{2}$ pipe diameter downstream, respectively, were connected to a 36-inch differential manometer which was filled with a manometer oil of 2.94 specific gravity. Calibration of the orifice is given in Appendix II.

Measurement of Column Temperature and Pressure

The column temperature was measured with a calibrated dial-type thermometer placed in the air stream approximately $4\frac{1}{2}$ feet below the liquid injector. By adjusting the liquid flow through the heat

exchanger, the column temperature could be kept fairly close to 68°F ($\pm 2^\circ$) for all runs.

The column pressure was measured at the liquid injector point. A pressure tap was connected to one side of a 24-inch differential manometer filled with Mercury. The other side of the manometer was open to the atmosphere.

Measurement of Pressure Gradient

The pressure gradient was measured between two 1/16-inch pressure taps located 84.5 inches apart. The taps were placed in the column at points where the entrance and exit effects would be minimized. The first tap was placed 86 inches (over 40 equivalent diameters) above the calming section. Work by Quarmby has shown that the hydrodynamic entrance length for annuli is from 30 to 40 equivalent diameters. The pressure taps were connected to a 50-inch inclined manometer filled with manometer oil of 0.826 specific gravity.

Measurement of Shear Stress at the Outer Wall

A Preston tube, consisting of a section of one-inch long stainless steel hypodermic tubing (0.0544 inch nominal diameter) connected to a 1/8-inch brass tube, was mounted on the dry, outer wall to measure shear stress. The tip of the Preston tube was located at the same position in the column as the upper static pressure tap. Both the

static and kinetic pressure taps were connected to a 50-inch inclined manometer filled with manometer oil of 0.826 specific gravity. In Appendix III, the theory and calibration of the Preston tube is presented.

Measurement of Velocity

The velocity in the gas stream was measured with a .02-inch (O. D.) pitot tube. The pitot tube was mounted on a traversing mechanism, and its position was determined by means of a Tumico-dial-type indicator micrometer which had a one-inch range and .0005-inch scale divisions. The tip of the pitot tube was at the same column position as the uppermost static pressure tap. Both kinetic and static taps were connected to a 50-inch inclined manometer filled with manometer oil of 0.826 specific gravity.

Purge System and Manometers

All manometers and all lines leading to the manometers were connected to a high pressure source to allow for the purging of liquid from the lines. One 50-inch inclined manometer was used to measure pressure gradient, shear stress at the outer wall, and velocity profile. This manometer was filled with 0.826 specific gravity fluid. With the aid of plumb bobs, the manometer inclination was determined and found to be $16^{\circ}12'$. A schematic diagram of the purge system and manometer connection is given in Figure 6.

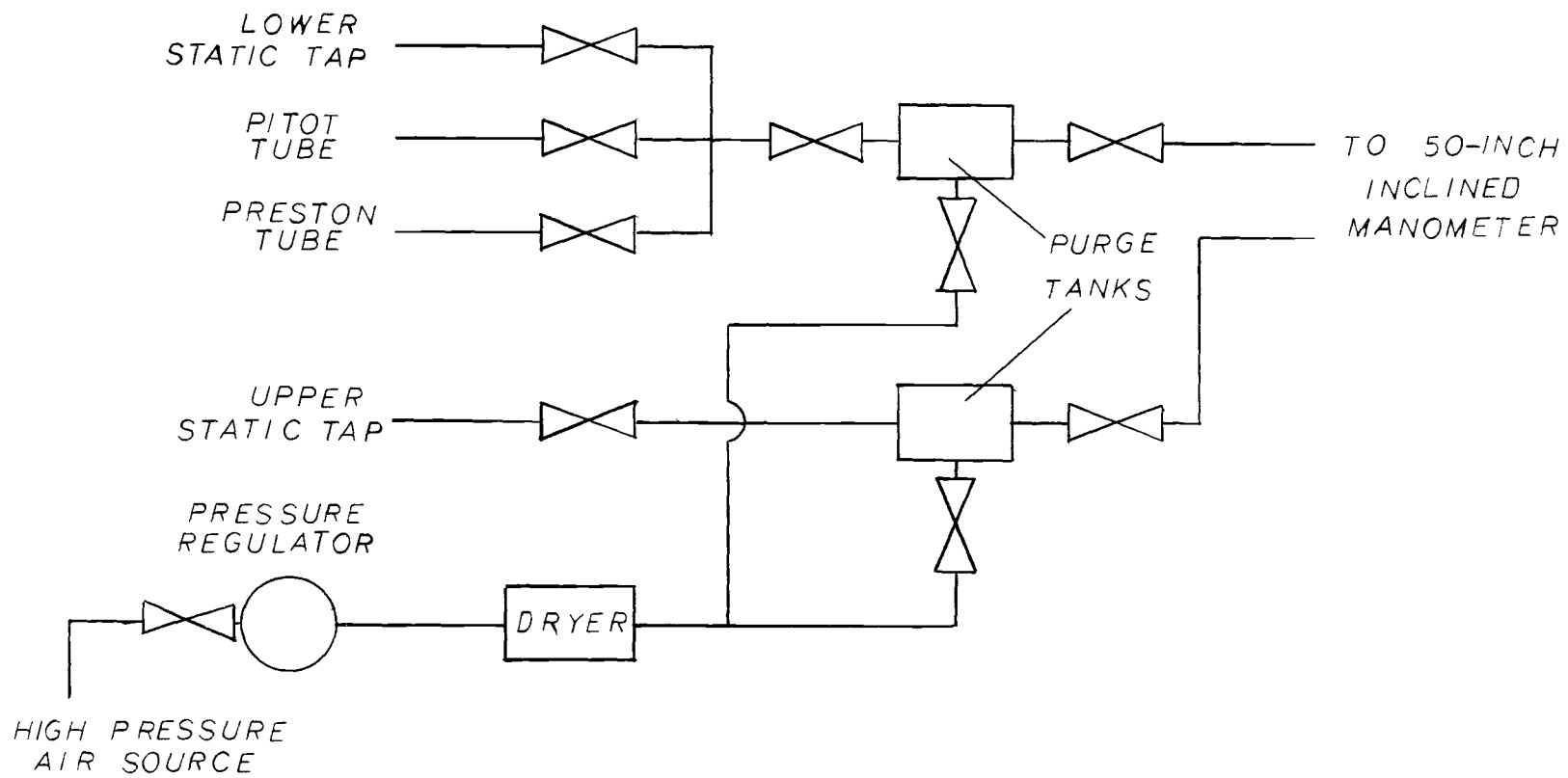


Figure 6. Purging system and manometer connections.

Measurement of Liquid Flow Rate

Liquid flow rates were measured with a Predictability Flowmeter no. FM10488 manufactured by the Manostat Corporation. A glass float was used for all liquids. The manufacturer had calibrated the rotameter and claimed calibration accurate to $\pm 2\%$. For each liquid, the calibration curve was tested at several flow rates and in every case the values obtained were within the $\pm 2\%$ range quoted by the manufacturer. The liquid flow rate was adjusted by means of (1) a bypass valve (which returned the liquid to the holding tank) located between the pump and the rotameter, and (2) a valve located immediately downstream from the rotameter.

The temperature of the liquid was controlled by circulating water through the jacketed holding tank. It was found that the liquid temperatures never varied significantly from the 68°F calibration temperature.

Measurement of the Liquid Films

Many techniques have been used to measure the thickness of the liquid films of annular flow. The United Kingdom Atomic Energy Authority research group at Harwell, England, has reported on several of these methods (Hewitt, King and Lovegrove; Hewitt and Lovegrove (1962); Hewitt, Lovegrove, and Nicholls (1964); Hewitt and Nicholls; Hewitt and Lovegrove (1969b); Hewitt and Roberts (1969); and Collier

and Hewitt (1964)). B. Scott has reviewed numerous techniques and has given a brief description of each. For other methods the reader is referred to Charvonia (1961) and Brown and Govier (1961). In the present study, high-speed motion picture photography was utilized to measure the characteristics of the liquid films.

The photographs were taken at a section 53.5 inches above the lower static pressure tap. The unit of the center tube which was to be photographed was made of acrylic plastic. It was found that the plastic tube effected much sharper film profiles than did the solid stainless steel rod; the latter caused extensive light scattering and reflection. Because the plastic rod allowed some light to pass through, reflection was not a problem.

A Fastax (model WF14S) high-speed 16mm camera, manufactured by the Revere-Wollensak Division of the Minnesota Mining and Manufacturing Company, was used in this study. The operating speed of the camera was controlled by regulating the voltage applied to the camera drive motors. An external control circuit called "Goose" served to achieve this voltage regulation. Manufactured by the Industrial Timer Corporation, the "Goose" control unit used (model J-515) was made specifically for Fastax cameras and allowed for film speeds of 1800 to 7000 frames/sec. Such high film velocities could thus be obtained without tearing the film during the starting transient.

It should be noted that setting a particular voltage on the "Goose" is not useful for measuring the exact film speed since the camera motor accelerates through virtually the entire run (most runs lasting one to three seconds). Because the film cannot be properly analyzed without the experimenter knowing the exact film speed during the duration of each run, time marks were exposed on the film edge at a known frequency. The timing light system will be described below.

All motion picture photography was carried out with the aid of a single 150 watt photo spotlight which backlighted the subject. It gave a sharp outline of either the air-water interface or the inner tube - wall interface, depending upon which was being photographed.

A two-inch extension tube was used in conjunction with a 50 mm, f/2, Wollensak Fastax Raptar lens. This lens system allowed for a five-inch focusing distance.

Two chromel wires ($.0396 \pm .0002$ inch diameter) were implanted in the column in such a manner that they protruded into the image field of the camera and could be used as reference distances to aid in film analysis. By photographing the wires and column when no liquid was flowing, the distance from the wall to the wires could be determined (this was approximately 1/8-inch). Once the liquid film was flowing, the wall could no longer be seen; therefore, the initial measurement was necessary for film analysis.

Two film types were necessary to cover the entire range of film speeds required; Plus-X 7276, ASA 40, and Tri-X 7278, ASA 160, were used. Both were double-perforated, 16 mm, black and white reversal films made by Kodak, and were used in 100 foot rolls. The film was processed by Evergreen Photo of Eugene, Oregon.

Appendix IV presents information about the camera settings used for all runs. In addition, the photographic technique used is briefly explained.

The analysis of the photographic film was extremely tedious and involved over 100 man-hours of work. Each roll of film (a total of 18 rolls were taken) was analyzed to find the average values for film thickness, wavelength, and celerity.

A time reference was necessary for film analysis and was provided by a $\frac{1}{2}$ watt Xenon light mounted within the camera housing, the terminals of which were connected to a 60 cycle a-c line. As a result, the photographic film was exposed on one edge every $1/120$ of a second. By counting the number of wave crests in a given period of time measured by the timing marks, the wave frequency was obtained. By counting the number of wave crests existing in a given distance of film, the wavelength could be found. Once the wavelength and frequency were determined, the wave celerity could be calculated. It should be pointed out that the wave crests were not always easy to find due to

the irregularity of the liquid surface and the differing relative wave speeds.

The average thickness of the liquid films were found by tracing single frame projections onto some previously weighed graph paper (calibrated to $\pm 2\%$ variation in area density). The projections were chosen at random to ensure a fair sampling of the profiles. The tracings were then cut out and weighed on a precision beam-balance. By knowing the length of the paper strips and the area from the weight determination, one could determine the average film thickness.

All photographic analysis was carried out with the help of a Bell and Howell 16 mm projector, Type D-1B. The projector had several features which made it invaluable for film analysis; namely, single frame projection capabilities, forward and reverse motion, manual operation capabilities, a frame counter, and variable speed control.

DISCUSSION OF RESULTS

Single-Phase Flow

In order to insure that the present experimental apparatus would yield valid two-phase flow data, it was necessary to take data for air flowing alone in the annulus and compare the resulting values with known single-phase correlations. The pressure loss, dP/dx , shear stress at the outer wall, τ_2 , and the radius of maximum velocity, r_m , were measured and compared to the values predicted by the empirical expressions previously presented.

Friction factors were calculated from the pressure loss data using Equation (8) and plotted in Figure 7a against the Reynolds number, Re , defined by Equation (9). The data cover a range $7 \times 10^4 < Re < 2 \times 10^5$ and have been presented along with the curves generated by relationships given by Knudsen and Katz, Equation (7), Brighton and Jones, Equation (14), and Meter and Bird, Equation (12). The present values lie very slightly below the Brighton and Jones curve.

Using the expressions presented by Rothfus and co-workers in Equations (1) and (2), and using the experimentally determined value for r_m , the values for f_2 and Re_2 can be calculated. These values are plotted in Figure 7b along with the Nikuradse smooth tube correlation (see Knudsen and Katz, p. 172). At the same time, τ_2 is calculated using Equation (4); this, in fact, is the method of calibrating

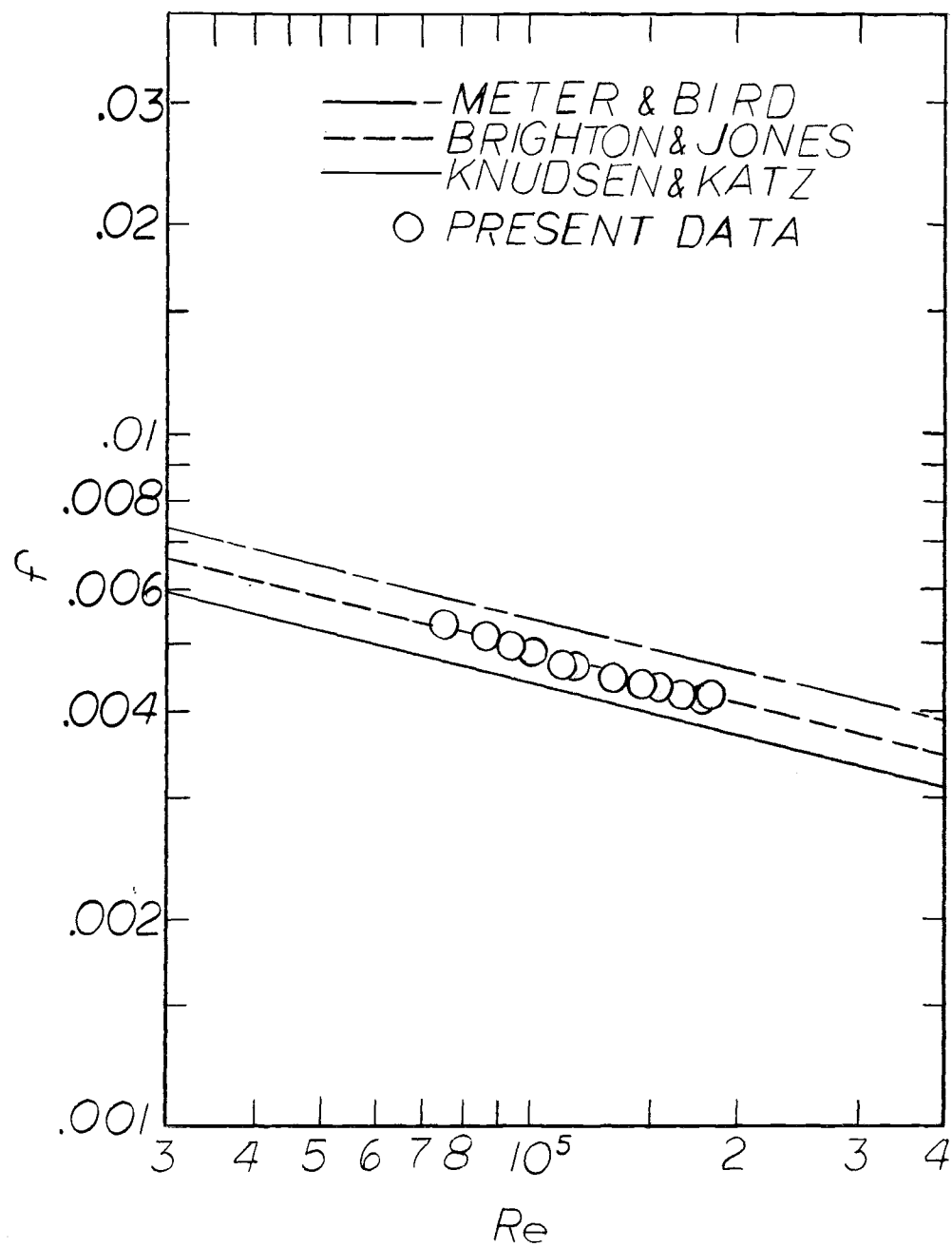


Figure 7a. Friction factor - Reynolds number for air data.

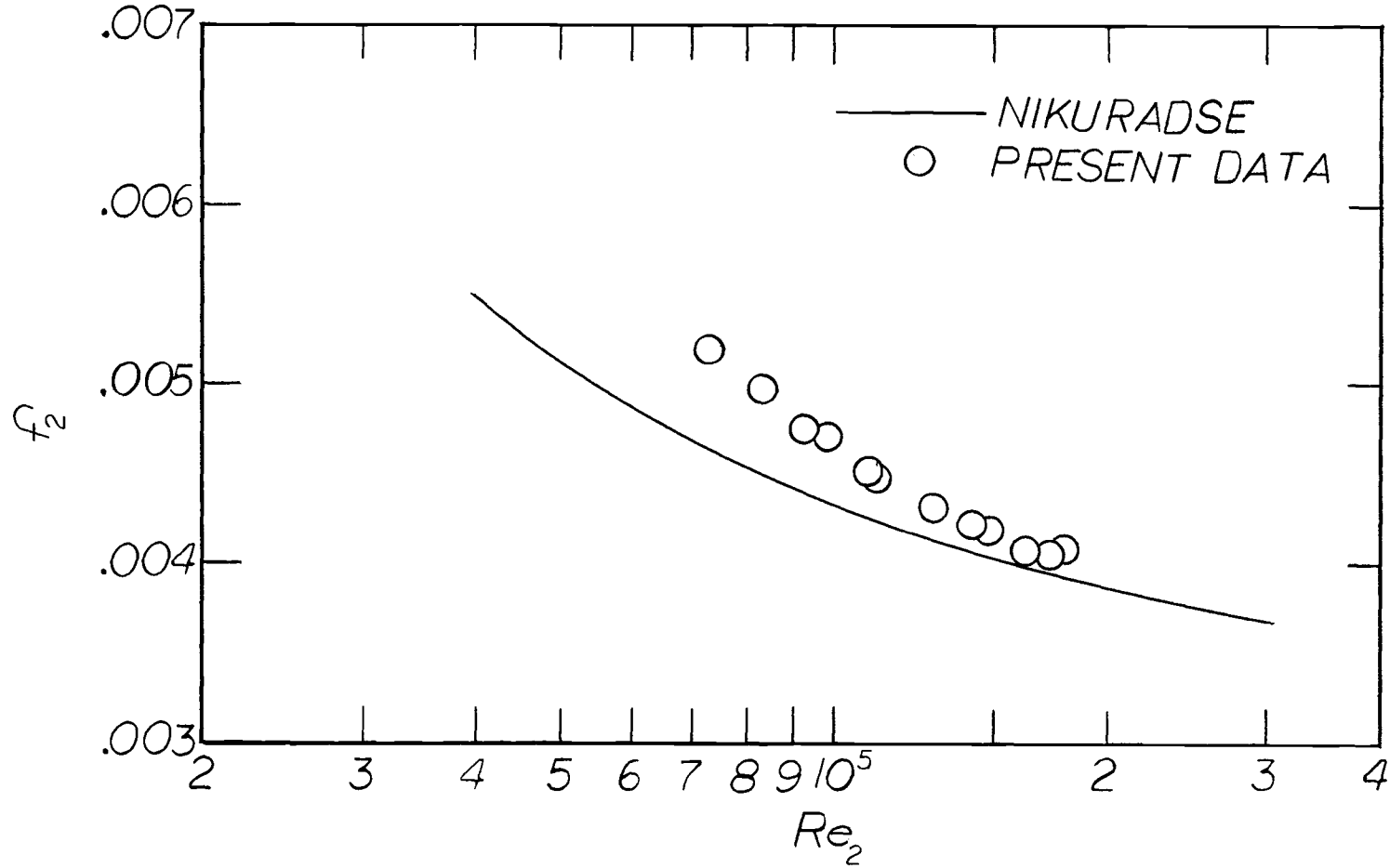


Figure 7b. Friction factor - Reynolds number for air data.

the Preston tube on the outer wall (see Appendix III). From Figure 6 it is observed that the annular values are 2% to 13% higher than values for the smooth tube. This agrees with Brighton and Jones, who reported annular friction factors 1% to 10% larger than the Nikuradse smooth tube values.

The experimental values of f_2 and Re_2 in the present system were correlated with the aid of *STEP, (Yates, 1969) which is a step-wise multiple linear regression analysis program written by the staff at the Oregon State University Statistics Department. This program allows one to enter and remove any number of independent variables; further, the resulting significance of each variable on the correlation is given by a correlation coefficient. The following correlation was found: ($R = .985$)

$$f_2 = 0.083 Re_2^{-.25} \quad (84)$$

This expression predicts values 6% greater than does Equation (6) given by Knudsen (1962).

The radius of maximum velocity was determined experimentally with the aid of a traversing pitot tube. The velocity was measured at several radii in the approximate vicinity of r_m . A least squares fit of the velocity vs. radius data was obtained by employing successive polynomials of order two and higher. The standard deviation about the regression line was examined for each polynomial fit and the order

which yielded the smallest standard deviation was chosen as the "best" fit. Since the point of maximum velocity is the radius at which the velocity gradient goes to zero, r_m could be found by taking the derivative of the chosen polynomial, setting to zero, and solving for r_m . The values for r_m showed no significant trend as the air Reynolds number was increased. The average value for r_m was found to be 0.892 in. ($\pm 5\%$). Table 1 compares this experimental value with the values predicted by the correlations for r_m given previously. The agreement with all of the correlations is quite good.

The pressure drop and outer wall shear stress are presented later in a subsequent section along with the air-liquid data. Both are linear functions of the air flow rate over the range of the data covered in this study.

It is concluded that the experimental apparatus and measuring equipment are predicting pressure drops, radii of maximum velocity, and the friction factors based upon these experimental values, in close agreement to published results.

Table 1. Predicted values of radius of maximum velocity.

| Correlation | r_m in | % Deviation |
|--------------------------------|-------------|-------------|
| Experimental Value | .892 | ----- |
| Kays and Leung Eq. (13) | .907 | + 1.6% |
| Rothfus <u>et al.</u> Eq. (18) | .901 | + 1.0% |
| Clump and Kwasnoski Eq. (19) | .913 | + 2.3% |

Two-Phase Flow Pressure Drop

The pressure drop was measured at a number of air and liquid flow rates for each liquid. For water and Shellsolv, the liquid flow rates used were 0.305, 0.59, and 0.755 lb_m/min ; for the light oil, 0.10 lb_m/min ; and for the iso-octyl alcohol, 0.10 and 0.305 lb_m/min . The pressure drops are plotted against the mass flow rate of the air in Figure 8, 9, 10, and 11. Each figure compares the two-phase pressure drop for a particular liquid flow rate with that for air alone. As expected, for each liquid, as the liquid flow rate is increased the pressure drop increases. Table 2 summarizes the results shown in the four figures and gives the approximate percent increase in pressure drop above that of air for each liquid flow rate. The pressure drop increases linearly with increasing gas flow rate over most of the data range. At the low air flow rates, the data appear to deviate from this linear trend. Sutey, among others, has shown that, at low air flow rates, the pressure drop curve appears to go through a minimum. This minimum in pressure drop is reported to correspond to the point of incipient downflow in the liquid film adjacent to the wall. The air-liquid interface is extremely rough and unstable under the conditions of very low air flow rate and liquid downflow. Thus, it is argued, more energy must be transferred from the gas to the liquid to maintain the climbing film.

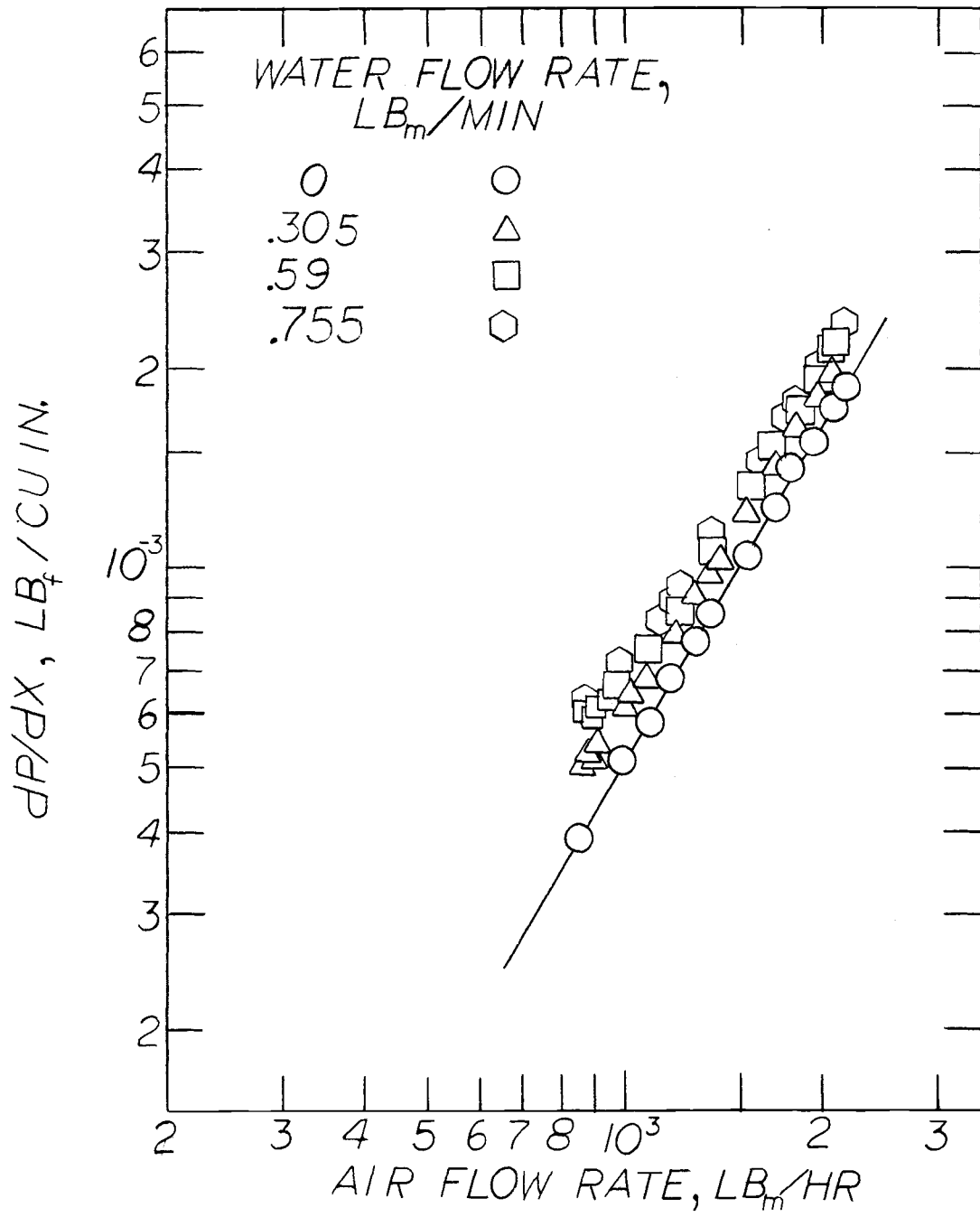


Figure 8. Pressure drop vs. air flow rate - water.

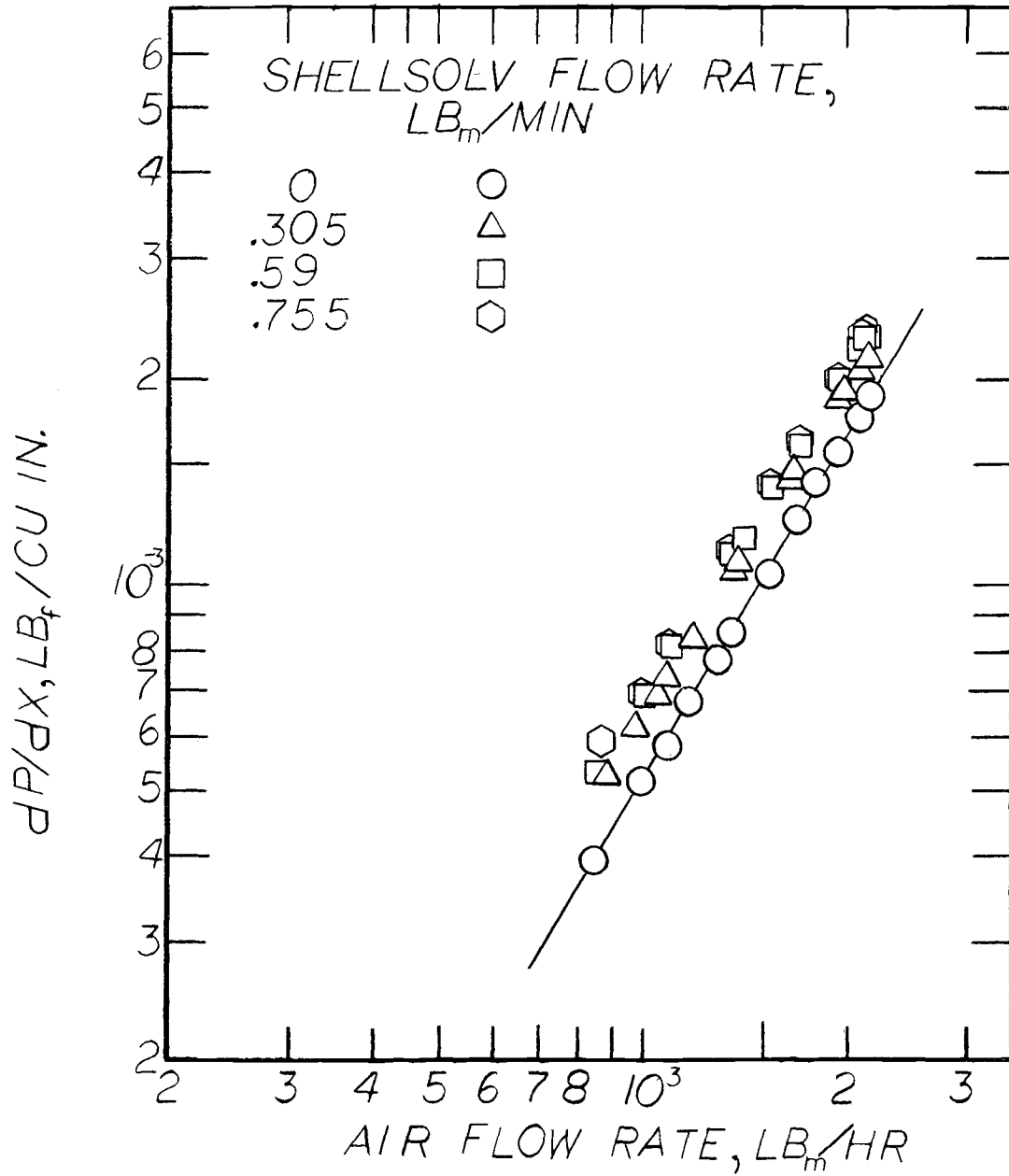


Figure 9. Pressure drop vs. air flow rate - Shellsolv.

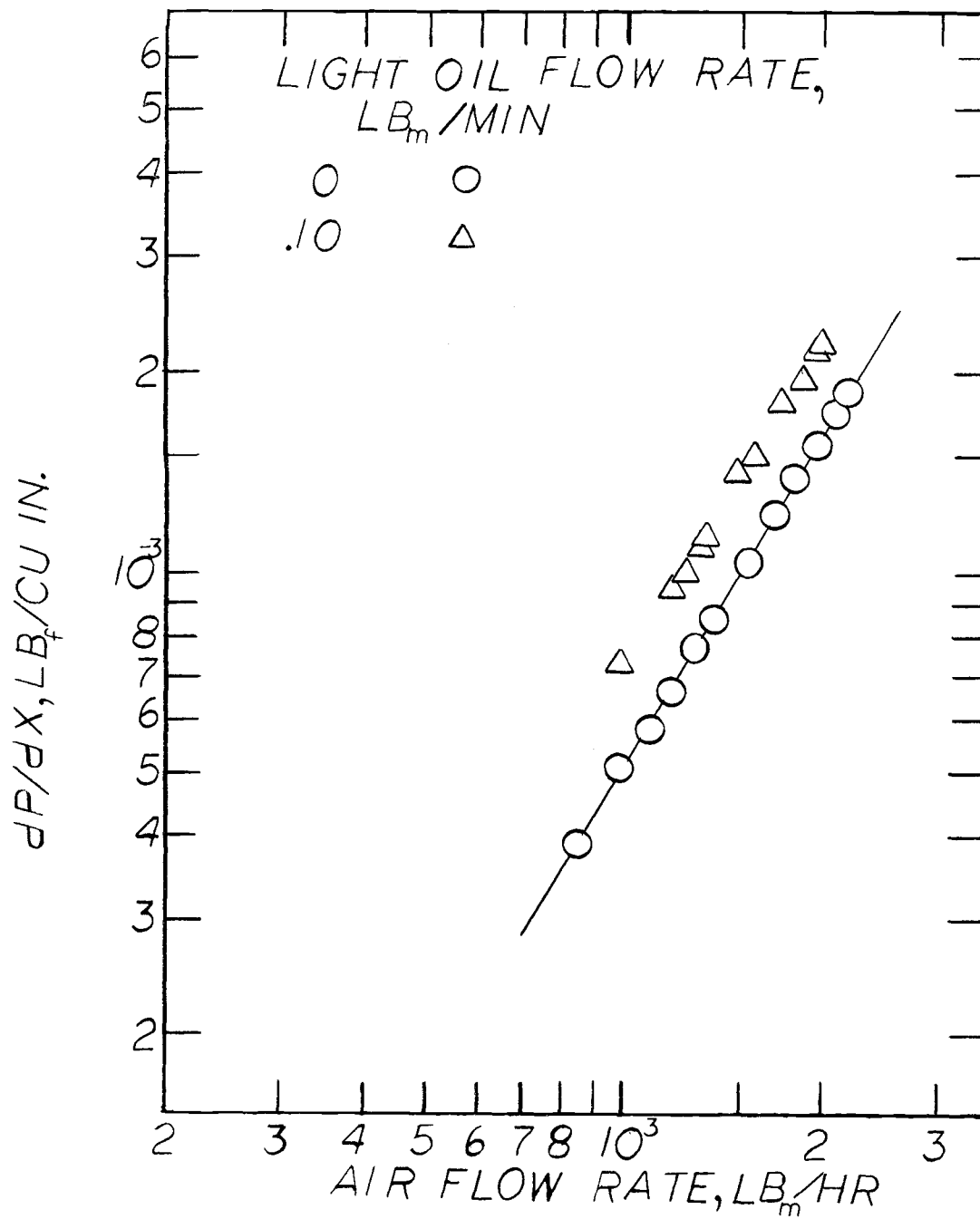


Figure 10. Pressure drop vs. air flow rate - light oil.

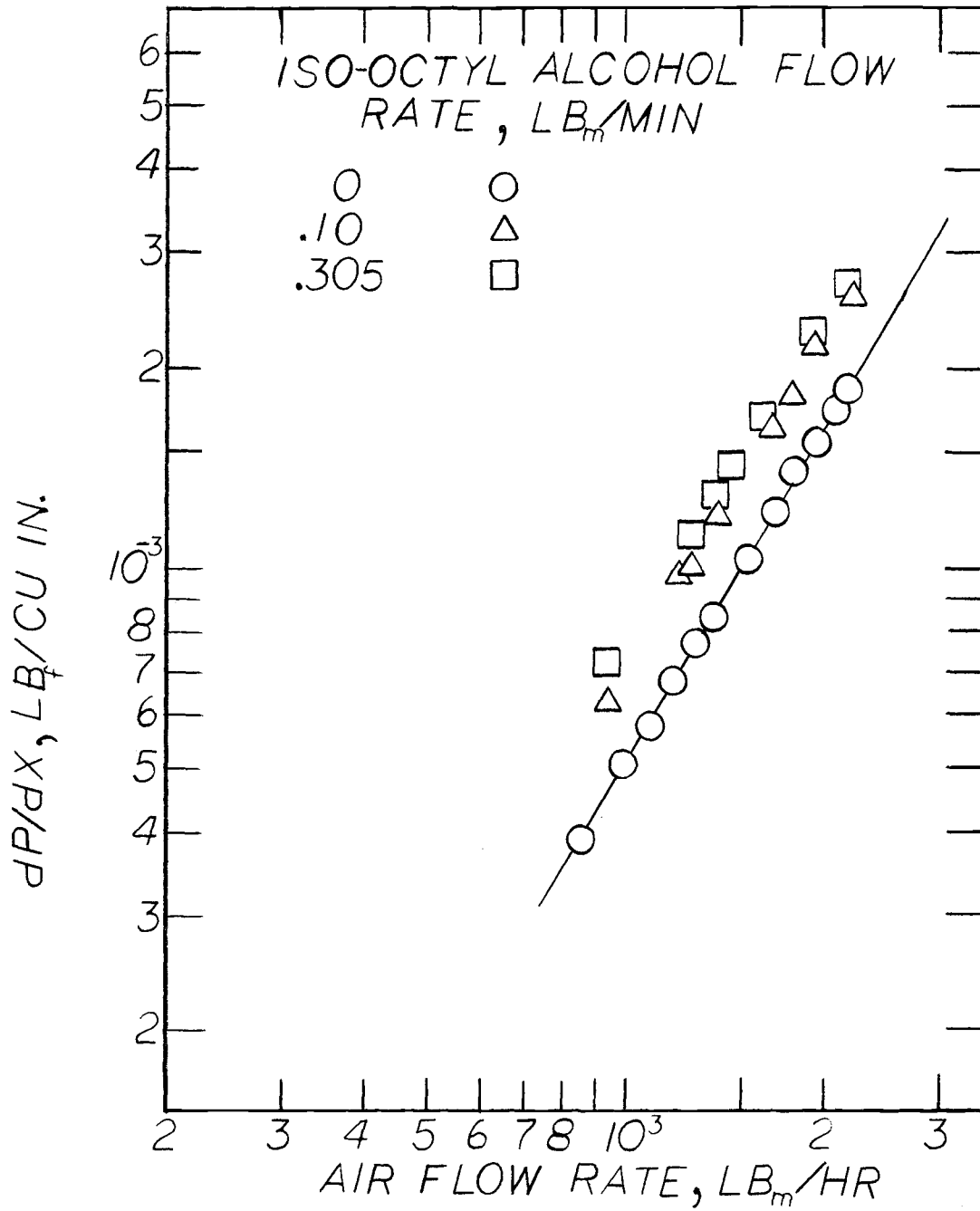


Figure 11. Pressure drop vs. air flow rate - iso-octyl alcohol.

Table 2. Comparison of single- and two-phase pressure drop and friction factor.

| Liquid | Liquid Rate lb _m /min. | % Increase above single-phase pressure drop | % Increase above single-phase friction factor |
|----------------|--------------------------------------|---|---|
| Water | .305 | 15 | 10 |
| Water | .59 | 23 | 20 |
| Water | .755 | 32 | 24 |
| Shellsolv | .305 | 20 | 16 |
| Shellsolv | .59 | 27 | 24 |
| Shellsolv | .755 | 31 | 27 |
| Light Oil | .10 | 34 | 30 |
| Iso-Octyl Alc. | .10 | 34 | 29 |
| Iso-Octyl Alc. | .305 | 48 | 41 |

It is observed that the data points tend to converge slightly at the higher air flow rates indicating that the two-phase pressure losses are approaching the single-phase pressure losses. This is expected since the liquid film is thinner at the higher air flow rates than at the lower air flow rates. Hartley and Roberts reasoned that if the liquid film is thinner than the gas boundary layer thickness, then there is no change in the pressure gradient from that of a gas flowing alone.

For the same liquid flow rate, the water and Shellsolv have essentially the same pressure drop. The light oil and the iso-octyl

alcohol also exhibit a similar pressure drop with the latter two showing considerably larger pressure drops than the former two. The water and Shellsolv have nearly the same density and viscosity, but water has three times the surface tension of Shellsolv. The oil and alcohol also have surface tensions about 1/3 that of water, are slightly less dense, but much more viscous. It would appear that the liquid surface tension has little effect on two-phase pressure drop in the climbing film regime. The liquid viscosity appears to have a significant effect on the pressure drop.

The pressure drop data can be presented in a different form by calculating friction factors as defined by Equation (9). These are shown for each liquid in Figures 12, 13, 14 and 15. In each figure, the friction factor at every liquid flow rate is given along with the single-phase air values. Table 2 lists the percent increase above the air data for each liquid flow rate. As expected, the curves show the same trends as the raw pressure drop data already presented. At the lower gas Reynolds numbers, the curves tend upward. This is the same region of incipient downflow and increased liquid entrainment which has been discussed elsewhere in this paper.

Shear Stress at the Outer Wall

The shear stress at the outer wall, τ_2 , is plotted vs. the air flow rate in Figures 16, 17, 18 and 19 (each figure shows values for a

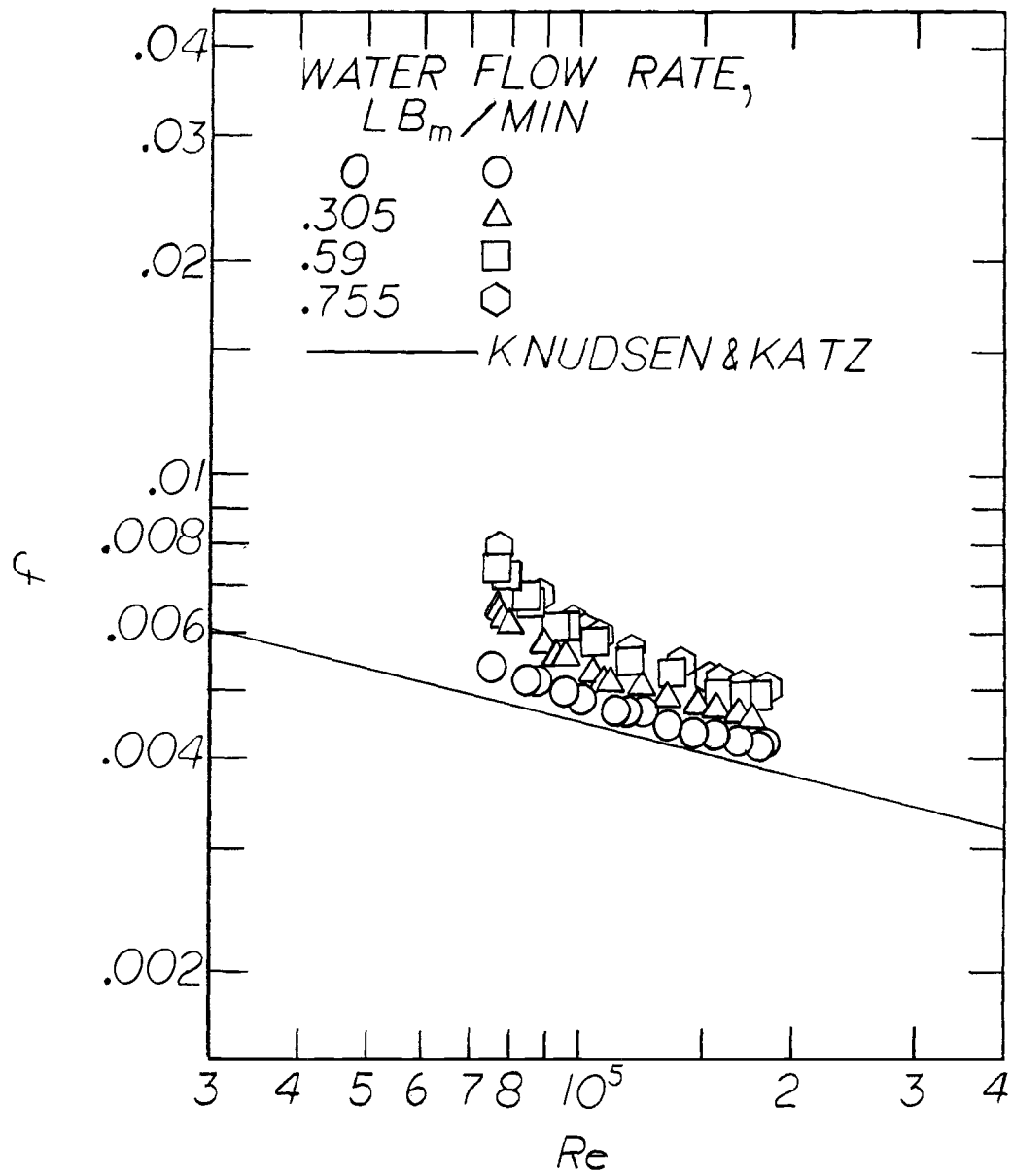


Figure 12. Friction factor vs. Reynolds number - water.

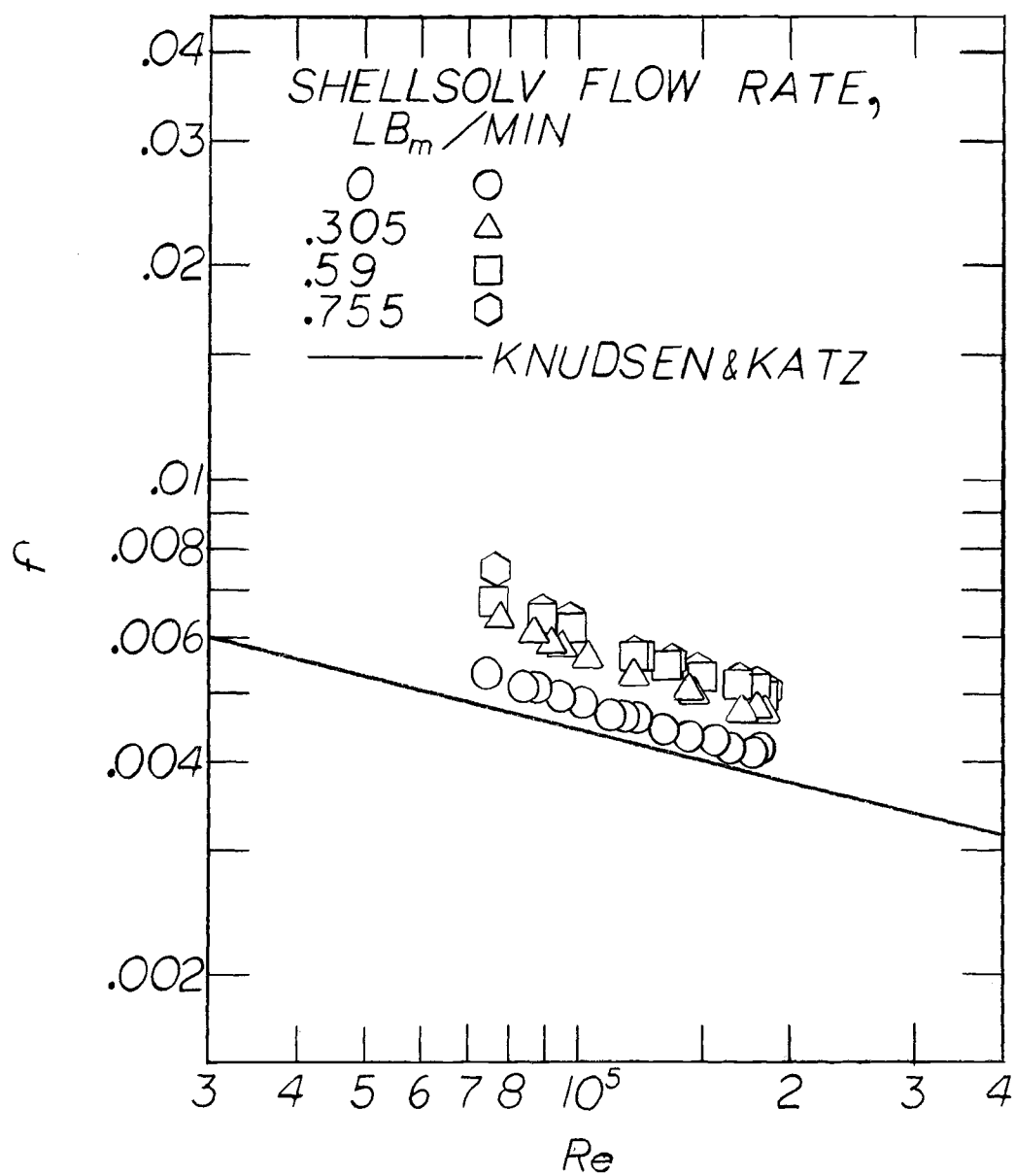


Figure 13. Friction factor vs. Reynolds number - ShellsoLV.

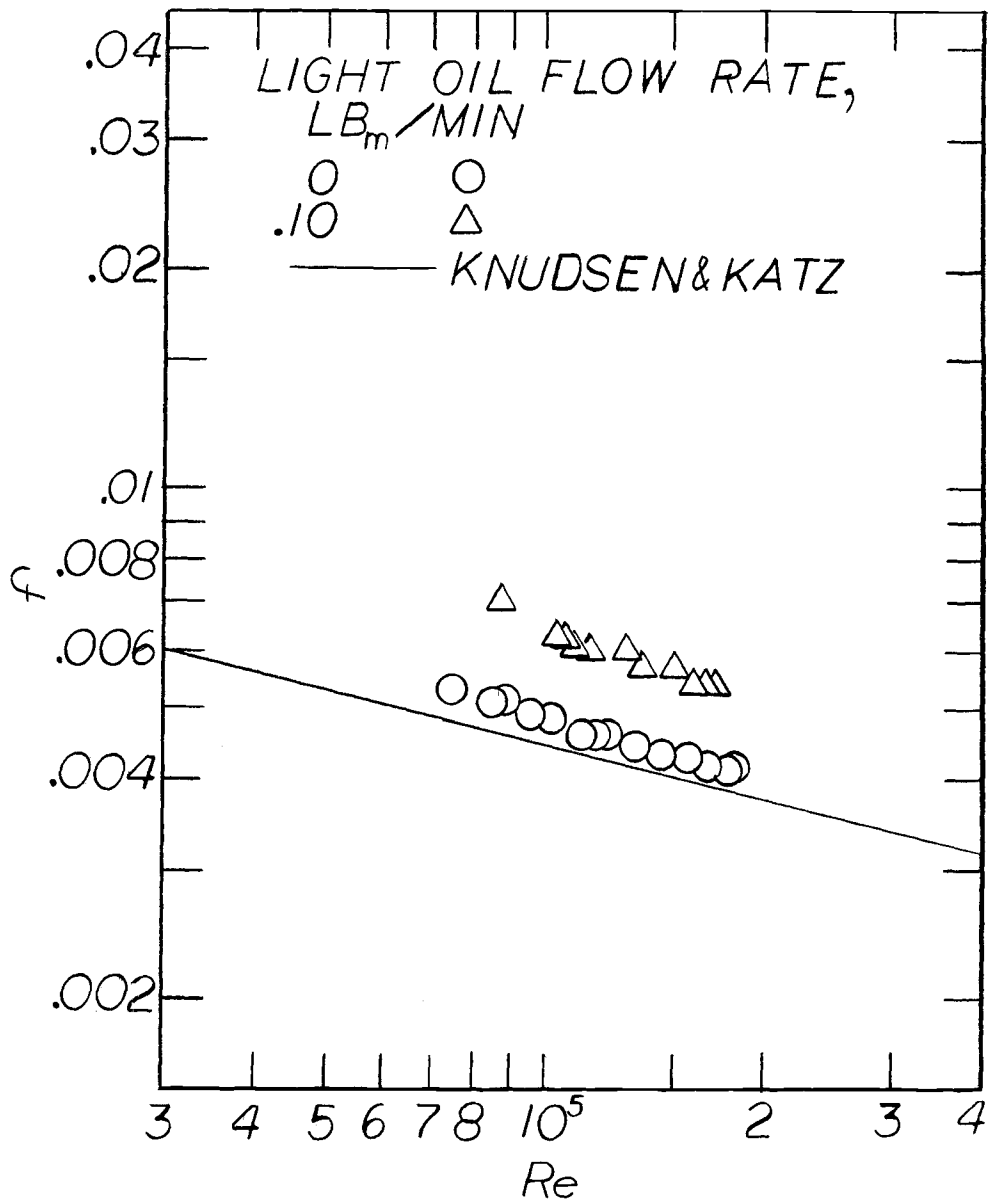


Figure 14. Friction factor vs. Reynolds number - light oil.

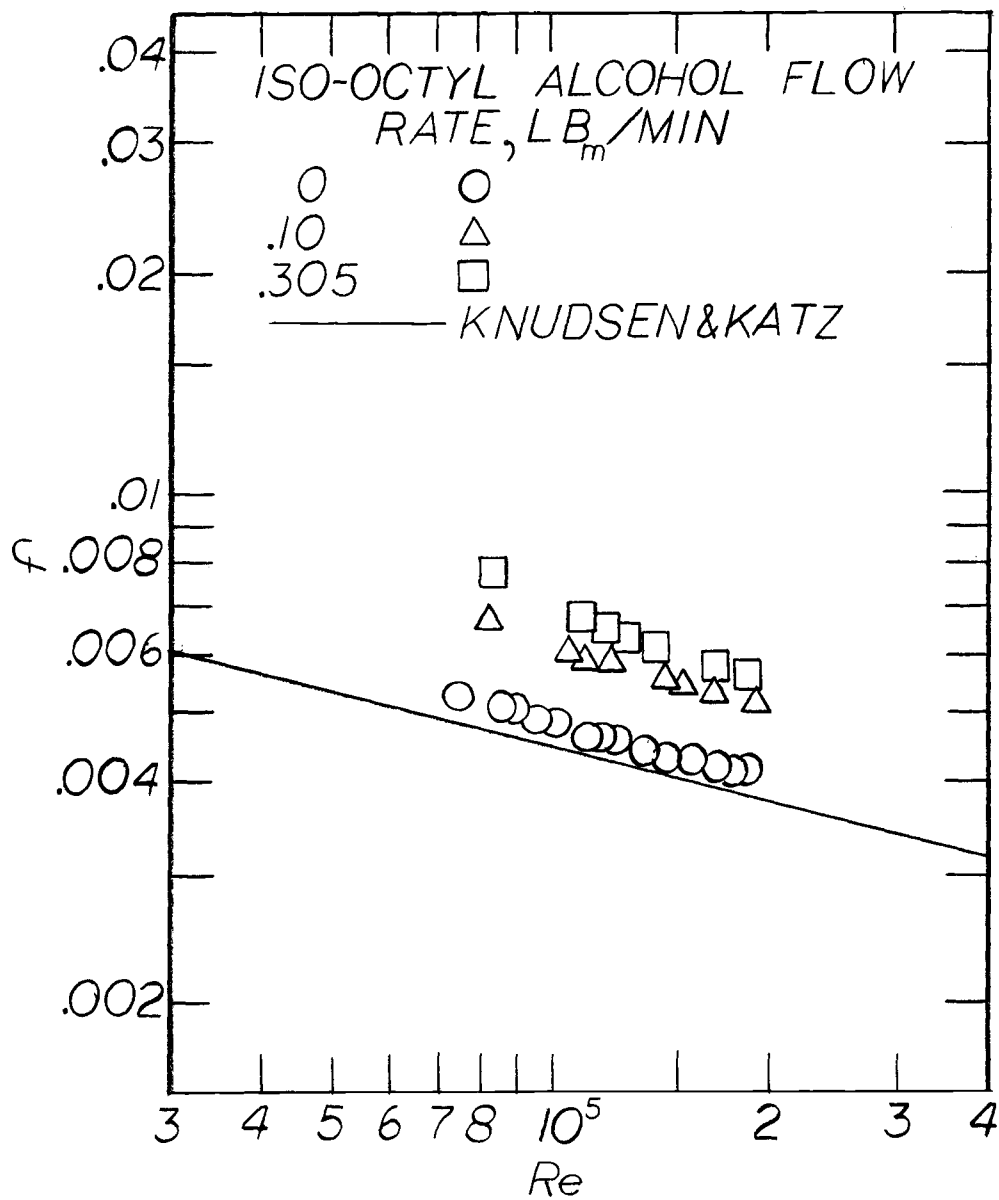


Figure 15. Friction factor vs. Reynolds number - iso-octyl alcohol.

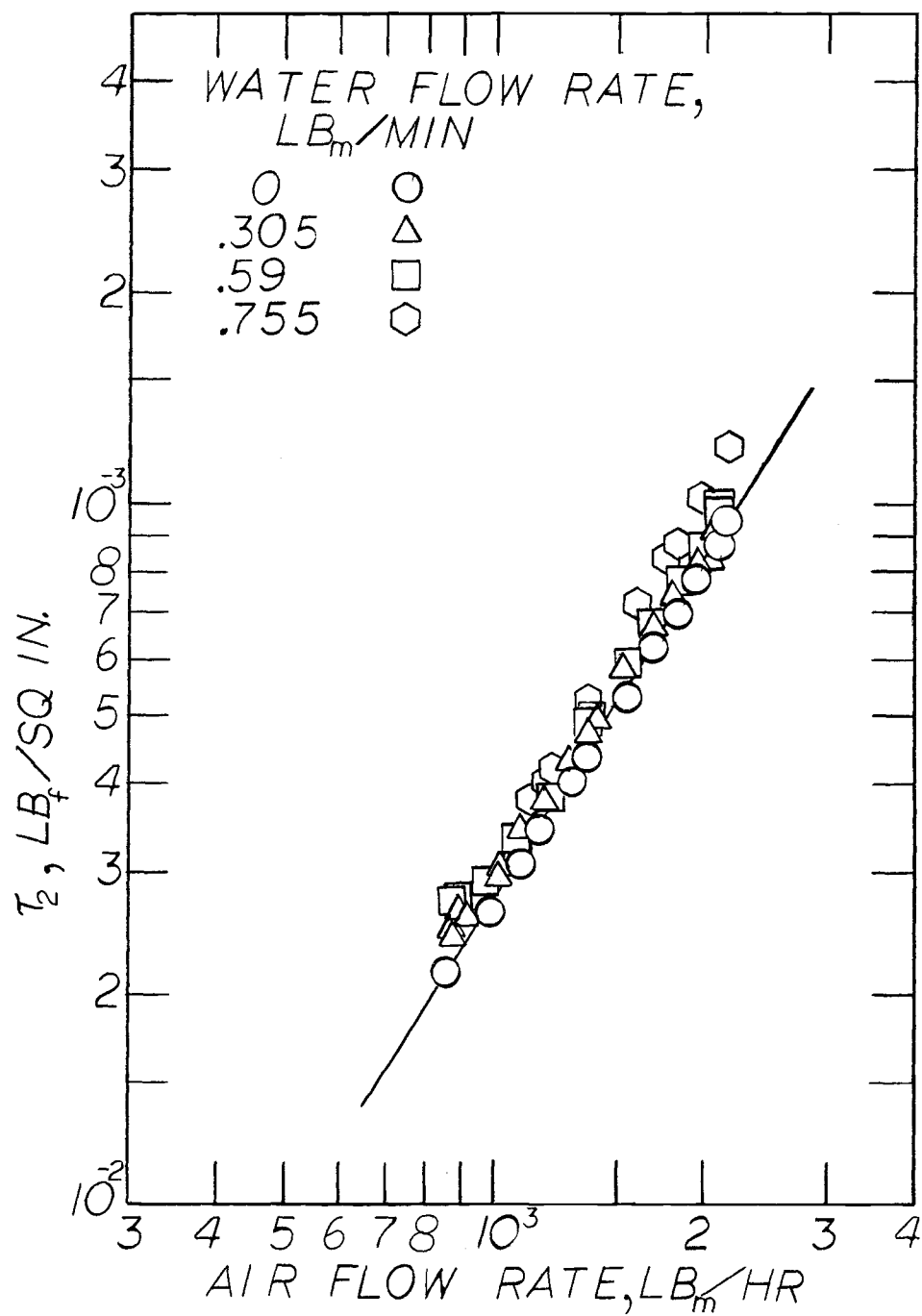


Figure 16. Shear stress at outer wall vs. air flow rate - water.

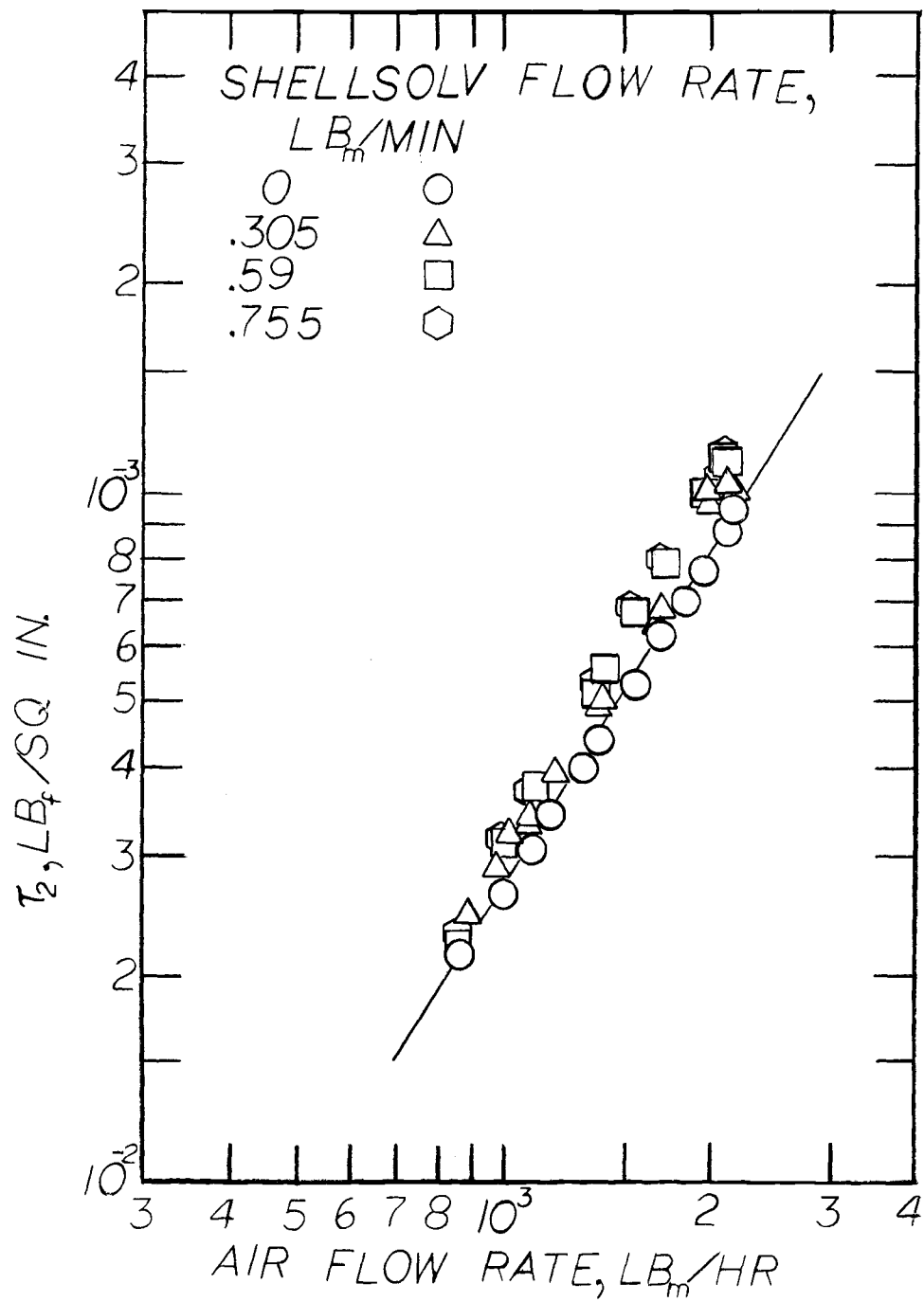


Figure 17. Shear stress at outer wall vs. air flow rate - Shellsolv.

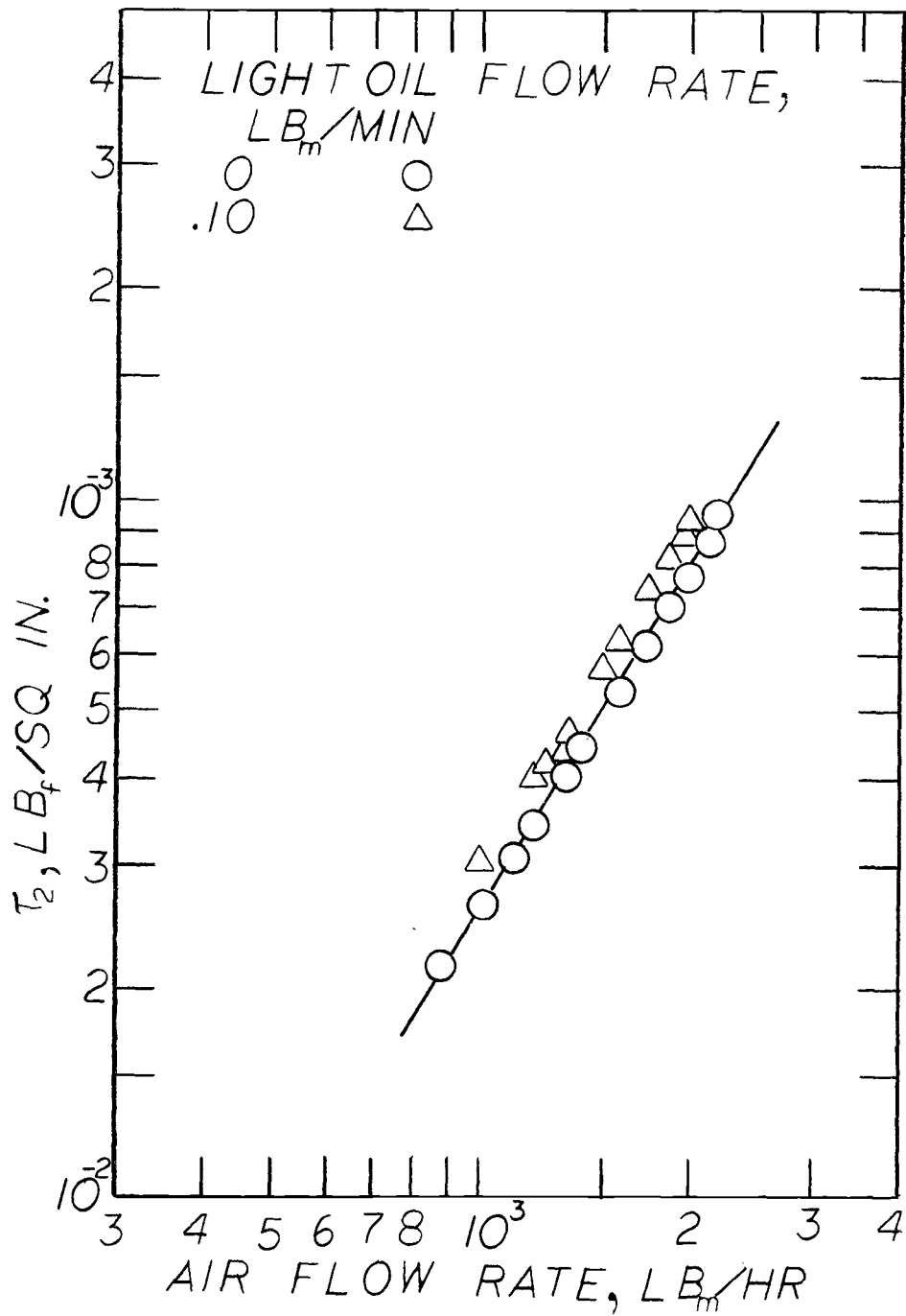


Figure 18. Shear stress at outer wall vs. air flow rate - light oil.

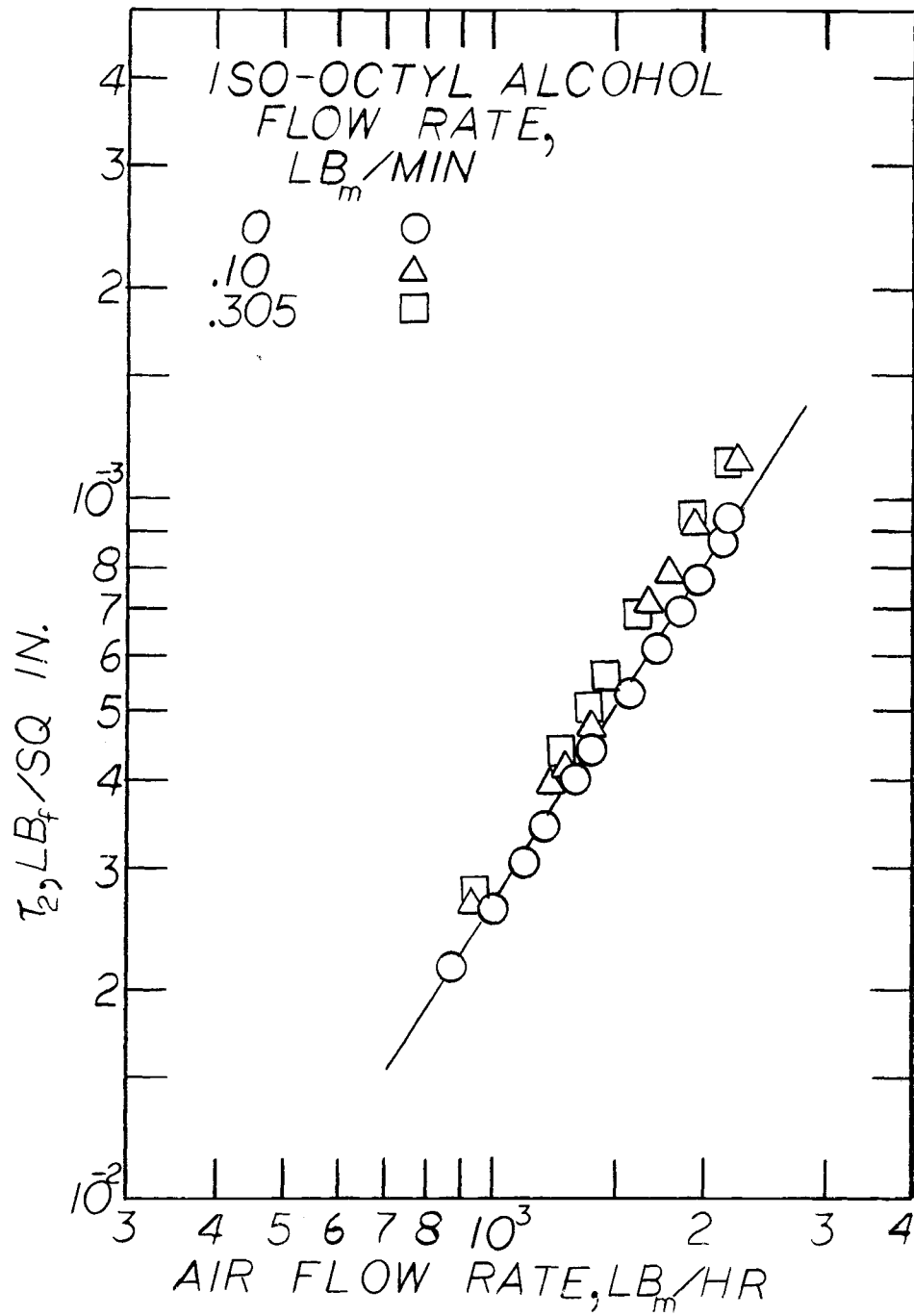


Figure 19. Shear stress at outer wall vs. air flow rate - iso-octyl alcohol.

different liquid). It can be seen from these figures that the two-phase values for τ_2 do not differ a great deal from the single-phase values (Kim's air-water data show deviations in τ_2 of magnitudes similar to those in the present study). The percent increase in the two-phase values of τ_2 above those for single-phase flow are given in Table 3.

It is interesting to note that the percent increases in the two-phase τ_2 values above the single-phase values are much smaller than the corresponding pressure drop increases given previously. This indicates that the region near the dry wall is relatively insensitive to the presence of a liquid film on the inner wall.

Whatever increases in two-phase values occur can probably be related to entrainment. At the higher liquid flow rates, liquid may be entrained, and the entrained liquid will impinge upon the outer wall, resulting in a rough wall effect. If the liquid droplets on the outer wall are of significant numbers, an increase in τ_2 will occur.

At high flow rates, water, having the highest surface tension and the lowest viscosity of the liquids, should exhibit the lowest degree of entrainment and, consequently, the lowest degree of impingement on the outer wall. In Figure 16, water does show the smallest deviation from the single-phase values of τ_2 . On the other hand, the higher viscosity, lower surface tension liquids should be more easily entrained and, in fact, these liquids show the largest deviations from

the single-phase curve. See Appendix V for further discussion of entrainment.

Table 3. Comparison of single- and two-phase outer wall shear stress.

| Liquid | Liquid flow rate lb_m/min | % Increase in τ_2 over single-phase values |
|-------------------|--|--|
| Water | .305 | 3.5 |
| Water | .59 | 6.5 |
| Water | .755 | 14 |
| Shellsolv | .305 | 6 |
| Shellsolv | .59 | 13.5 |
| Shellsolv | .755 | 16 |
| Light Oil | .10 | 12 |
| Iso-Octyl Alcohol | .10 | 8 |
| Iso-Octyl Alcohol | .305 | 15.5 |

In this study, however, no liquid entrainment was observed at the higher air flow rates. In addition, the liquid impinged on the outer dry wall only at the lower air flow rates.

Kim, as well as Ellis and Gay, showed that the two-phase velocity profile in the region near the dry wall was essentially the same as for single-phase flow. The present data tends to support this finding to some degree. If, in fact, the hydrodynamics in the region near the

dry wall remain unchanged, or change only slightly, when a climbing film is present on the inner wall, it is thus possible that the friction factor and Reynolds number given by Rothfus and co-workers and defined in Equations (1) and (2) could be used to correlate the data for τ_2 . The liquid on the inner core causes a rough wall condition, shifting the radius of maximum velocity toward the outer wall. At the same time, the presence of the climbing film also causes a greater pressure drop. Examining Equation (1)

$$f_2 = \frac{r_2^2 - r_m^2}{r_2 \rho U^2} \frac{-dP_f}{dx} \quad (1)$$

where $dP_f/dx = dP/dx + g\rho$, it can be seen that if r_m and dP/dx increase at the same time they will have an offsetting effect on the magnitude of f_2 .

In Figure 20, the plot of f_2 vs. Re_2 for all liquid data falls in a fairly narrow band. Upon observation, it appears that the data could be described by two straight lines. For $Re_2 < 8 \times 10^4$, the liquid was observed to be entrained and impinged on the outer wall. Liquid impinging on the outer wall should cause an increase in f_2 . This increase is observed in Figure 20.

Correlations were found for the data in Figure 20 using *STEP. For all of the data the following expression was found ($R = .957$):

$$f_2 = 0.454 Re_2^{-.396} \quad (85)$$

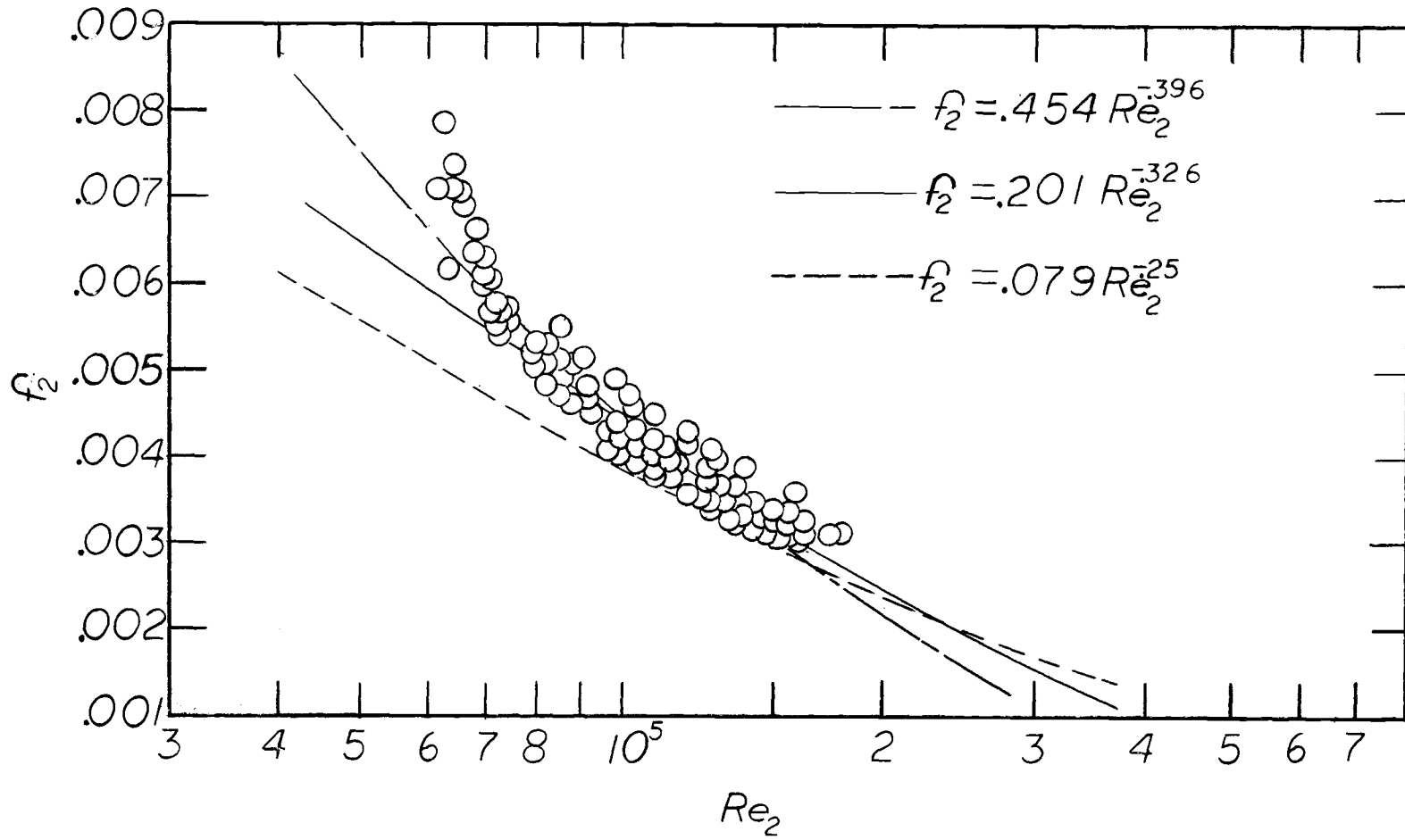


Figure 20. Two-phase friction factor, f_2 , vs. Reynolds number, Re_2 .

and for $Re_2 > 8 \times 10^4$, where the outer wall was observed to remain dry, it was found that ($R = .938$)

$$f_2 = 0.201 Re_2^{-.326} \quad (86)$$

The liquid properties were also inserted into the correlations in order to examine their effect on the correlation coefficient. Only the viscosity was found to have any effect on the correlation. For all the data it was found that ($R = .961$)

$$f_2 = 0.441 Re_2^{-.397} \left(\frac{\mu_L}{\mu_G}\right)^{.0093} \quad (87)$$

and for $Re_2 > 8 \times 10^4$ the following expression was obtained ($R = .959$):

$$f_2 = 0.174 Re_2^{-.320} \left(\frac{\mu_L}{\mu_G}\right)^{.014} \quad (88)$$

Although the liquid viscosity has an effect on the correlation, it is so slight that nothing conclusive can be said regarding its effect on f_2 .

It is interesting to note that, in the region for $Re_2 > 8 \times 10^4$, the friction factor varies approximately with $Re_2^{-.32}$. Recall that Hewitt used Equation (15)

$$f_k = .00070 + .0625 Re_k^{-.32} \quad (15)$$

(referred to earlier as the Koo Equation) to predict the friction factor at the outer wall. This expression was correlated from data for single-phase flow in an annulus with a smooth outer wall and an artificially roughened inner surface. Although the friction factor and Reynolds number defined in the Koo Equation are not exactly the same as in the present correlation, both are based on choosing the region between r_m and r_2 as the hydraulic flow region. In both correlations, the similar dependence of friction factor on Reynolds number implies that the case of an artificially roughened wall and that of a liquid flowing as a film on the inner wall are similar.

The use of friction factors of the type defined by Rothfus and co-workers, as well as those of the type serving as a basis for the Koo Equation, necessitates either the experimental determination of r_m or the prediction of r_m with the aid of correlations. Both methods of determining r_m are represented in the next section.

Radius at the Point of Maximum Velocity

The radius at the point of maximum velocity was experimentally determined for each liquid and air flow rate. The same technique described previously for determining r_m with air flowing alone in the annulus was employed when the liquid film was climbing on the inner wall.

For a constant liquid flow rate the value for r_m showed no significant trend with a change in air flow rate. Hence, for each liquid flow rate studied, the values of r_m obtained at each air flow rate were averaged to give an average value over the range of air flows investigated. Figure 21 shows the values of y_m ($\pm 5\%$), the distance from the inner wall to the point of maximum velocity ($y_m = r_m - r_l$), plotted against the liquid flow rate.

The data show that as the liquid flow rate increases, y_m increases. The Shellsolv and the water differ in surface tension by a factor of three, yet there is only a slight change in y_m between the two liquids. It is apparent, therefore, that y_m has little dependence on the surface tension. The liquid viscosity, however, does seem important. For a given flow rate, the most viscous liquid exhibits the highest values for y_m .

An empirical correlation was sought for y_m as a function of the liquid flow rate and viscosity. For convenience, a dimensionless correlation was attempted and the following variables used: (1) a dimensionless distance from the outer wall

$$y^* = \frac{y_{MTP} - y_{MAIR}}{y_{MAIR}} \quad (89)$$

where y_{MTP} and y_{MAIR} are two-phase and single-phase values for y_m , respectively, (2) a liquid Reynolds number of the type used in

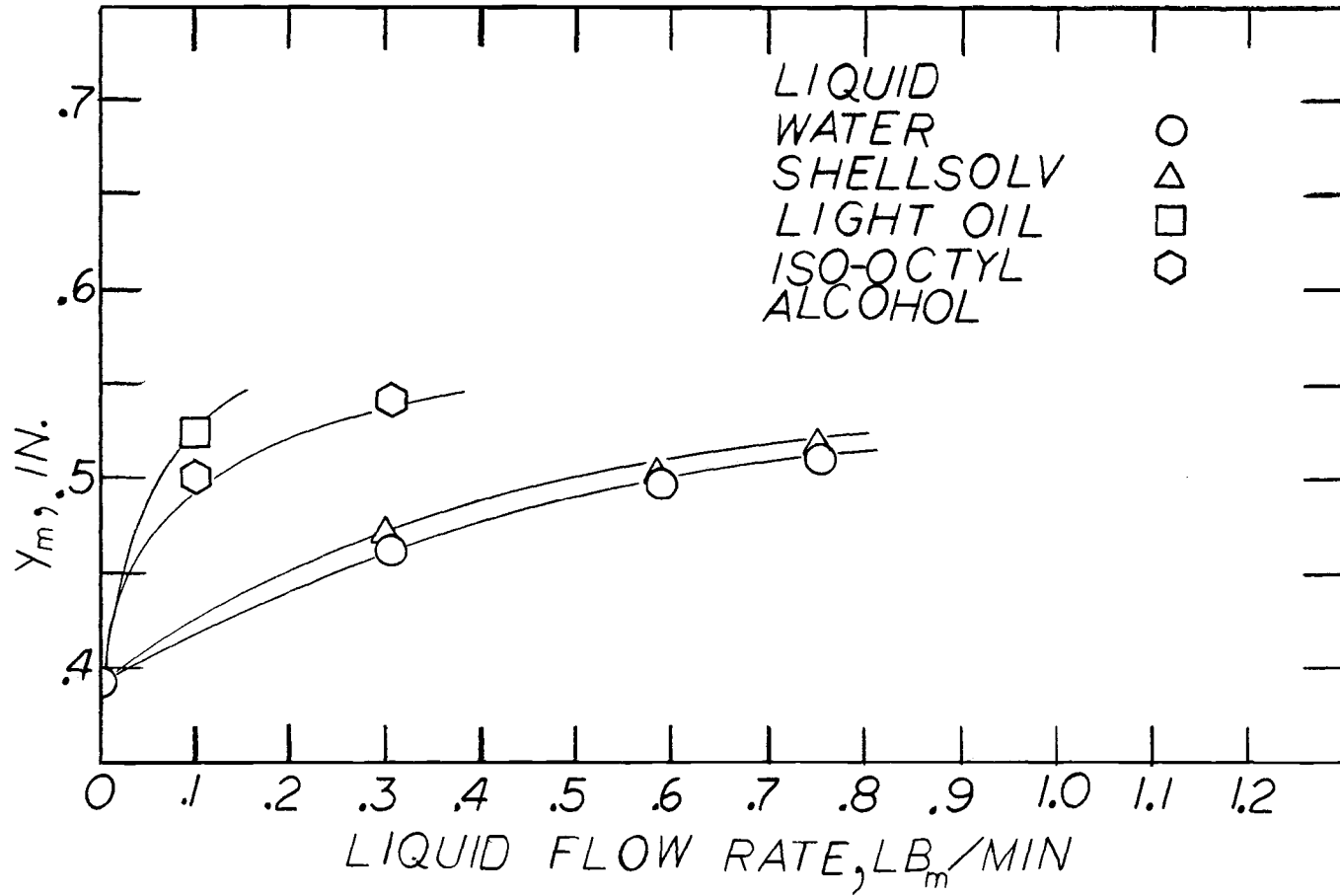


Figure 21. Radius of maximum velocity vs. liquid flow rate.

defining film flow

$$\text{Re}_L = \frac{4 \Gamma_L}{\mu} \quad (90)$$

where Γ_L is the mass liquid flow rate per unit of wetted perimeter, and (3) a dimensionless viscosity,

$$\mu^* = \frac{\mu_L}{\mu_G} \quad (91)$$

Using *STEP, a correlation was sought for

$$y^* = y^*(\text{Re}_L, \mu^*) \quad (92)$$

and was found as ($R = .9996$)

$$y^* = 0.01 \text{Re}_L^{.246} \mu^{*.48} \quad (93)$$

Figure 22 plots this regression line with the data to show the scatter about the line.

This final expression is probably not general since the radius ratio, r^* , is undoubtedly a significant variable in any correlation attempting to predict r_m . More data at different values of r^* are necessary before a general correlation can be found.

However, for the present system, the above correlation is extremely valuable. Ability to predict r_m permits the investigator to determine the shear stresses and the film characteristics.

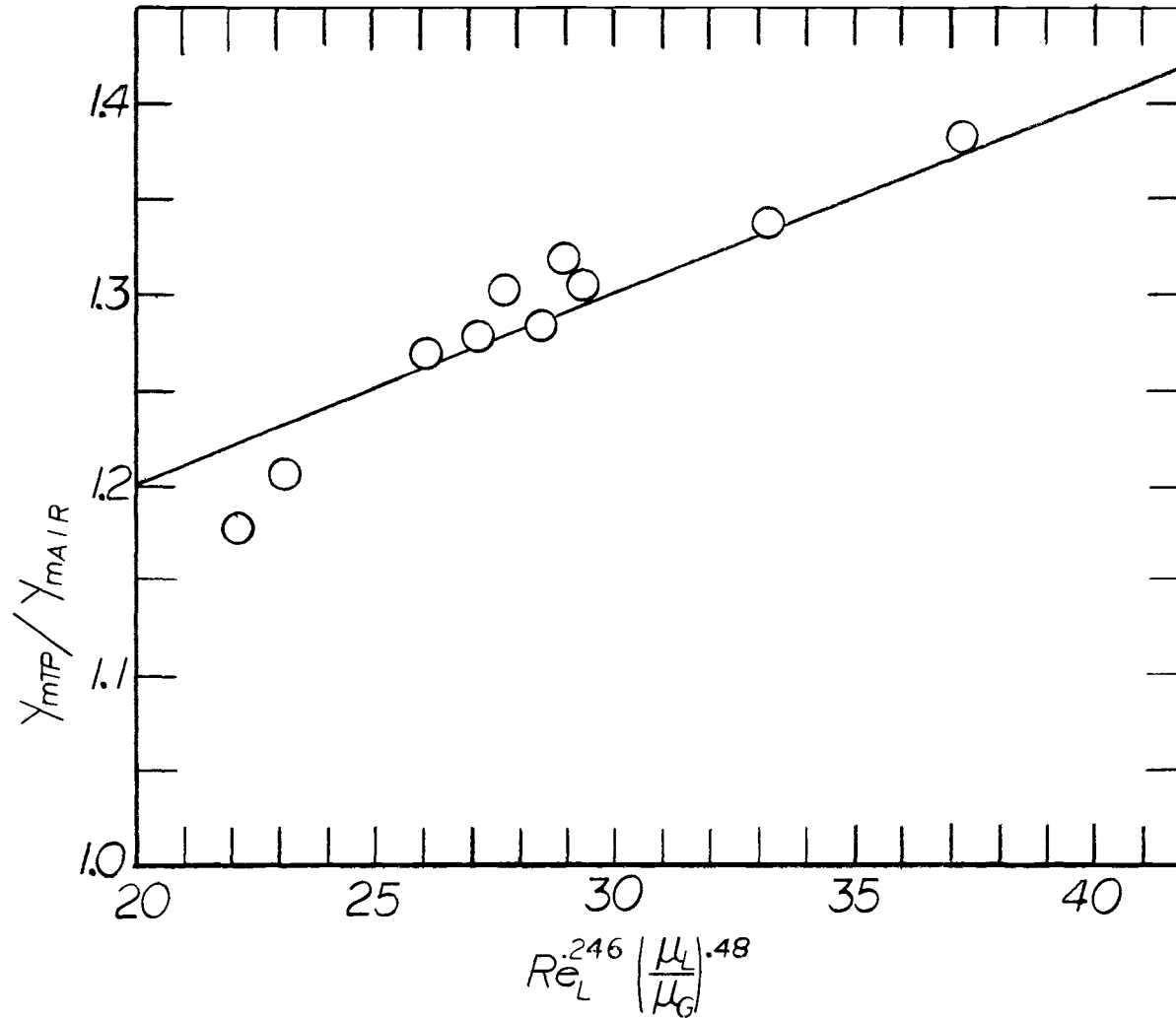


Figure 22. Correlation for radius of maximum velocity.

Two-Phase Pressure Drop Correlations

The two-phase pressure drop data were used to evaluate the comparative accuracy of the following three pressure drop correlations:

(1) Orkiszewski's correlation for vertical two-phase flow, (2) the Lockhart-Martinelli correlation derived for horizontal flow, and (3) a modified Martinelli correlation for vertical flow presented by Wallis (1966).

Orkiszewski presented four different sets of equations, each corresponding to a particular flow regime in vertical flow. In addition, he gave parameters for determining the flow regime. The flow-regime criterion of Orkiszewski predicts that the regime of the present study is the annular-mist regime.

In the annular-mist flow regime, a friction pressure loss term, τ_f , is defined by Orkiszewski as

$$\tau_f = \frac{f_{TP} \rho_G U_{GS}^2}{2g_c D} \quad (94)$$

where f_{TP} is a two-phase friction factor, U_{GS} the superficial gas velocity in the duct, and D the hydraulic diameter of the duct. A Reynolds number, Re_{GS} (based on U_{GS}), and a corrective term designated as a relative roughness, ϵ/D , are used to find values for f_{TP} on a single-phase friction factor chart. A correlation based on σ , ρ_G , U_{GS} , and D is given to calculate ϵ/D . After determining f_{TP} , Equation (94) is used to find τ_f . The final step in the calculation

of pressure drop involves making a momentum balance on the vertically flowing mist. The momentum balance includes an approximation of the kinetic energy changes in the flow tube, the effect of frictional drag, and the losses due to gravity.

The pressure drops calculated using the Orkiszewski correlation for water at a liquid flow rate of $.305 \text{ lb}_m/\text{min}$ are compared with the experimental values in Figure 23. As can be seen, the predicted values are 250% to 400% larger than the experimental values. It would appear that the application of the annular-mist flow regime correlations are not applicable to the present data. This is reasonable since flow rates were maintained low enough so that entrainment was believed to be insignificant.

The second pressure drop correlation investigated was that of Lockhart and Martinelli. Hewitt, King and Lovegrove fit the $\Phi_G - \chi$ curves of Martinelli with a fifth-degree polynomial for various flow regimes. The polynomial for a turbulent gas phase and a viscous liquid phase which they derived was used in this analysis. The predicted and experimental values for pressure drop are given in Figures 24, 25 and 26. In Figure 24 the air-water data are in excellent agreement with the predicted values; the maximum deviation ranging from -6% to +3%. Kim also found that the Martinelli correlation agreed well with his pressure drop data for air-water climbing film flow. Figure 25, for the Shellsolv data, and Figure 26, giving the light oil and

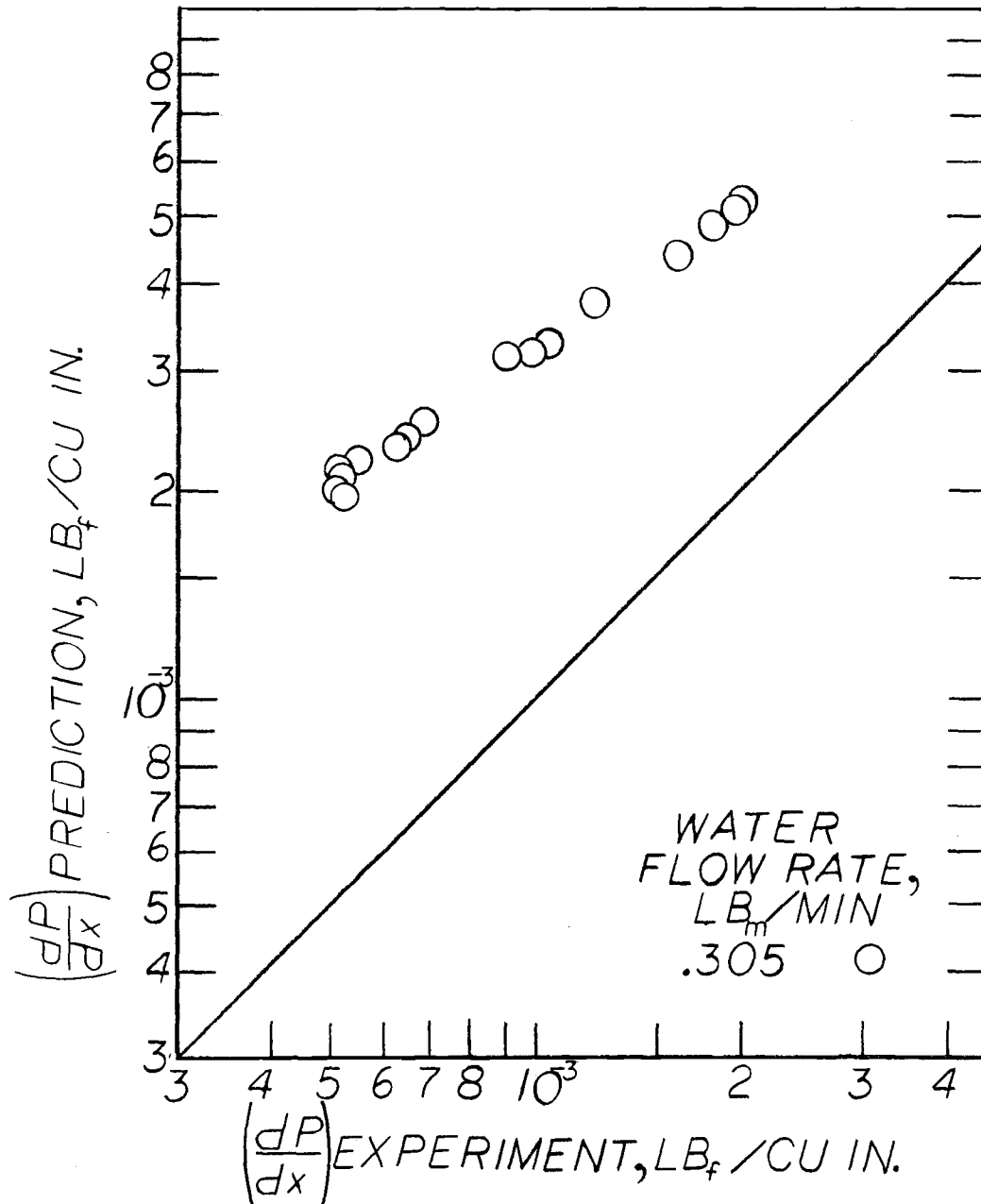


Figure 23. Orkiszewski pressure drop correlation - water.

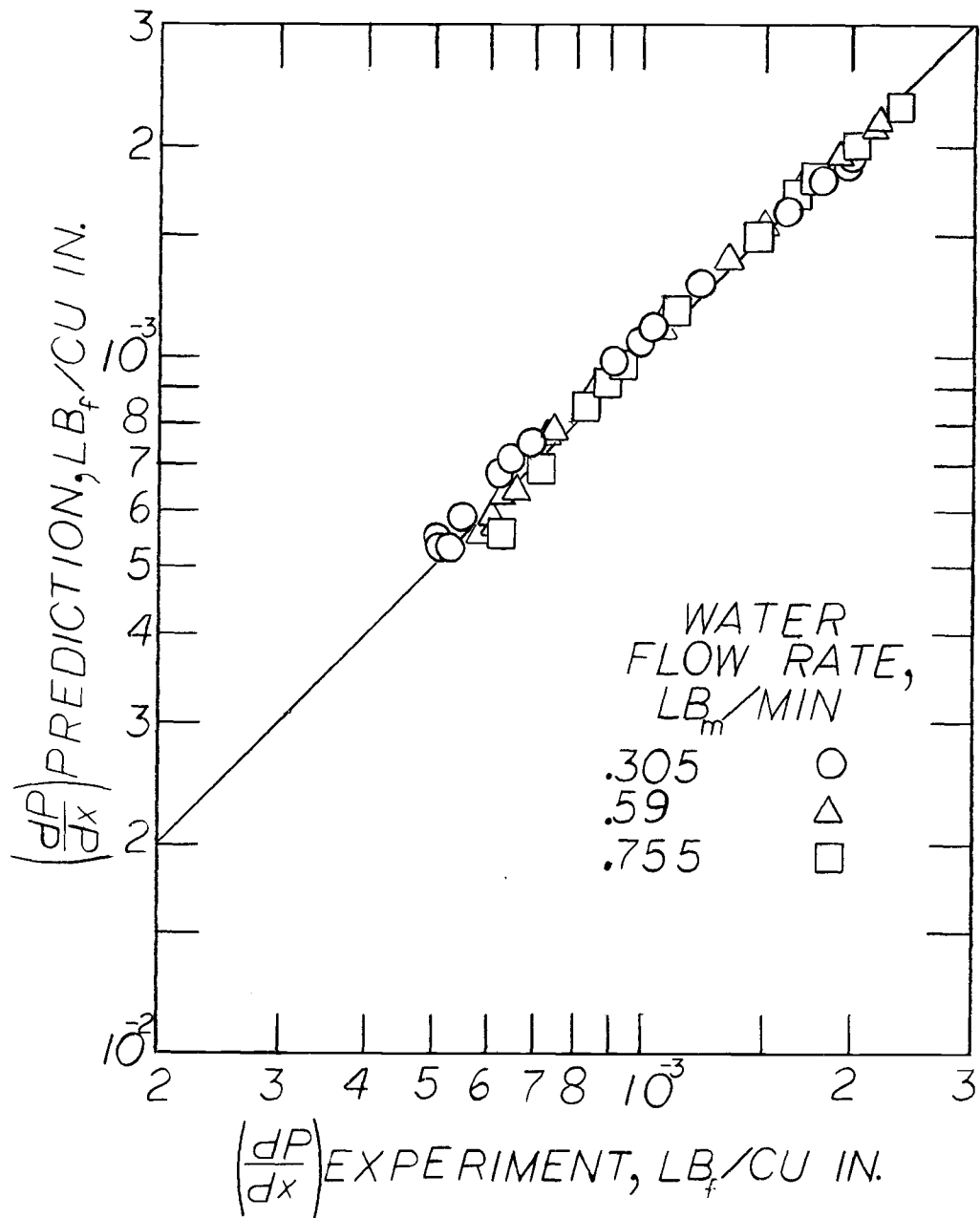


Figure 24. Lockhart-Martinelli pressure drop correlation - water.

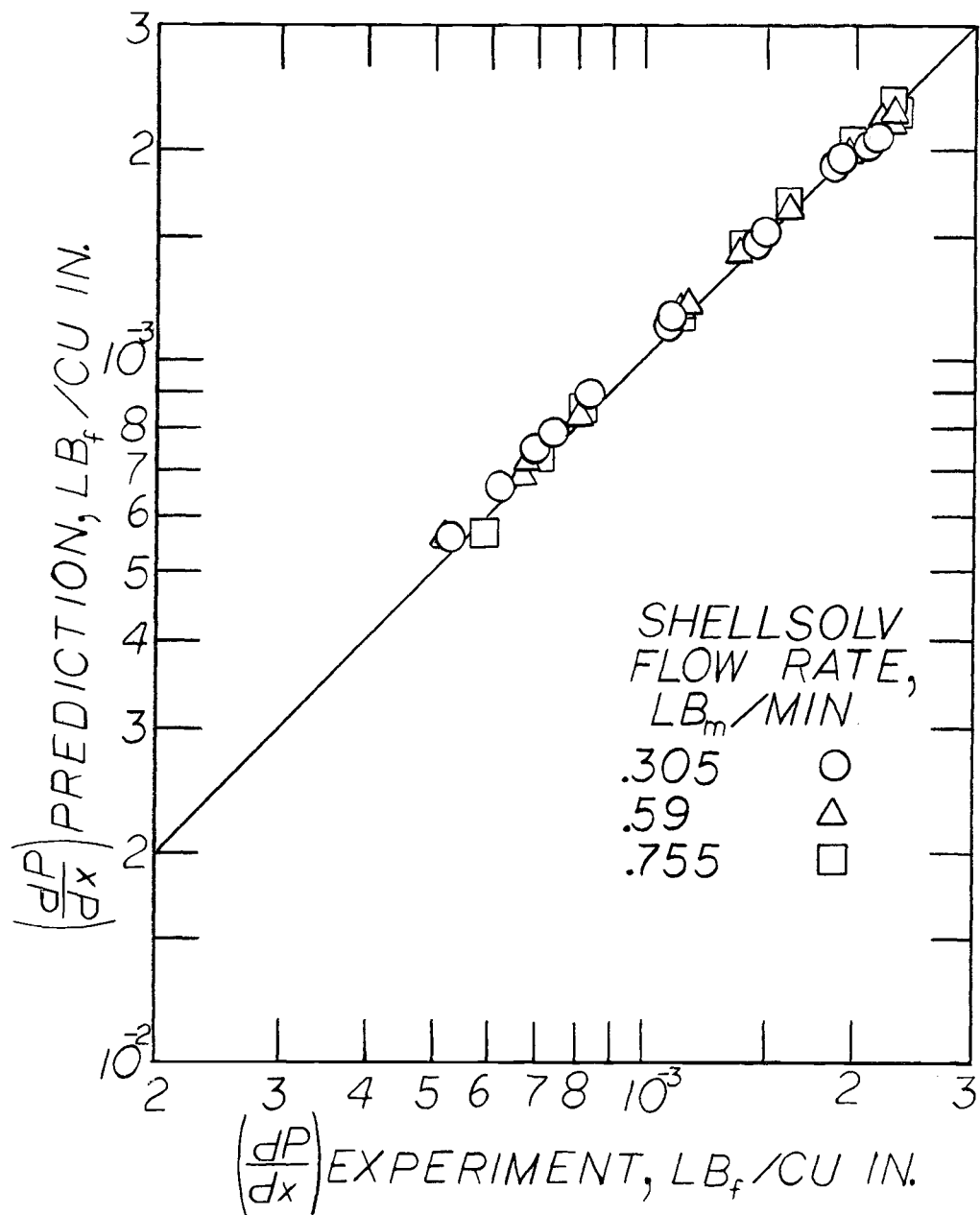


Figure 25. Lockhart-Martinelli pressure drop correlation - Shellsolv.

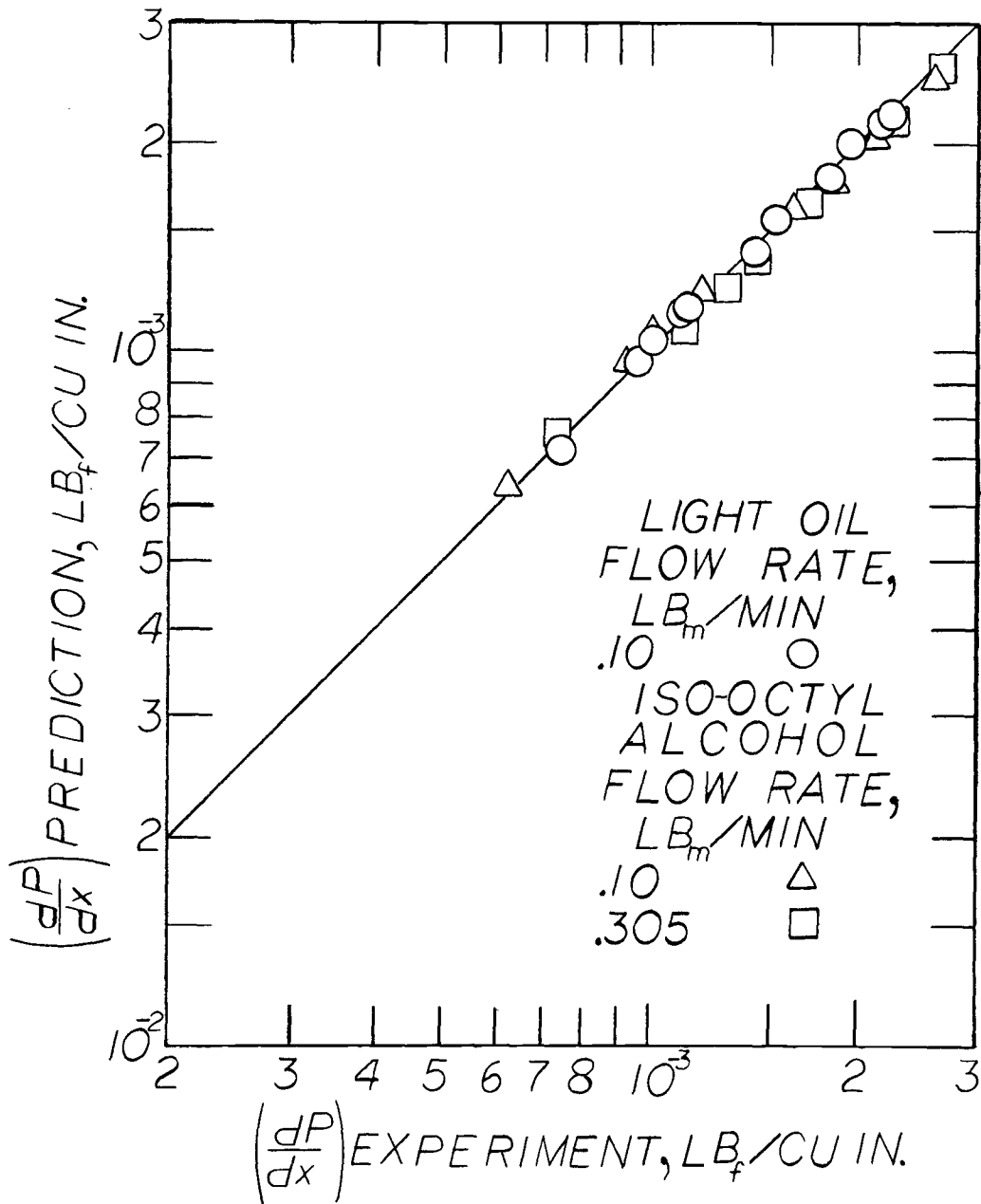


Figure 26. Lockhart-Martinelli pressure drop correlation - light oil and iso-octyl alcohol.

iso-octyl alcohol data, also show similar agreement between predicted and measured two-phase pressure drops. It appears that the Martinelli correlation predicts the pressure drop well in climbing film flow for air and liquids which have a wide range of physical properties.

Wallis (1966) modified the Martinelli correlation so that it would apply to vertical as well as horizontal flow by considering body forces. He claims that his modified model can be applied to vertical two-phase flow in all cases except when the dimensionless gas velocity $j_G^* \gg 2$. At high gas velocities, the shear stress dominates the flow and corrections for body forces are negligible. Unfortunately, the liquid flow rates used in the present study were too low for Wallis's curves to be used: Wallis presented curves with a minimum value of the dimensionless liquid velocity, j_L^* , of 0.02, and in the present study values ranged from 0.0003 to 0.0025.

The dimensionless gas velocities in the present study ranged from 1.08 to 2.92. Since the Martinelli correlation predicted pressure drop successfully, and since it was not true that, for this study, $j_G^* \gg 2$, it appears that the Wallis criteria need some qualification. Complete criteria for the use of the modified Martinelli correlation for vertical flow should take the liquid flow rate into consideration.

Liquid Film Thickness and Shear Stress Distribution

The thickness of the liquid film was obtained by analyzing photographs taken with a high-speed motion picture camera. In Figures 27, 28 and 29, the average film thickness is plotted against the average air velocity in the annulus for a constant liquid flow rate of 0.10, 0.305, and 0.59 lb_m/min , respectively. It is deduced from all of these figures that the film thickness decreases as the air velocity increases. In addition, it can be seen from a comparison of the three figures that, for a given liquid, the film thickness increases as the liquid flow rate increases.

In Figure 27 the film thicknesses of iso-octyl alcohol and light oil at 0.10 lb_m/min are compared. It is evident that at the lower air velocity light oil has the larger film thickness; conversely, at the higher air velocity there is little difference in the film thickness of the two liquids. Since the light oil has twice the viscosity of the iso-octyl alcohol, and since the surface tension of these two liquids differs only slightly, it appears that the higher viscosity causes the thicker liquid film.

In Figure 28, the film thicknesses of water, Shellsolv, and iso-octyl alcohol are compared. Although the Shellsolv and water values are not significantly different, they are important in that they are both considerably smaller than the values for the more viscous iso-octyl alcohol.

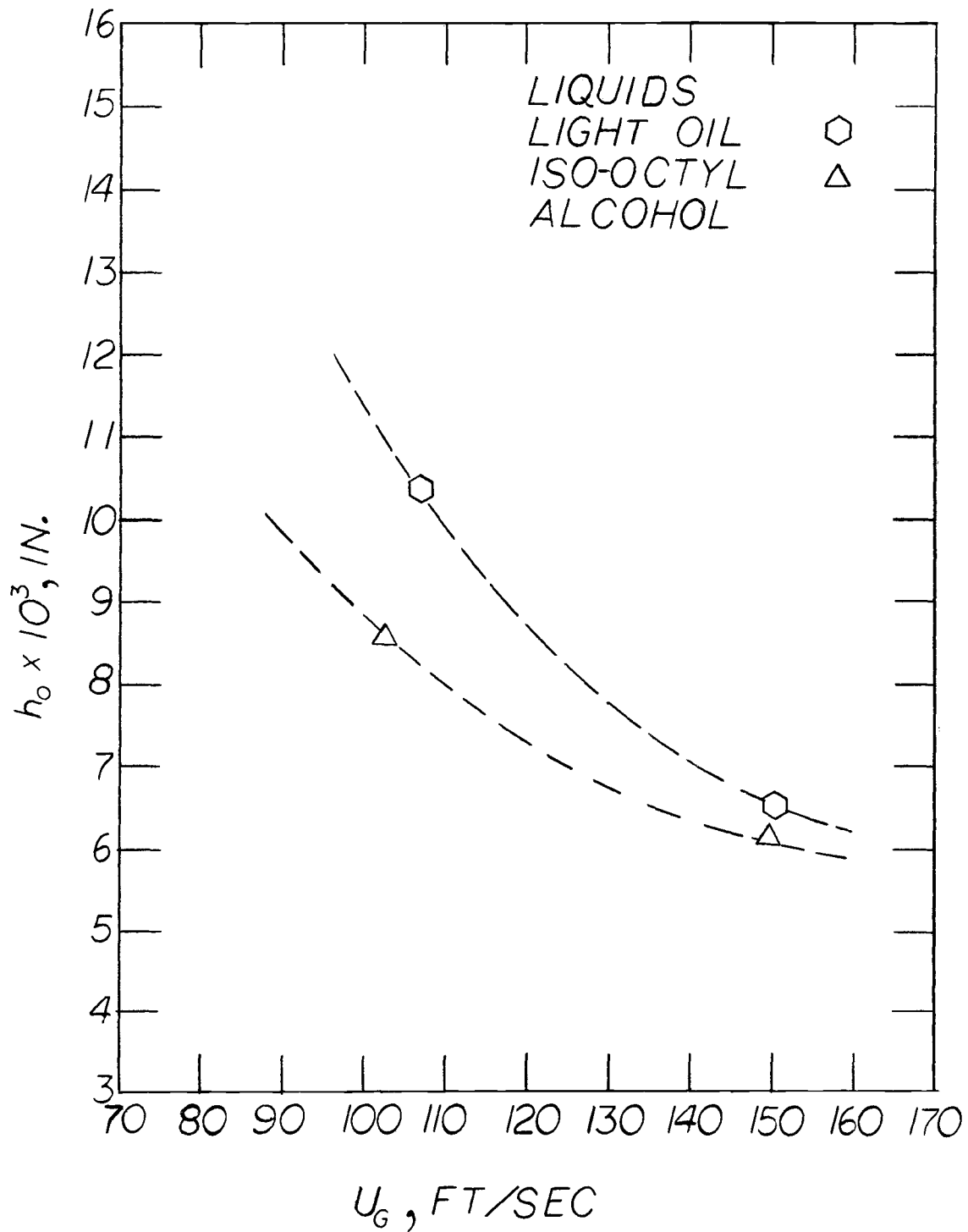


Figure 27. Film thickness vs. average air velocity: liquid flow rate . 10 lb_m/min.

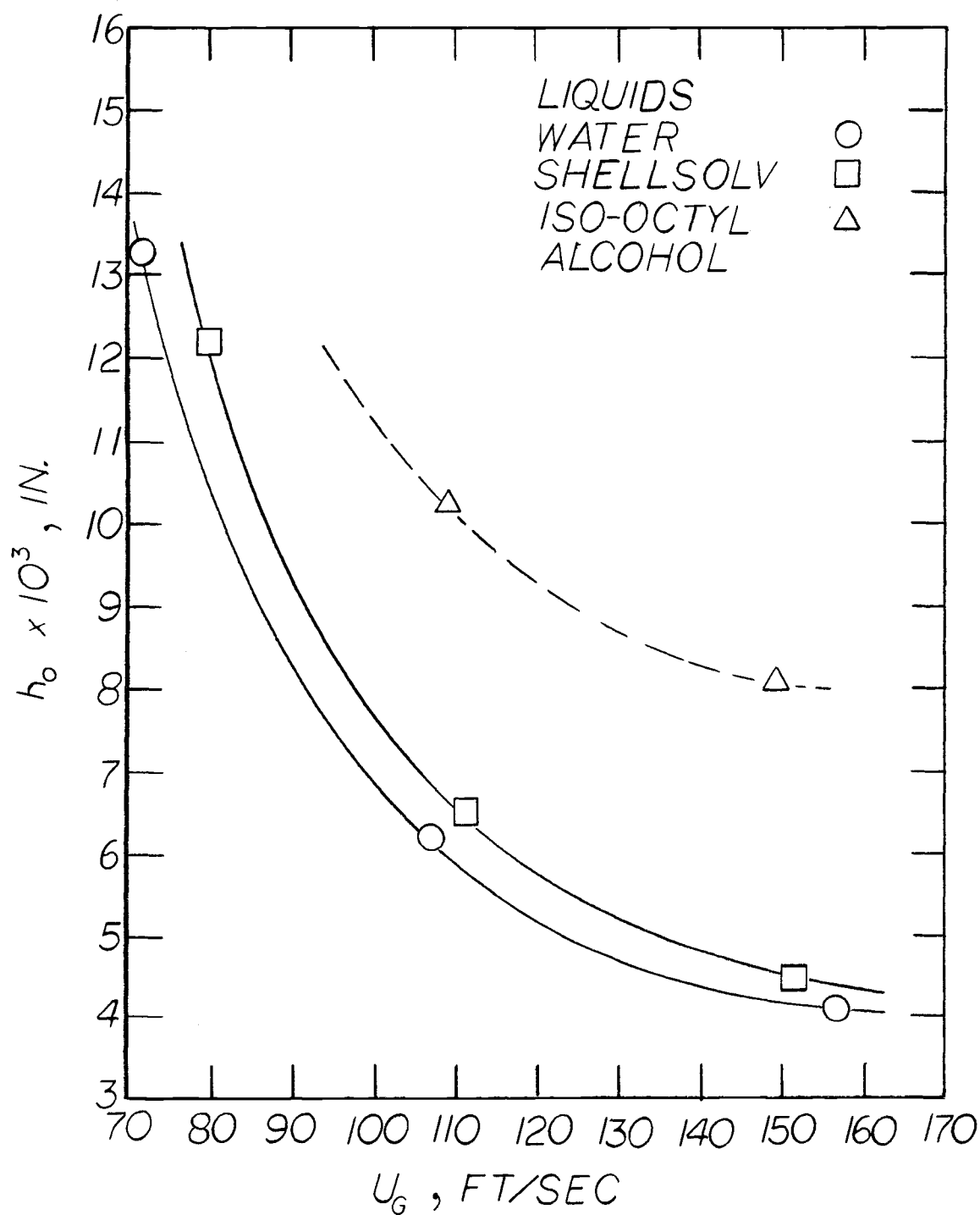


Figure 28. Film thickness vs. average air velocity: liquid flow rate . 305 $\text{lb}_m/\text{min.}$

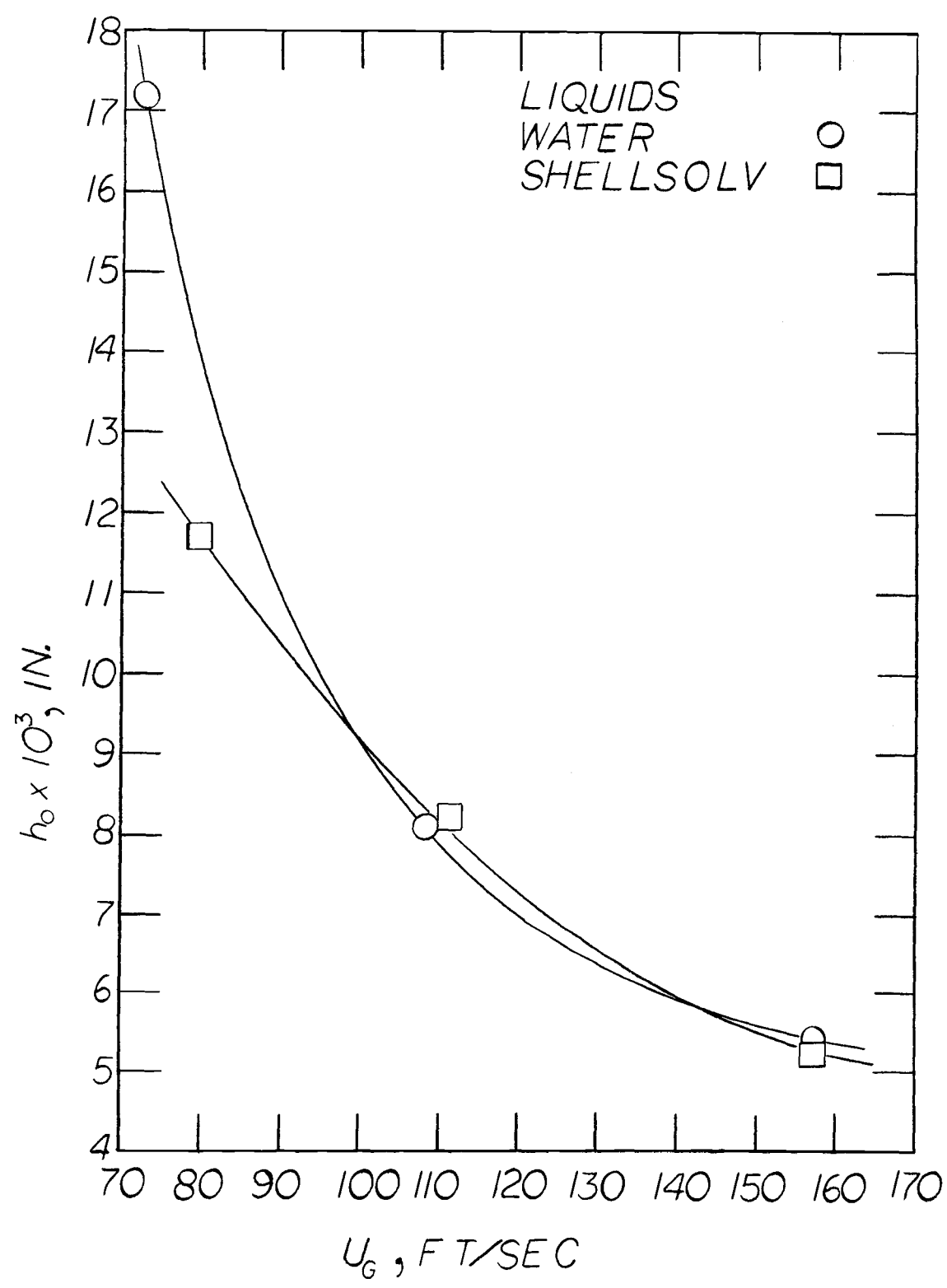


Figure 29. Film thickness vs. average air velocity: liquid flow rate . 59 lb_m /min.

In Figure 29, the film thicknesses of water and Shellsolv are compared. It is observed that the film thicknesses of both liquids are similar in magnitude. It is evident that the film thickness has small dependence on the surface tension. It is also noted that at the very low air velocity the liquid film becomes very thick, at an increasingly rapid rate. At such low velocities, the region is approached where the liquid film may break up and become entrained in the air phase.

The values of the film thicknesses were predicted using Equation (70) in conjunction with Equation (83) using a successive substitution technique. When the laminar film model predictions are compared with the experimental data (see Table 4), a maximum deviation of -36.5% to +34.5% is observed. Within the experimental accuracy of the film thickness measurements ($\pm 10\%$), the predicted values appear to be reasonable.

The comparison of predicted and experimental film thickness values indicate that the laminar film model tends to underpredict the experimental values of h_o for the less viscous liquids and overpredicts these values for the more viscous liquids. It is inferred that the film thickness is not as strong a function of liquid viscosity as suggested by the laminar film model (Equation (70)), which indicates that h_o is approximately directly proportional to, or slightly less than, ν . The present data indicates that $h_o \sim \nu^{.3}$.

Table 4. Prediction of liquid film thickness.

| Liquid | Liquid Flow Rate lb /min m | Air Velocity ft/sec | h_o Exper. in | h_o Pred. in | % Deviation |
|----------------|-------------------------------------|---------------------------|-----------------------|----------------------|----------------|
| Water | .305 | 71.25 | .0133 | .00981 | -26.2 |
| Water | .305 | 108.88 | .0062 | .00466 | -24.8 |
| Water | .305 | 156.96 | .0041 | .00310 | -24.3 |
| Water | .590 | 72.91 | .0172 | .01092 | -36.5 |
| Water | .590 | 108.46 | .0081 | .00592 | -26.9 |
| Water | .590 | 157.76 | .00542 | .00394 | -27.3 |
| Shellsolv | .305 | 79.92 | .0122 | .00816 | -33.1 |
| Shellsolv | .305 | 111.38 | .0065 | .00533 | -18.5 |
| Shellsolv | .305 | 151.21 | .00447 | .00366 | -18.1 |
| Shellsolv | .590 | 79.94 | .0117 | .01104 | -5.6 |
| Shellsolv | .590 | 111.34 | .0082 | .00668 | -18.5 |
| Shellsolv | .590 | 157.89 | .00531 | .00454 | -14.5 |
| Light Oil | .10 | 106.89 | .0104 | .01170 | +12.5 |
| Light Oil | .10 | 150.22 | .0065 | .00749 | +15.2 |
| Iso-octyl Alc. | .10 | 102.52 | .0086 | .00943 | +9.6 |
| Iso-octyl Alc. | .10 | 149.88 | .00614 | .00560 | +8.8 |
| Iso-octyl Alc. | .305 | 109.36 | .01026 | .01380 | +34.5 |
| Iso-octyl Alc. | .305 | 149.79 | .0081 | .00897 | +10.7 |

The experimental film thicknesses were also compared using the holdup correlations given by Lockhart and Martinelli, Hughmark and Pressburg, and Wallis, Steen and Turner. These correlations, when applied to annular flow, gave a direct measurement of the liquid film thickness. Using the present liquid film thickness data, the liquid holdup was calculated using the expression

$$R_L = \frac{r_i^2 - r_l^2}{r_o^2 - r_l^2}$$

and these values for R_L were subsequently compared with the values of R_L predicted by the correlations.

Lockhart and Martinelli used a dimensionless variable χ to correlate experimentally determined values of R_L . Hewitt, King and Lovegrove later fit the $R_L - \chi$ curves of Lockhart and Martinelli to a polynomial and extended them with their own data (taken from experiments in a tube with relatively high entrainment occurring) to the lower liquid holdup region. The polynomial presented by these investigators was used to determine R_L in the present study.

Figure 30 presents the extended Martinelli curve for R_L vs. χ along with the data of the present study and that of Kim (as represented by the dashed line). Both the present data and that of Kim fall below the extended Martinelli curve, but the data and the curve appear to intersect at $\chi \approx .01$. Assuming that the data and correlation are

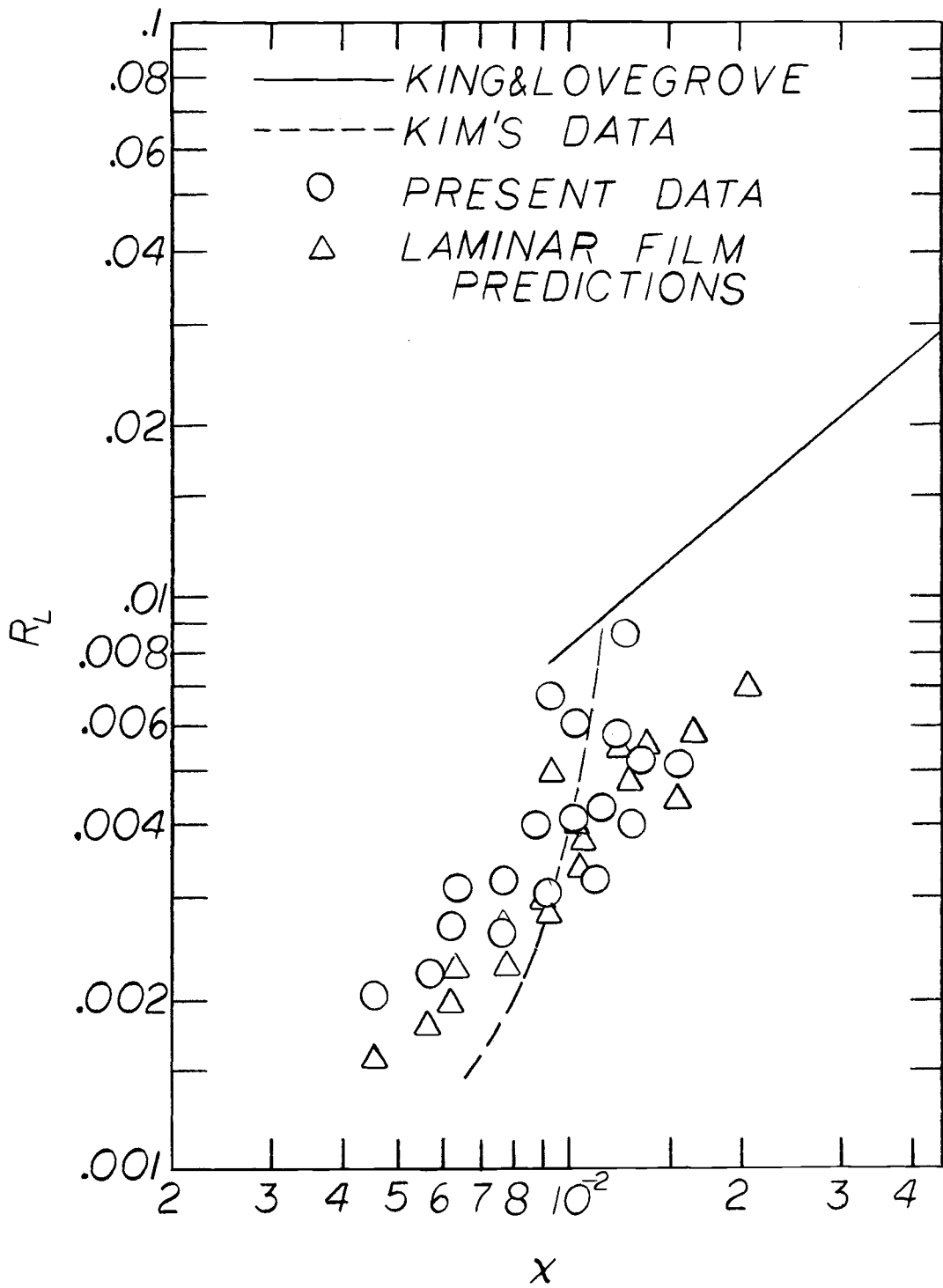


Figure 30. Lockhart-Martinelli void fraction correlation.

general for any duct configuration, it is possible that $\chi \approx .01$ may represent a transition point between flow regimes. Kim mentioned this possibility in his study. However, until more data at higher liquid flow rates are available (the liquid flow rates in the present study were limited by the experimental apparatus), only guarded conclusions can be made concerning a possible transition point. However, it is felt that, since transition from annular to churn flow is gradual, the transition on the $R_L - \chi$ curve, if one exists, will be over a region of flow rather than a point.

As a further illustration of the predicting ability of the Martinelli correlation in the annular flow regime, Figure 31 compares the experimental values of R_L with those predicted by this correlation. The Martinelli correlation overpredicts R_L by as much as 190%.

Hughmark and Pressburg analyzed upward two-phase flow for six liquids. They obtained a correlation that must be extrapolated to the low liquid flow rate region for comparison with the present data. As presented, their correlation indicates that, at low liquid flow rates, R_L is constant at a value of approximately .004.

The Dartmouth correlation presented by Wallis, Steen and Turner was obtained with data for $R_L > .05$. The correlation was based on the hypothesis that there exists a regime of annular flow in which viscous and surface-tension forces are small, and the fluid dynamics are governed by a balance between hydrostatic forces and

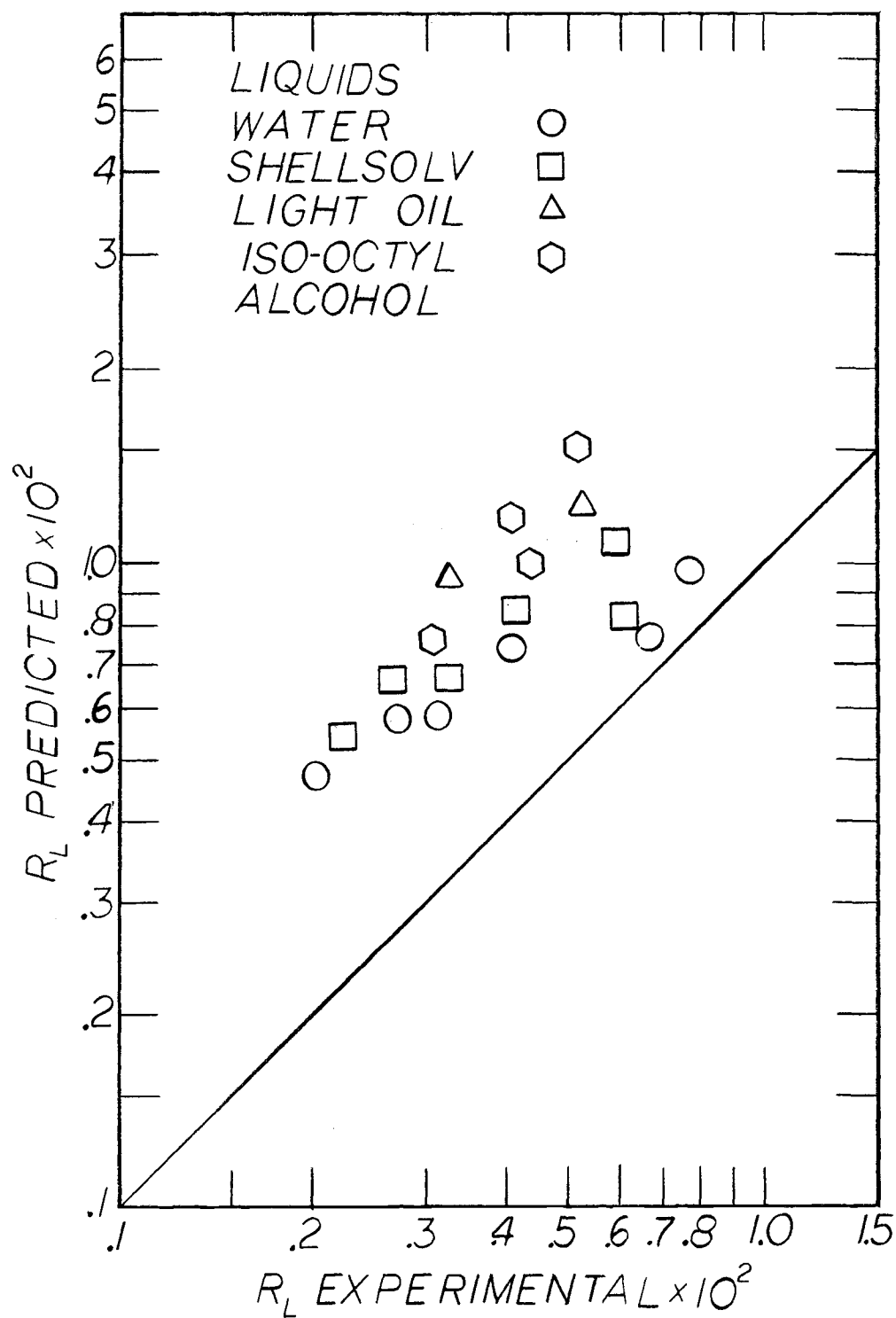


Figure 31. Comparison of Martinelli correlation with experimental values of R_L .

inertia forces in the gas and the liquid. The correlation was checked against the data from the present study and found to overpredict film thickness by as much as 50 times.

For purposes of comparison, the laminar film model was also used to predict R_L and is compared in Figure 32 with the experimental values. Deviations in R_L from the experimental values are the same as those for h_o .

The experimental determination of the liquid film thickness makes possible the determination of the shear stress distribution through the liquid film. Using Equation (80) and (83) along with the experimental values for r_m , dP/dx , τ_2 , and h_o , the shear stress at the inner wall, τ_1 , and the air-liquid interface, τ_i , were determined. The experimentally determined values of τ_1 , τ_i , and τ_2 are presented in Table 5.

It is noted that τ_i is always the largest of the shear stresses and that $\tau_1 > \tau_2$ (except for the low air velocity region). τ_i is shown to be greater than τ_2 by 33% to 52%. τ_i is greater than τ_1 by as much as 130% at the lower air flow rates, and as little as 7% greater at the higher air flow rates. This implies that the velocity profile in the film approaches linearity at high air flow rate. The shear stress at the outer wall has already been discussed. However, as pointed out previously, τ_2 remains fairly invariant with changes in the liquid flow rate.

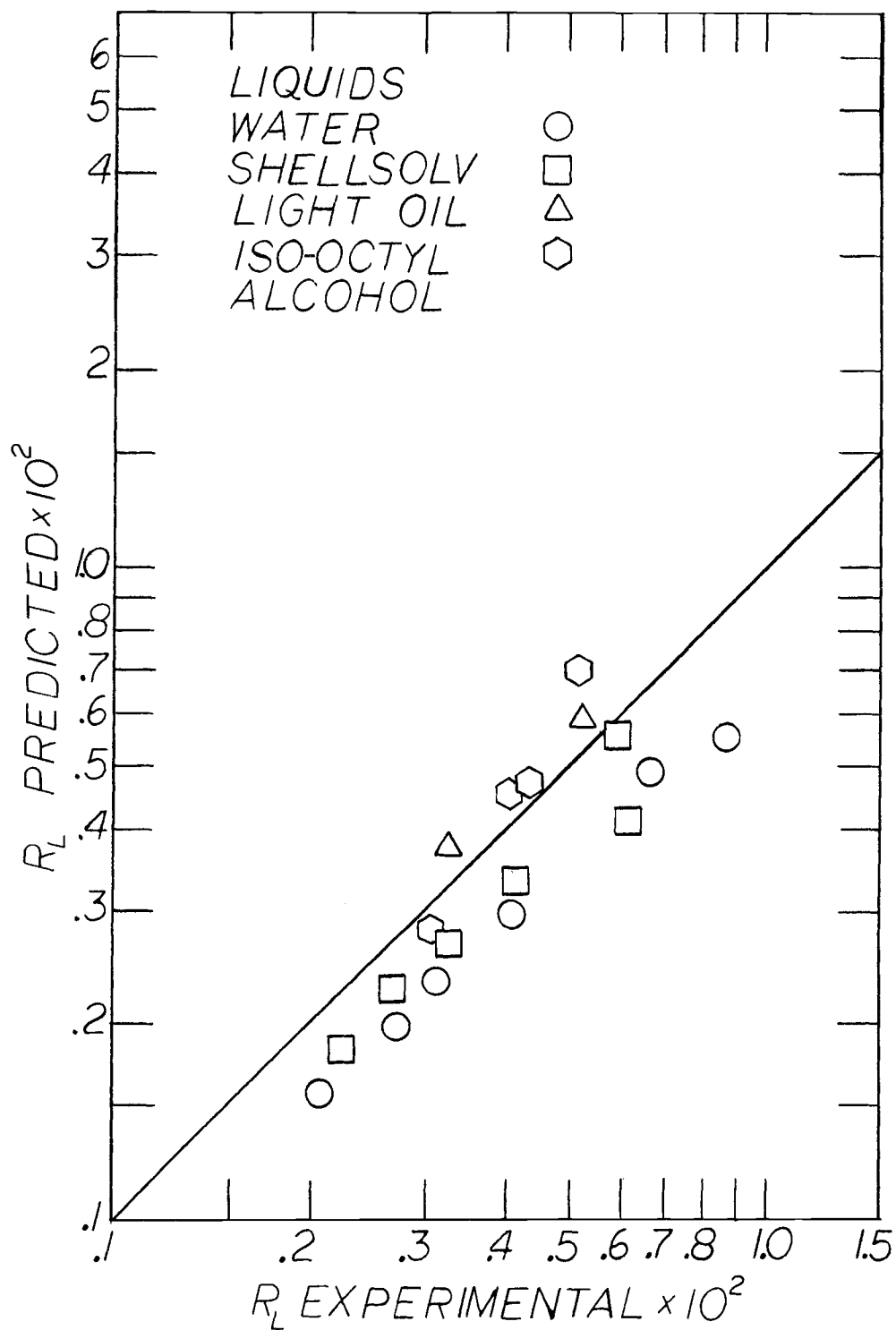


Figure 32. Comparison of laminar film model with experimental values of R_L .

Table 5. Distribution of shear stress.

| Liquid | Liquid Flow Rate lb _m /min | Air Velocity ft/sec | $\tau_1 \times 10^4$ lb _f /in ² | $\tau_i \times 10^4$ lb _f /in ² | $\tau_2 \times 10^4$ lb _f /in ² |
|----------------|---|------------------------|--|--|--|
| Water | .305 | 71.25 | -1.151 | 3.679 | 2.469 |
| Water | .305 | 108.88 | 4.909 | 7.132 | 4.720 |
| Water | .305 | 156.96 | 12.957 | 14.406 | 9.494 |
| Water | .590 | 72.91 | -1.524 | 4.727 | 2.740 |
| Water | .590 | 108.46 | 5.756 | 8.648 | 4.924 |
| Water | .590 | 157.76 | 15.371 | 17.267 | 9.780 |
| Shellsolv | .305 | 79.92 | 1.011 | 4.526 | 2.891 |
| Shellsolv | .305 | 111.38 | 6.138 | 7.986 | 5.044 |
| Shellsolv | .305 | 151.21 | 14.213 | 15.451 | 9.720 |
| Shellsolv | .590 | 79.94 | 1.923 | 5.280 | 2.989 |
| Shellsolv | .590 | 111.34 | 7.517 | 9.828 | 5.526 |
| Shellsolv | .590 | 157.89 | 17.925 | 19.372 | 10.830 |
| Light Oil | .10 | 106.89 | 5.892 | 9.112 | 4.645 |
| Light Oil | .10 | 150.22 | 15.724 | 17.683 | 8.945 |
| Iso-octyl Alc. | .10 | 102.52 | 4.845 | 7.403 | 4.148 |
| Iso-octyl Alc. | .10 | 149.88 | 14.956 | 16.731 | 9.329 |
| Iso-octyl Alc. | .305 | 109.36 | 7.674 | 10.693 | 5.067 |
| Iso-octyl Alc. | .305 | 149.79 | 17.898 | 20.201 | 9.532 |

Water exhibits negative values for τ_1 at the lowest air velocities. This indicates that the liquid near the inner wall is flowing downward. Sutey verified that the laminar film model prediction of incipient downflow in the liquid film compares favorably with the prediction obtained from mass transfer studies at the solid-liquid interface. The negative shear stress at the wall and the positive shear stress at the air-liquid interface indicate that the liquid film is moving in two directions and that a plane of zero shear exists in the liquid film.

The curves presented previously for pressure drop suggest that the flow conditions corresponding to the region of incipient downflow in the liquid film are near the region where the pressure drop approaches an apparent minimum. Hewitt, Lacey, and Nicholls (1965) suggested that these two hydrodynamic phenomena occur concurrently.

Wave Characteristics of the Liquid Film

The experimental values of frequency, \tilde{f} ($\pm 10\%$), and wavelength, λ ($\pm 20\%$), were determined by analyzing the motion picture film. The results are presented in Table 6. The waves appearing on the surface of the liquid film were generally quite irregular. The surface deformations were not uniform sinusoids moving at regular intervals along the liquid surface; rather, they were a combination of fast and slow moving waves of varying sizes. Therefore, analysis of

Table 6. Wave characteristics.

| Liquid | Liquid Flow Rate lb /min m | Average Air Velocity ft/sec | \tilde{f} Experiment cps | \tilde{f} Predicted cps | λ Experiment in | λ Predicted in | c Experiment ft/sec | c Predicted ft/sec |
|--------------|-------------------------------------|-----------------------------------|----------------------------------|---------------------------------|-------------------------------|------------------------------|---------------------------|--------------------------|
| Water | .305 | 71.25 | 30.37 | ---- | .260 | ---- | .66 | .1042 |
| Water | .305 | 108.88 | 89.43 | 233.86 | .182 | .0746 | 1.35 | 1.454 |
| Water | .305 | 156.96 | 304.86 | 751.8 | .098 | .0373 | 2.48 | 2.339 |
| Water | .590 | 72.91 | 47.27 | ---- | .392 | ---- | 1.54 | .4927 |
| Water | .590 | 108.46 | 116.89 | 472.08 | .341 | .0558 | 3.33 | 2.195 |
| Water | .590 | 157.76 | 322.40 | 1541.5 | .141 | .0277 | 3.78 | 3.556 |
| Shellsolv | .305 | 79.92 | 136.0 | 82.45 | .254 | .1219 | 2.86 | .8377 |
| Shellsolv | .305 | 111.38 | 275.5 | 422.31 | .231 | .0462 | 5.32 | 1.624 |
| Shellsolv | .305 | 151.21 | 542.6 | 1215.3 | .116 | .0246 | 5.28 | 2.496 |
| Shellsolv | .590 | 79.94 | 142.2 | 105.76 | .431 | .1220 | 5.12 | 1.0754 |
| Shellsolv | .590 | 111.34 | 345.82 | 898.7 | .322 | .0335 | 9.25 | 2.5068 |
| Shellsolv | .590 | 157.89 | 752.21 | 2662.4 | .199 | .01757 | 12.45 | 3.898 |
| Light Oil | .10 | 106.89 | 85.0 | 3.66 | .604 | .634 | 4.28 | .1937 |
| Light Oil | .10 | 150.22 | 197.2 | 16.25 | .319 | .2632 | 5.22 | .3563 |
| Iso-Oct Alc. | .10 | 102.52 | 96.8 | 7.66 | .581 | .4016 | 4.68 | .2564 |
| Iso-Oct Alc. | .10 | 149.88 | 233.0 | 40.38 | .228 | .1503 | 4.44 | .5058 |
| Iso-Oct Alc. | .305 | 109.36 | 133.6 | 27.03 | .571 | .2355 | 6.38 | .5305 |
| Iso-Oct Alc. | .305 | 149.79 | 262.0 | 112.84 | .304 | .1013 | 6.63 | .9524 |

the liquid surface was rendered quite difficult and, unfortunately, relatively subjective. The average wave frequency values, it is felt, are the more reliable of the measured quantities since they represent an average of a larger number of samples than the wavelength values. Further, the wavelengths were not fixed distances, but tended to shrink and expand due to the relative wave celerities. The wave celerities calculated using $c = \bar{f}\lambda$ are also presented in Table 6.

For all liquids tested, it appears that the frequency is not as strong a function of the liquid flow rate as of the air velocity. The Shellsolv has a frequency two to three times that of water and approximately two times that of iso-octyl alcohol. In turn, iso-octyl alcohol exhibits a slightly larger frequency than light oil. One may therefore conclude that the wave frequency decreases as the liquid viscosity or the liquid surface tension increases.

It appears that the wave celerity increases as the average air velocity or liquid flow rate increases. Further, the wave celerity varies from 1.0% to 8.3% of the average air velocity, with most of the data falling between 3% and 6%. In this connection, recall that Hall-Taylor and Hewitt found by experimental measurement that wave celerity was 5% to 10% of the average air velocity.

The laminar film model (using Equations (69) and (73) along with the predicted average film thicknesses) was used to predict values for \bar{f} , λ , and c . These values are presented in Table 6. The predicted

frequencies range from 4.7 times the experimental values for the water to 23 times smaller for the light oil. The wavelength predictions are as large as six times smaller than the experimental values for the water and Shellsolv, and they predict well the wavelength values for the liquids of higher viscosity.

When the motion pictures were viewed qualitatively, it was noticed that the liquid surface was composed of roll waves. The more rapidly moving liquid disturbances would overtake and encompass the slower moving disturbances, capturing some of the liquid of the slower waves, and generating smaller waves in their wake. The large waves would build to significant heights, the fronts of the waves would then steepen, and the tops would tend to roll in a downward motion. This rolling resembled the action of waves building and breaking on a beach. Upon completion of this rolling action, the roll waves would leave an irregular film surface in their wake.

The water and Shellsolv waves were particularly illustrative of the roll wave phenomenon, especially at the higher liquid flow rates. In contrast, the more viscous liquids exhibited long stretches of little surface deformation followed by an infrequent roll wave, moving usually in a rather sluggish manner. The smaller waves seemed to be considerably damped in the higher viscosity liquids.

Although the Shellsolv and water were both characterized by large numbers of energetic roll waves, the shape and character of the

surface disturbances were quite different for these two liquids. The water waves exhibited the closer resemblance to a uniform wave form. These water waves had rather smooth wave fronts and gradually tapering wakes. It was observed that ripples were superimposed on the tail of the waves, but the ripples were not obtrusively evident.

The Shellsolv disturbances, on the other hand, were rather like amorphous masses of liquid flowing on top of the liquid surface. The waves exhibited very little coherence and tended to undulate in amoeba-like fashion as they rolled over the film surface.

This disparity in the wave shape of water and Shellsolv is probably directly related to the difference in surface tension of the two liquids. Disturbances on the water surface had relatively large surface tension-induced restoring forces acting upon them. In contrast, Shellsolv had smaller restoring forces acting upon the surface disturbances. With smaller restoring forces acting upon them, disturbances on the surface tended to extend from the surface in all shapes and all directions.

CONCLUSIONS

1. Friction factors for air flowing alone in the annulus in a Reynolds number range of 7×10^4 to 2×10^5 are 2% to 13% larger than for smooth tube air flow. The radius of maximum velocity for the present data is not a function of the air Reynolds number. For the present annulus, with $r^* = .333$, the experimental value for $r_m = .892$ is predicted well by existing correlations.

2. As the liquid or air flow rate increases, the two-phase pressure loss increases. At a constant liquid flow rate, the more viscous liquids give rise to two-phase pressure losses above those for single-phase flow. Water at $.305 \text{ lb}_m/\text{min}$ exhibits a 15% increase above single-phase pressure loss values, while iso-octyl alcohol at the same flow rate exhibits a 48% increase. The two-phase pressure losses in climbing film flow show little dependence on liquid surface tension.

3. A liquid film flowing on the inner wall causes an increase in the shear stress at the outer wall. The increase in τ_2 above the single-phase values is less than the corresponding pressure loss increase. Water and iso-octyl alcohol at $.305 \text{ lb}_m/\text{min}$ exhibit increases in τ_2 above single-phase values of 3.5% and 15.5%, respectively. The percent increase in τ_2 is larger at higher liquid flow rates and larger for the more viscous liquids. The two-phase data

for f_2 and Re_2 fall in a narrow band. A correlation for all of the data is ($R = .957$)

$$f_2 = 0.454 Re_2^{-.396}$$

and for the region of low entrainment at $Re_2 > 8 \times 10^4$ ($R = .938$)

$$f_2 = 0.201 Re_2^{-.326}$$

The case of a liquid film flowing on the inner wall of an annulus appears to be hydrodynamically similar to the case of a gas flowing in an annulus with an artificially roughened inner wall and a smooth outer wall.

4. The radius at the point of maximum velocity was observed to be independent of the air Reynolds number. The radius at the point of maximum velocity increases as the liquid flow rate increases and is greater for the more viscous liquids. An empirical correlation for the point of maximum velocity is ($R = .9996$)

$$y^* = 0.01 Re_L^{.246} \mu^{*.48}$$

5. The Lockhart and Martinelli pressure drop correlation predicts two-phase pressure drops for climbing-film flow, for air and a variety of liquids (with a wide range of physical properties), with a maximum deviation of -6% to +3%.

6. The liquid film thickness increases as the liquid flow rate increases and as the air velocity decreases. Film thicknesses are larger for the more viscous liquids and are independent of the liquid surface tension.

The laminar film model predicts h_o with an accuracy of -36.5% to +34.5%. The model underpredicts the less viscous liquids and overpredicts the more viscous liquids, indicating $h_o \sim v^n$, where n appears to be approximately .3.

7. The available liquid holdup correlations predict poorly the liquid film thickness in the low liquid flow rate climbing film regime. The intersection of the data with the Lockhart and Martinelli $R_L - \chi$ curve at $\chi \approx .01$ indicate that this may be near a region of transition from the annular to the churn flow regime.

8. The shear stress at the air-liquid interface is from 33% to 52% larger than the shear stress at the outer wall and 7% to 130% larger than that at the inner wall.

9. The wave frequency increases with increasing air flow rate and increases to a less degree with increasing liquid flow rate. Frequency is larger for the less viscous liquids and also larger for the liquids with the lower surface tension.

The wave celerity increases with increases in air or liquid flow rate. The celerity is 3% to 6% of the average air velocity in the annulus.

The laminar film model in general predicts poorly the frequency and wavelength. However, the model predicts wavelength of the more viscous liquids very well.

RECOMMENDATIONS FOR FURTHER WORK

1. Experimental data are needed from studies using annular ducts of different diameter ratios. Correlations for flow in an annulus cannot be considered general until the effect of r^* is known.
2. Climbing film data at higher liquid flow rates are needed to extend the present work. Accurate definition of the regime boundaries for annular flow in a number of duct cross-sections, for both climbing and falling film flow and for a wide range of liquids, would be extremely valuable.
3. The experimental apparatus should be modified so that both climbing and falling film flow (influenced by either a co-current or a counter-current flowing gas phase) can be studied using the same equipment.
4. Entrainment studies (using sampling probes, for example) should be part of all future experimental work in annular flow.
5. A more continuous and less tedious method (possibly using a conductance probe technique) of determining liquid film thicknesses and wave characteristics should be used in future work.

BIBLIOGRAPHY

- Anderson, G. H. and B. F. Mantzouranis. 1960. Two-phase (gas-liquid) flow phenomena. Part I. Pressure drop and hold-up for two-phase flow in vertical tubes. *Chemical Engineering Science* 12:109-126.
- Anderson, R. J. and T. W. F. Russell. 1965. Designing for two-phase flow. Part I. *Chemical Engineering*, Dec. 6, 1965, p. 139-144.
- Anshus, B. E. and S. L. Goren. 1966. A method for getting approximate solutions to the Orr-Sommerfeld equation for flow on a vertical wall. *A. I. Ch. E. Journal* 12:1004-1008.
- Benjamin, T. B. 1957. Wave formation in laminar flow down an inclined plane. *Journal of Fluid Mechanics* 2:554-574.
- Bennett, J. A. R. 1958. Two-phase flow in gas-liquid systems: A literature survey. Harwell, Berkshire, England, 58 p. (United Kingdom Atomic Energy Authority. AERE-CE/R-2497)
- Berbente, C. D. and E. Ruckenstein. 1968. Hydrodynamics of wave flow. *A. I. Ch. E. Journal* 14:772-779.
- Brighton, J. A. and J. B. Jones. 1964. Fully developed turbulent flow in annuli. *Transactions of the American Institute of Mechanical Engineers*, ser. D. 86:835-844.
- Brodkey, R. S. 1967. *The phenomena of fluid motions*. Boston, Addison-Wesley. 737 p.
- Brown, R. A. S. and G. W. Govier. 1961. High-speed photography in the study of two-phase flow. *Canadian Journal of Chemical Engineering* 39:159-164.
- Calvert, S. and B. Williams. 1955. Upward cocurrent annular flow of air and water in smooth tubes. *A. I. Ch. E. Journal* 1:78-86.
- Cannon, M. R. and M. R. Fenske. 1938. Viscosity measurement. *Industrial and Engineering Chemistry* 10:297-301.
- Casagrande, I., L. Cravarolo, A. Hassid and E. Pedrocchi. 1963. Adiabatic dispersed two-phase flow: Further results on the influence of physical properties on pressure drop and film

thickness. 75 p. (Centro Informazione Studi Esperienze. Topical Report no. 6. CISE-R-73; European Atomic Energy Commission. EURAEC-712)

Charvonia, D. A. 1961. An experimental investigation of the mean liquid film thickness and the characteristics of the interfacial surface in annular, two-phase flow. Paper presented at the Winter Annual Meeting of the American Society of Mechanical Engineers, New York, Nov. 26-Dec. 1.

Clump, C. W. and D. Kwasnoski. 1968. Turbulent flow in concentric annuli. *A. I. Ch. E. Journal* 14:164-168.

Collier, J. G. 1961. Burnout in liquid cooled reactors. Part I. *Nuclear Power* 6:61-66.

Collier, J. G. and G. F. Hewitt. 1961. Data on the vertical flow of air-water mixtures in the annular and dispersed flow regimes. Part II. Film thickness and entrainment data and analysis of pressure drop measurements. *Transactions of the Institution of Chemical Engineers (London)* 39:127-136.

_____. 1964. Film thickness measurements. Harwell, Berkshire, England. 18 p. (United Kingdom Atomic Energy Authority. AERE-R-4684)

Cooper, K. D., G. F. Hewitt and B. Pinchin. 1963. Photography of two-phase flow. Harwell, Berkshire, England. 11 p. (United Kingdom Atomic Energy Authority. AERE-R-4301.

Daniels, F. et al. 1963. *Experimental physical chemistry*. 6th ed. New York, McGraw-Hill. 625 p.

DeGance, A. and R. W. Atherton. 1970. Chemical engineering aspects of two-phase flow. Part VI. Vertical and inclined-flow correlations. *Chemical Engineering*, Oct. 5, 1970, p. 87-94.

Dukler, A. E. 1960. Fluid mechanics and heat transfer in vertical falling-film systems. In: *Heat transfer-Storrs*. New York, American Institute of Chemical Engineers. p. 1-10. (Chemical Engineering Progress Symposium Series, no. 30)

Dukler, A. E. and O. P. Berglin. 1952. Characteristics of flow in falling liquid films. *Chemical Engineering Progress* 48:557-563.

- Ellis, S. R. M. and B. Gay. 1959. The parallel flow of two fluid streams: Interfacial shear and fluid-fluid interaction. *Transactions of the Institution of Chemical Engineers (London)* 37:206-213.
- Fulford, G. D. 1964. The flow of liquid in thin films. *Advances in Chemical Engineering* 5:151-236.
- Gill, L. E., G. F. Hewitt and P. M. C. Lacey. 1963. Sampling probe studies of the gas core in annular two-phase flow. Part II. Studies of the effect of phase flow rates on phase and velocity distribution. Harwell, Berkshire, England. 26 p. (United Kingdom Atomic Energy Authority. AERE-R-3955)
- Gollan, A. and S. Sideman. 1969. On the wave characteristics of falling films. *A. I. Ch. E. Journal* 15:301-303.
- Hall-Taylor, N. and G. F. Hewitt. 1962. The motion and frequency of large disturbance waves in annular two-phase flow of air-water mixtures. Harwell, Berkshire, England. 20 p. (United Kingdom Atomic Energy Authority. AERE-R-3952)
- Hanks, R. W. and W. F. Bonner. 1971. Transitional flow phenomena in concentric annuli. *Industrial and Engineering Chemistry Fundamentals* 10:105-113.
- Hanratty, T. J. and J. M. Engen. 1957. Interaction between a turbulent air stream and a moving water surface. *A. I. Ch. E. Journal* 3:299-304.
- Hanratty, T. J. and A. Hershmann. 1961. Initiation of roll waves. *A. I. Ch. E. Journal* 7:488-497.
- Harkins, W. D. and H. F. Jordan. 1930. A method for the determination of surface and interfacial tension from the maximum pull on a ring. *Journal of the American Chemical Society* 52:1751-1772.
- Hartley, D. E. and D. C. Roberts. 1961. A correlation of pressure drops for two-phase annular flows in vertical channels. 46 p. (London, Queen Mary College. Nuclear Engineering Laboratory Memorandum Q 6)
- Hewitt, G. F. 1964. Interpretation of pressure drop data from an annular channel. Harwell, Berkshire, England. 16 p. (United Kingdom Atomic Energy Authority. AERE-R-4340)

- Hewitt, G. F., R. D. King and P. C. Lovegrove. 1962. Techniques for liquid film and pressure drop studies in annular two-phase flow. Harwell, Berkshire, England. 39 p. (United Kingdom Atomic Energy Authority. AERE-R-3921)
- Hewitt, G. F., P. M. C. Lacey and B. Nicholls. 1965. Transitions in film flow in a vertical tube. Harwell, Berkshire, England. 18 p. (United Kingdom Atomic Energy Authority. AERE-R-4614)
- Hewitt, G. F. and P. C. Lovegrove. 1962. The application of the light absorption technique to continuous film thickness recording in annular two-phase flow. Harwell, Berkshire, England. 9 p. (United Kingdom Atomic Energy Authority, AERE-R-3953)
- _____. 1969a. A mirror-scanner velocitometer and its application to wave velocity measurement in annular two-phase flow. Harwell, Berkshire, England. 5 p. (United Kingdom Atomic Energy Authority. AERE-R-3958)
- _____. 1969b. Frequency and velocity measurements of disturbance waves in annular two-phase flow. Harwell, Berkshire, England. 6 p. (United Kingdom Atomic Energy Authority. AERE-R-4304)
- Hewitt, G. F., P. C. Lovegrove and B. Nicholls. 1964. Film thickness measurement using a fluorescence technique. Part I. Description of the method. Harwell, Berkshire, England. 7 p. (United Kingdom Atomic Energy Authority. AERE-R-4478)
- Hewitt, G. F. and B. Nicholls. 1969. Film thickness measurement in annular two-phase flow using a fluorescence spectrometer technique. Part II. Studies of the shape of the disturbance waves. Harwell, Berkshire, England. 6 p. (United Kingdom Atomic Energy Authority. AERE-R-4506)
- Hewitt, G. F. and D. N. Roberts. 1969. Investigation of interfacial phenomena in annular two-phase flow by means of the axial view technique. Harwell, Berkshire, England. 8 p. (United Kingdom Atomic Energy Authority. AERE-R-6070)
- Hughmark, G. A. and B. S. Pressburg. 1961. Holdup and pressure drop with gas-liquid flow in a vertical pipe. A. I. Ch. E. Journal 7:677-682.
- Hyzer, W. G. 1962. Engineering and scientific high-speed photography. New York, Macmillan. 537 p.
- Hoogendoorn, C. J. 1959. Gas-liquid flow in horizontal pipes. Chemical Engineering Science 9:205-217.

- Jeffreys, H. 1925. On the formation of water waves by wind. Proceedings of the Royal Society of London, ser. A, 107:189-205.
- Jones, L. O. and S. Whitaker. 1966. An experimental study of falling liquid films. A. I. Ch. E. Journal 12:525-529.
- Kapitza, P. L. 1948. Flow in thin layers of viscous liquid. Part I. Free flow. Journal of Experimental and Theoretical Physics 18:3-18. (Translated from Zhurnal Eksperimental i Theoretichkoi Fiziki) (U. S. Atomic Energy Commission. AEC-TR-5514) (Microfiche)
- Kays, W. M. and E. Y. Leung. 1963. Heat transfer in annular passages - Hydrodynamically developed turbulent flow with arbitrarily prescribed heat flux. International Journal of Heat and Mass Transfer 6:537-557.
- Kim, D. H. 1965. Momentum transfer in climbing film flow in an annular duct. Doctoral dissertation. Corvallis, Oregon State University. 148 numb. leaves.
- Kinsman, B. 1965. Wind waves; their generation and propagation on the ocean surface. Englewood Cliffs, Prentice-Hall. 676 p.
- Knudsen, J. G. 1949. Heat transfer, friction and velocity gradients in annuli containing plain and fin tubes. Doctoral dissertation. Ann Arbor, University of Michigan. 215 numb. leaves.
- Knudsen, J. G. 1962. Note on j-factors for turbulent flow. A. I. Ch. E. Journal 8:565-568.
- Knudsen, J. G. and D. L. Katz. 1958. Fluid dynamics and heat transfer. New York, McGraw-Hill. 576 p.
- Krantz, W. B. and S. L. Goren. 1970. Finite-amplitude long waves on liquid films flowing down a plane. Industrial and Engineering Chemistry Fundamentals 9:107-113.
- _____. 1971a. Stability of thin liquid films flowing down a plane. Industrial and Engineering Chemistry Fundamentals 10:91-101.
- _____. 1971b. Bimodal wave formation on thin liquid films flowing down a plane. A. I. Ch. E. Journal 17:494-496.

- Lacey, P. M. C., G. F. Hewitt and J. G. Collier. 1962. Climbing film flow. Harwell, Berkshire, England. 22 p. (United Kingdom Atomic Energy Authority. AERE-R-3962)
- Levich, V. G. 1962. Physicochemical hydrodynamics, tr. by Scripta Technica Inc. Englewood Cliffs, Prentice-Hall. 700 p.
- Levich, V. G. and V. S. Krylov. 1969. Surface-tension-driven phenomena. *Annual Review of Fluid Mechanics* 1:293-316.
- Lighthill, M. J. and G. B. Whitham. 1955. On kinematic waves. Part II. A theory of traffic flow on long crowded roads. *Proceedings of the Royal Society of London, ser. A*, 229:317-345.
- Lilleleht, L. U. and T. J. Hanratty. 1961. Relation of interfacial shear stress to the wave height for concurrent air-water flow. *A. I. Ch. E. Journal* 7:548-550.
- Lockhart, R. W. and R. C. Martinelli. 1949. Proposed correlation of data for isothermal two-phase, two-component flow in pipes. *Chemical Engineering Progress* 45:39-48.
- Lorenz, F. R. 1932. Uber turbulente Stromung durch Rohre mit keisringformigen Querschnitt. *Communications of the Institute of Fluid Mechanics, Karlsruhe* 2:26-66.
- Ludwig, H. 1950. Instrument for measuring the wall shearing stress of turbulent boundary layers. Washington. 22 p. (Translated from the German) (U. S. National Advisory Committee for Aeronautics. Technical Memorandum 1284)
- Ludwig, H. and W. Tillmann. 1950. Investigations of the wall shearing stress in turbulent boundary layers. Washington. 25 p. (Translated from the German) (U. S. National Advisory Committee for Aeronautics. Technical Memorandum 1285)
- Macagno, E. D. and D. W. McDougall. 1966. Turbulent flow in annular pipes. *A. I. Ch. E. Journal* 12:437-444.
- Martinelli, R. C. et al. 1944. Isothermal pressure drop for two-phase two-component flow in a horizontal pipe. *Transactions of the American Society of Mechanical Engineers* 66:139-151.
- Massot, C., F. Irani and E. N. Lightfoot. 1966. Modified description of wave motion in a falling film. *A. I. Ch. E. Journal* 12:445-455.

- Meter, D. M. and R. B. Bird. 1961. Turbulent Newtonian flow in annuli. *A. I. Ch. E. Journal* 7:41-45.
- Nicol, A. A. and J. O. Medwell. 1964. Velocity profiles and roughness effects in annular pipes. *Journal of Mechanical Engineering Science* 6:110-115.
- Nusselt, W. 1916. Die Oberflochenkondensation des Wasserdampfes. *Zeitschrift des Vereines Deutscher Ingenieure* 60:541-546.
- Orkiszewski, J. 1967. Predicting two-phase pressure drops in vertical pipe. *Journal of Petroleum Technology* 19:829-838.
- Perry, J. H. (ed.). 1963. *Chemical engineers' handbook*. 4th ed. New York, McGraw-Hill, n. p.
- Prengle, R. S. and R. R. Rothfus. 1955. Transition phenomena in pipes and annular cross sections. *Industrial and Engineering Chemistry* 47:379-386.
- Preston, J. H. 1954. The determination of turbulent skin friction by means of pitot tubes. *Journal of the Royal Aeronautical Society* 58:109-121.
- Quarmby, A. 1967. An experimental study of turbulent flow through concentric annuli. *International Journal of Mechanical Sciences* 9:205-221.
- Rothfus, R. R., C. C. Monrad and V. E. Senecal. 1950. Velocity distribution and fluid friction in smooth concentric annuli. *Industrial and Engineering Chemistry* 42:2511-2520.
- Rothfus, R. R., W. K. Sartory and R. I. Kermode. 1966. Flow in concentric annuli at high Reynolds numbers. *A. I. Ch. E. Journal* 12:1086-1091.
- Rothfus, R. R. et al. 1955. Isothermal skin friction in flow through annular sections. *Industrial and Engineering Chemistry* 47: 913-918.
- Schneider, F. N., P. D. White and R. L. Huntington. Oct., 1954. Horizontal two-phase oil and gas flow. *Pipe Line Industry* 1: 47-51

- Scott, B. 1969. Motion picture study of a vertical climbing film in an annular duct. Master's thesis. Corvallis, Oregon State University. 99 numb. leaves.
- Scott, D. S. 1963. Properties of cocurrent gas-liquid flow. *Advances in Chemical Engineering* 4:199-277.
- Semenov, P. A. 1950. The flow of liquid in thin layers. *Zhurnal Tekhnicheskoi Fiziki* 20:980-990. (Personally translated from the Russian for the author)
- Shearer, C. J. and R. M. Nedderman. 1965. Pressure gradient and liquid film thickness in co-current upwards flow of gas/liquid mixtures: Application to film-cooler design. *Chemical Engineering Science* 20:671-683.
- Stainthorp, F. P. and J. M. Allen. 1965. The development of ripples on the surface of a liquid film flowing inside a vertical tube. *Transactions of the Institution of Chemical Engineers (London)* 43:85-91.
- Sutey, A. M. 1967. Mass transfer at the solid-liquid interface for climbing film flow in an annular duct. Doctoral dissertation. Corvallis, Oregon State University. 170 numb. leaves.
- Tailby, S. R. and S. Portalski. 1962. The determination of the wavelength on a vertical film of liquid flowing down a hydrodynamically smooth plate. *Transactions of the Institution of Chemical Engineers (London)* 40:114-121.
- Telles, A. C. D. S. 1968. Liquid film characteristics in vertical two-phase flow. Doctoral dissertation. Houston, University of Houston. 268 numb. leaves.
- Tong, L. S. 1965. Boiling heat transfer and two-phase flow. New York, Wiley. 242 p.
- Van Rossum, J. J. 1959. Experimental investigation of horizontal liquid films; wave formation, atomization, film thickness. *Chemical Engineering Science* 11:35-52.
- Vohr, J. H. 1960. Flow patterns of two-phase flow; a survey of the literature. 54 p. (U. S. Atomic Energy Commission. TID-11514)

- Wallis, G. B. 1966. Two-phase flow and boiling heat transfer. 110 p. (U. S. Atomic Energy Commission. NYO-3114-14)
- Wallis, G. B. 1969. One-dimensional two-phase flow. New York, McGraw-Hill. 408 p.
- Wallis, G. B. and D. A. Steen. 1964. The transition from annular to annular-mist co-current two-phase downflow. 75 p. (U. S. Atomic Energy Commission. NYO-3114-2)
- Wallis, G. B. , D. A. Steen and J. M. Turner. 1964. Two-phase flow and boiling heat transfer, quarterly progress report. 12 p. (U. S. Atomic Energy Commission. NYO-3114-1)
- Whitwell, J. C. 1938. Discharge rates from gas flowmeters; proper temperature and pressure corrections. *Industrial and Engineering Chemistry* 30:1157-1162.
- Willis, I. J. 1965. Upwards annular two-phase air-water flow in vertical tubes. *Chemical Engineering Science* 20:895-902.
- Woodmansee, D. E. and T. J. Hanratty. 1969. Base film over which roll waves propagate. *A. I. Ch. E. Journal* 15:712-715.
- Yates, T. L. (ed.). 1969. OSU statistical analysis program library. Rev. ed. Corvallis, Oregon State University. Department of Statistics. n. p.
- Yih, C. S. 1963. Stability of liquid flow down an inclined plane. *Journal of the Physics of Fluids* 6:321-334.
- Zhivaikin, L. Y. 1962. Liquid film thickness in film-type units. *International Chemical Engineering* 2:337-341.

APPENDICES

APPENDIX I

Physical Property Determination

PHYSICAL PROPERTY DETERMINATION

Measurement of the Specific Gravity of the Liquids

The specific gravity of each liquid was measured with a Cenco 16752 hydrometer set. Density measurements were accurate to $\pm .5\%$ and reproducible to $\pm .1\%$. In Figures I-1, I-2, I-3, and I-4, the density vs. temperature curves for the four liquids are given.

Measurement of the Viscosity of the Liquids

Liquid viscosity was measured by means of a calibrated Cannon-Fenske viscometer (no. 25-J413). Measurements were accurate to $\pm .5\%$ and reproducible to $\pm .2\%$. The method outlined in the paper by Canon and Fenske (1938) was followed. Viscosity vs. temperature curves are given in Figures I-5, I-6, I-7, and I-8.

Measurement of the Surface Tension of the Liquids with Air

Surface tension was measured by means of a Du Nuoy ring tensiometer. The method given in Daniels, et al. (1962) was followed. Correction factors given by Harkins and Jordan (1930) were employed to account for non-ideal liquid shape and ring dimensions. The measurements were found to be accurate to $\pm 2\%$ and reproducible to $\pm 1\%$. In Figures I-9, I-10, I-11, and I-12, the surface tension vs. temperature curves for the various liquids and air are given.

Measurement of Air Properties

The wet and dry bulb temperatures of the air were taken at the blower inlet. From a psychrometric chart the density of the air was derived. By measuring the column temperature and pressure, and by assuming ideal gas relationships, the actual air density in the column was obtained. The viscosity of the air was obtained from Perry (1963).

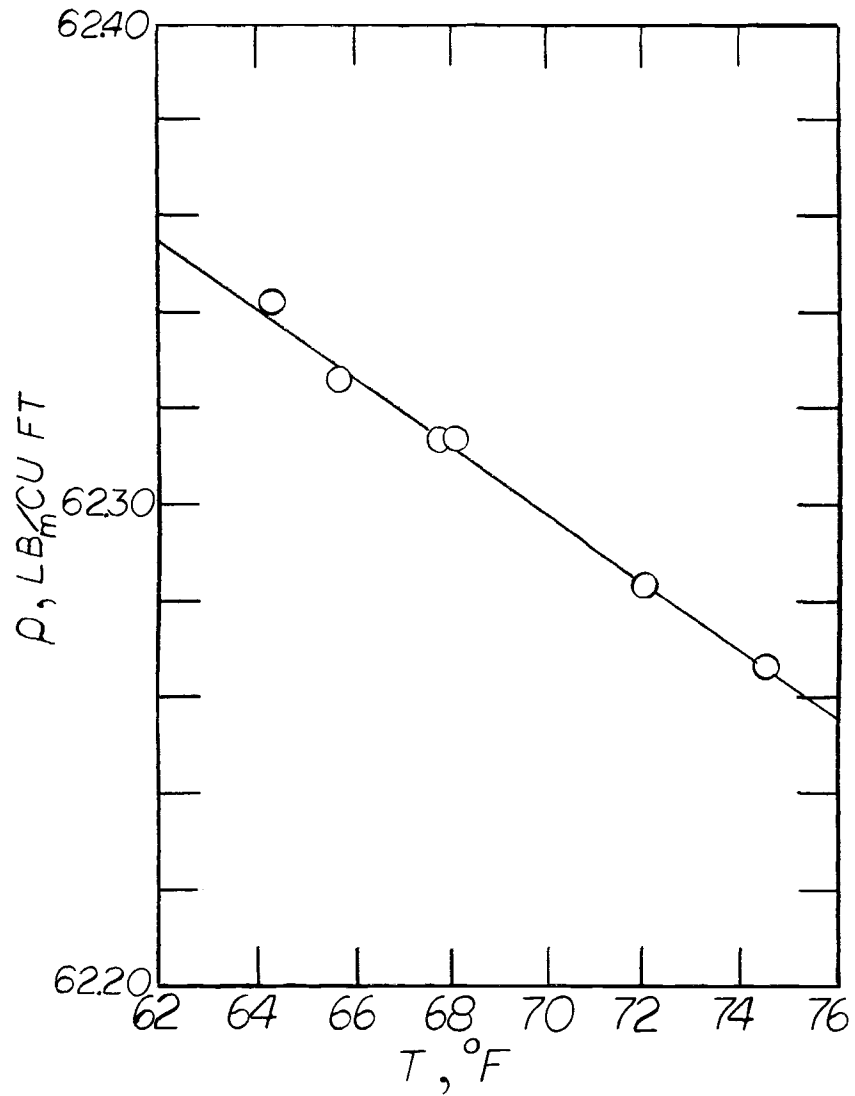


Figure I-1. Density vs. Temperature - water.

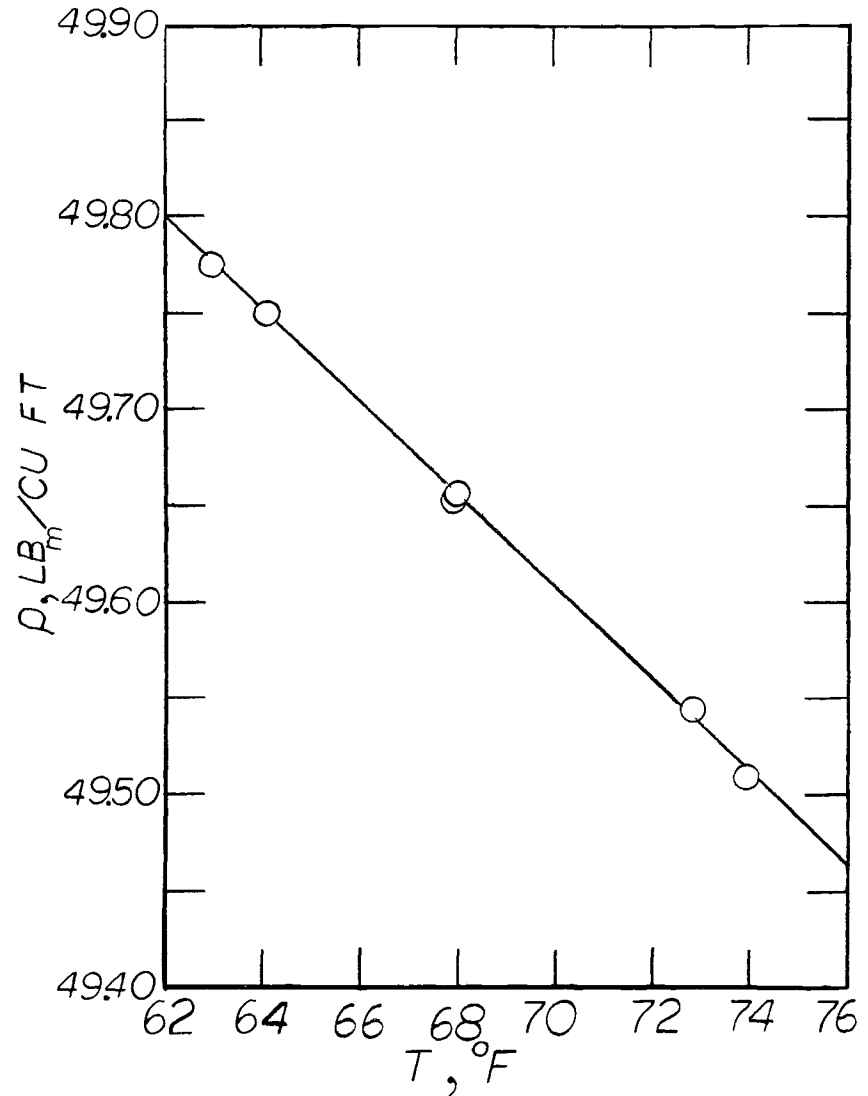


Figure I-2. Density vs. temperature - Shellsolv.

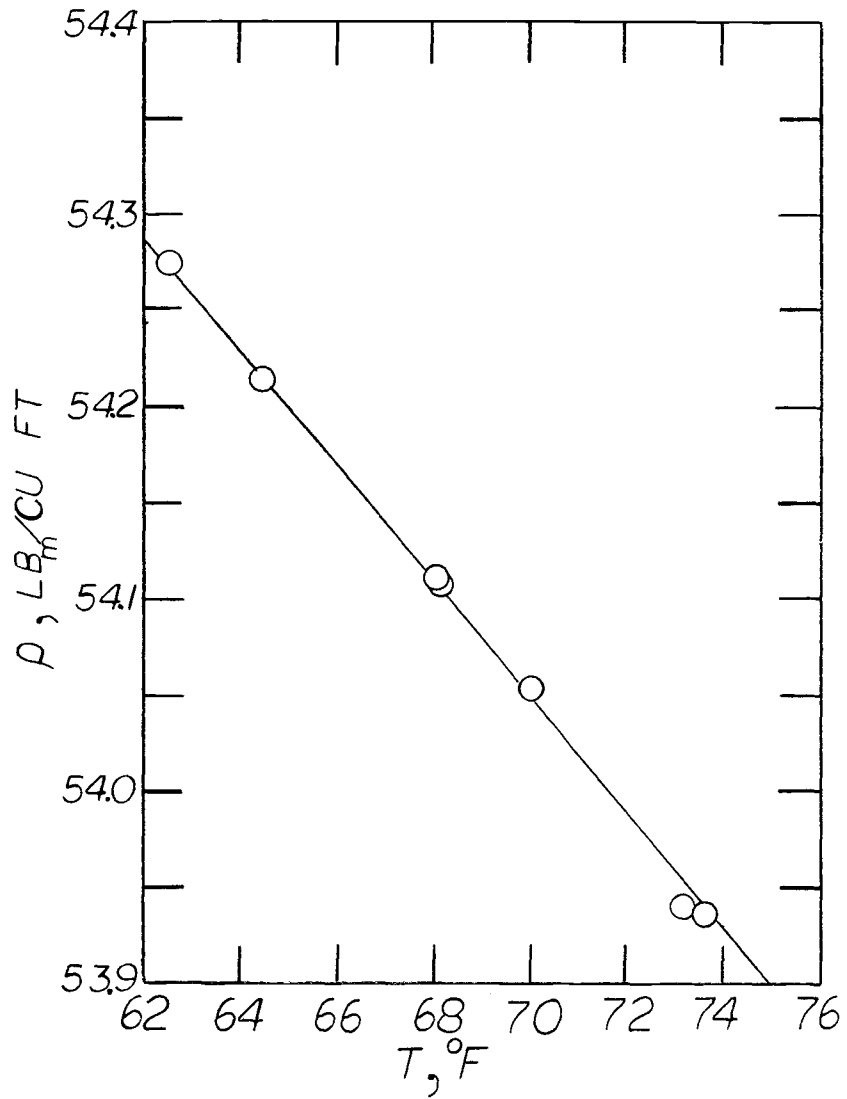


Figure I-3. Density vs. temperature - light oil.

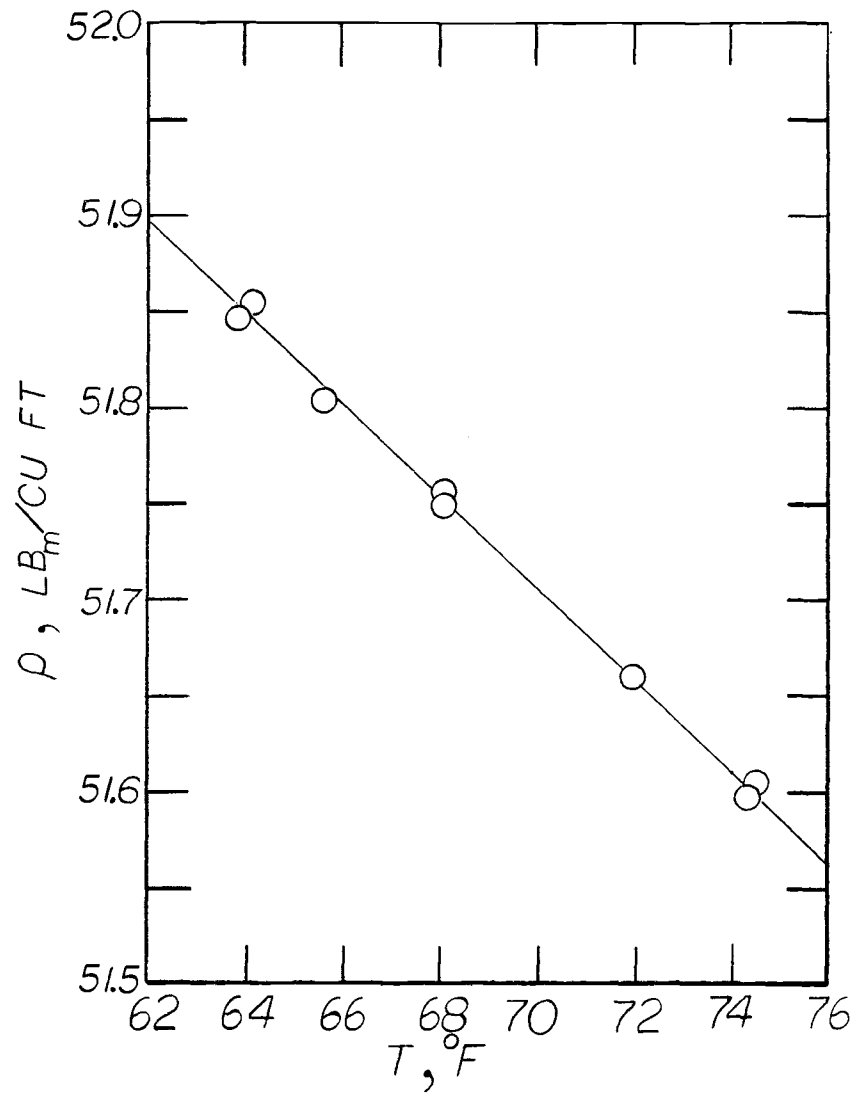


Figure I-4. Density vs. temperature - iso-octyl alcohol.

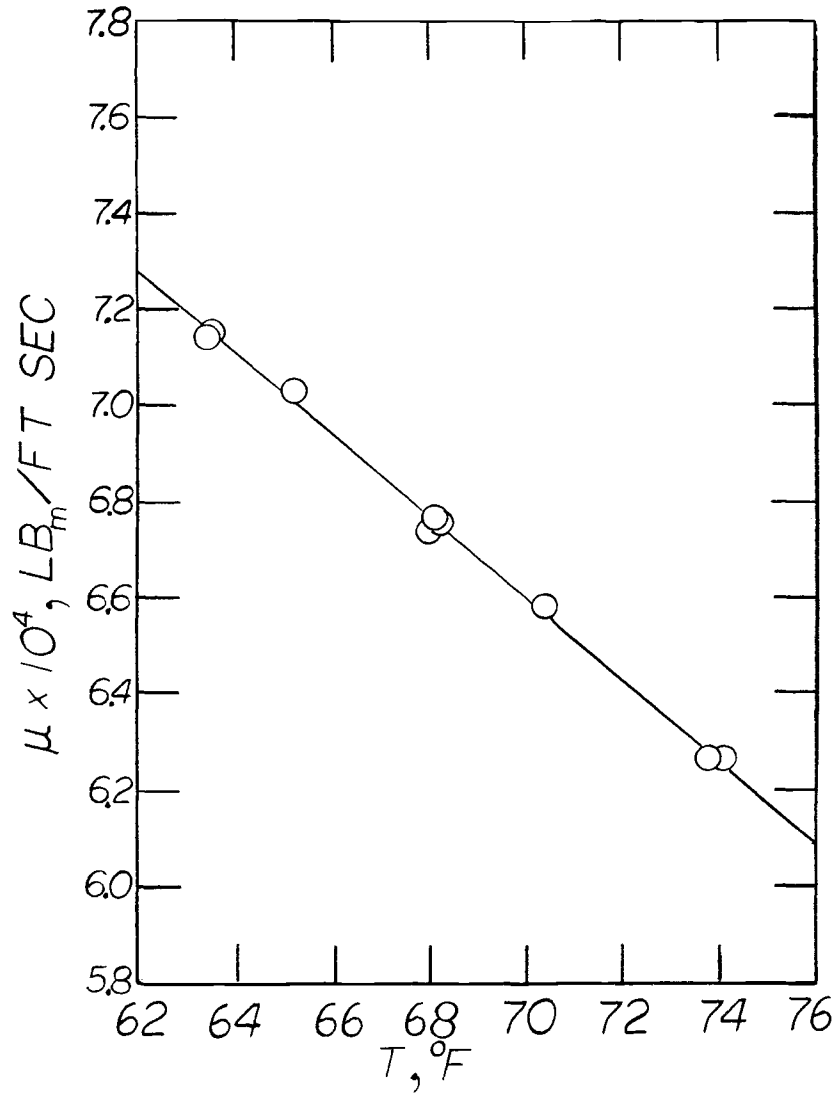


Figure I-5. Viscosity vs. temperature - water.

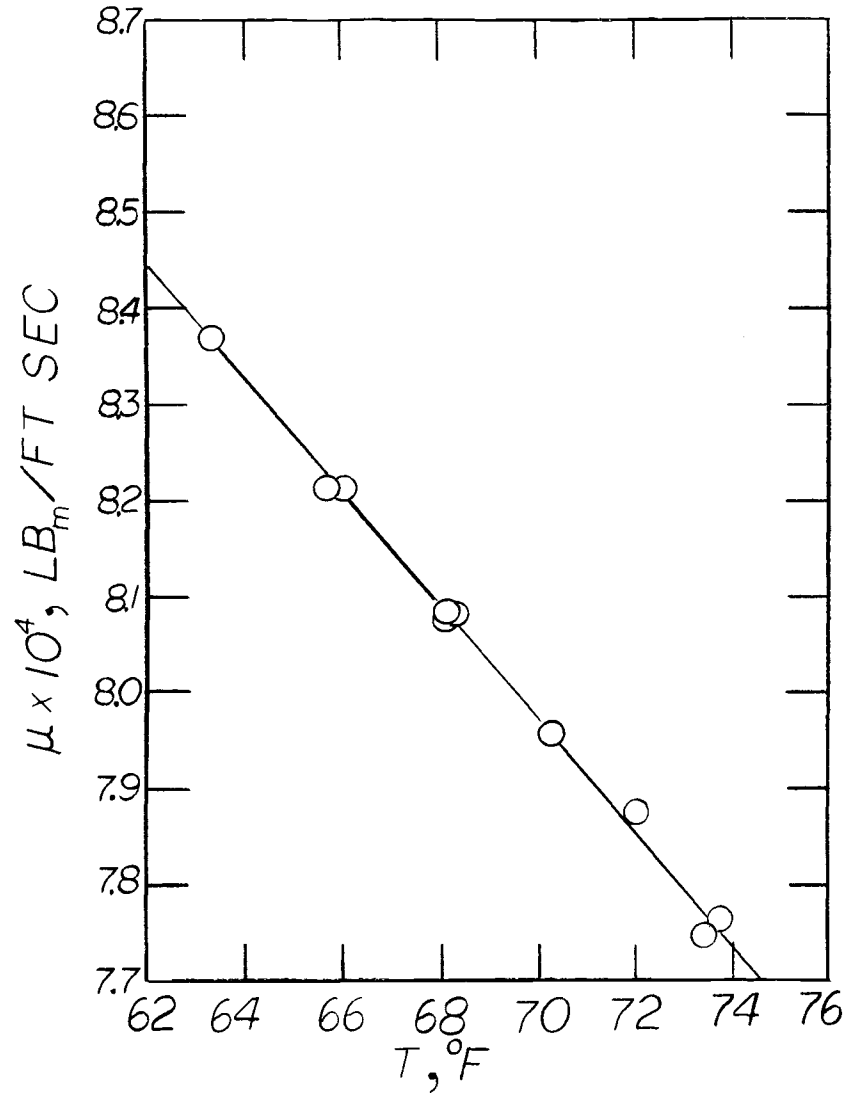


Figure I-6. Viscosity vs. temperature - Shellsolv.

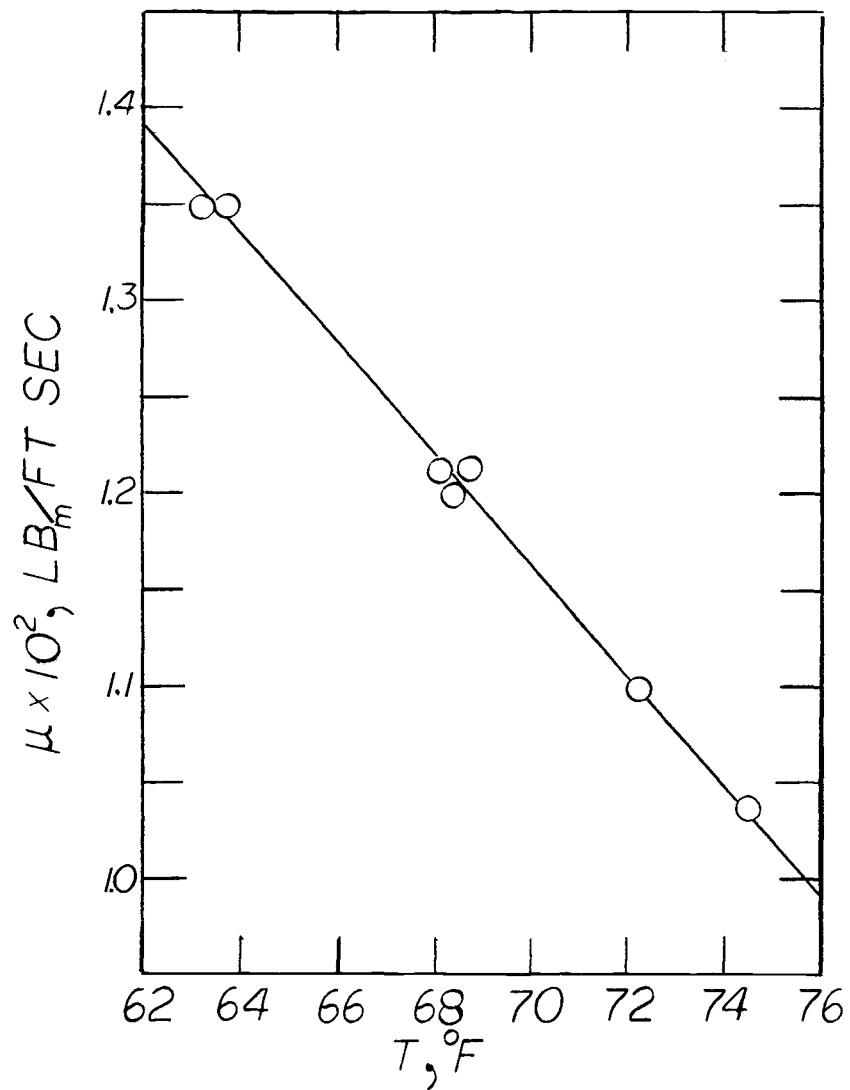


Figure I-7. Viscosity vs. temperature - light oil.

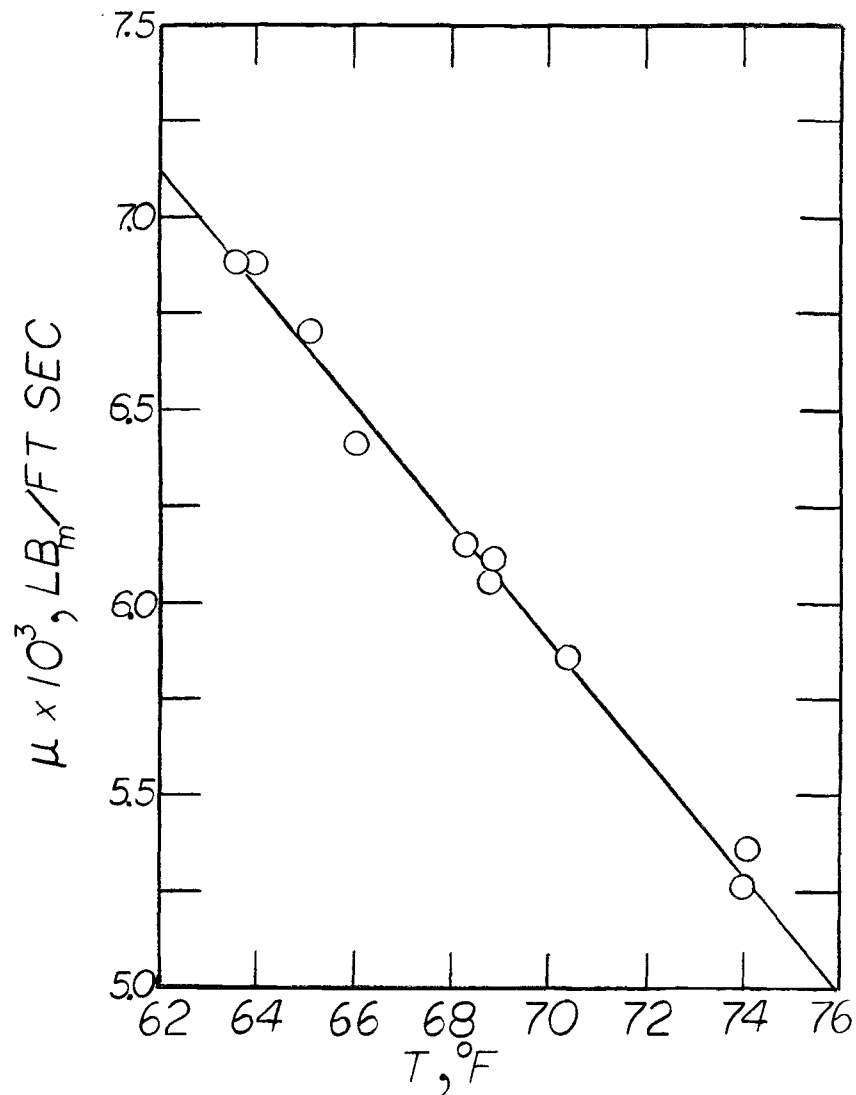


Figure I-8. Viscosity vs. temperature - iso-octyl alcohol.

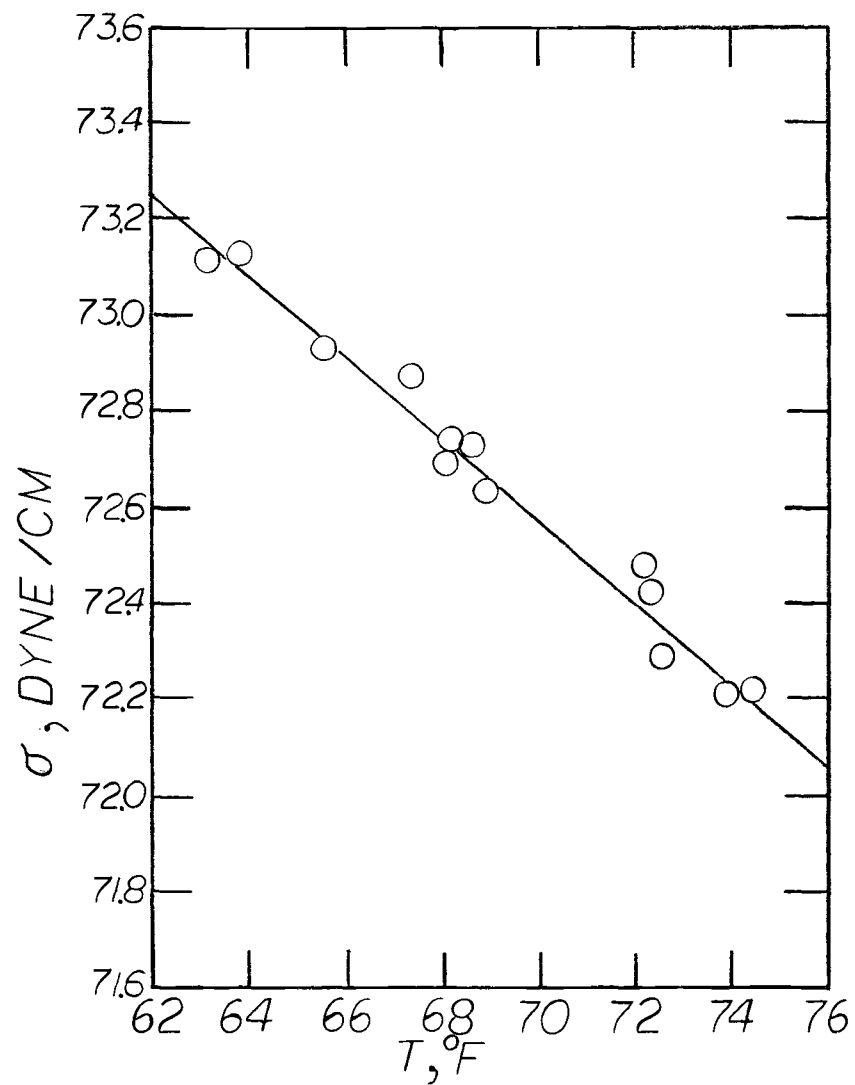


Figure I-9. Surface tension vs. temperature - water.

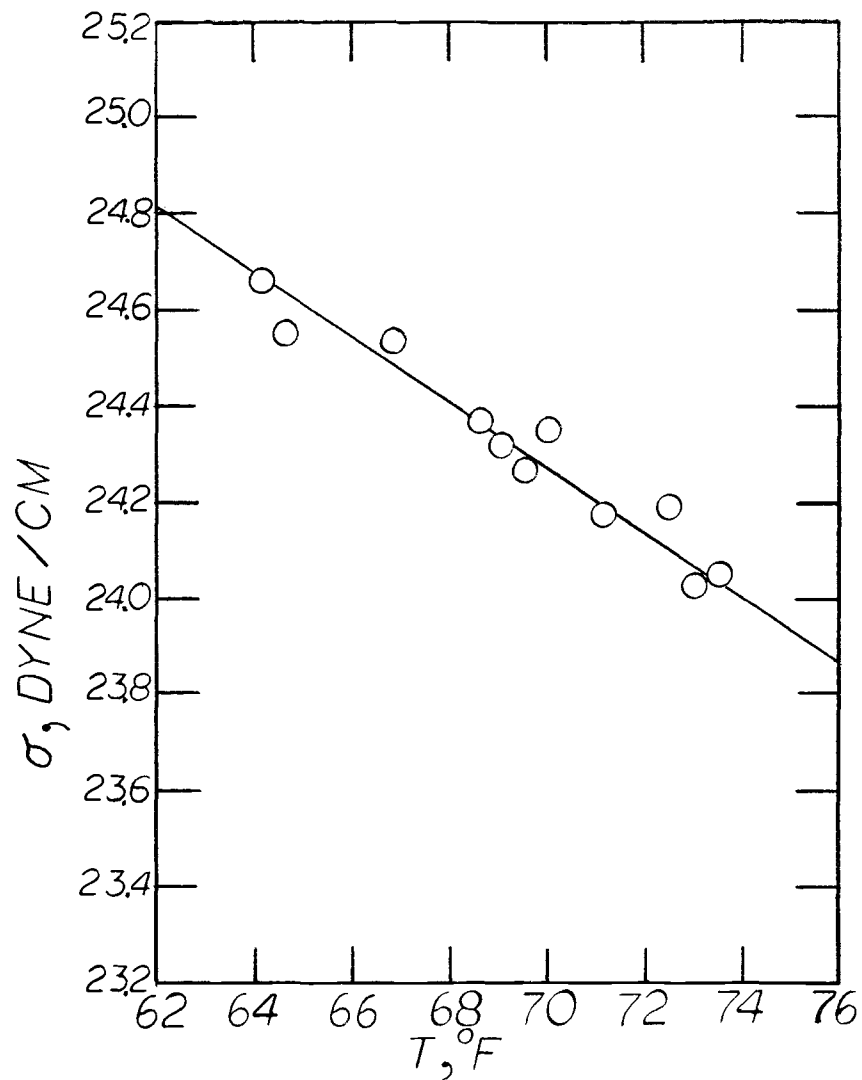


Figure I-10. Surface tension vs. temperature - Shellsoil.

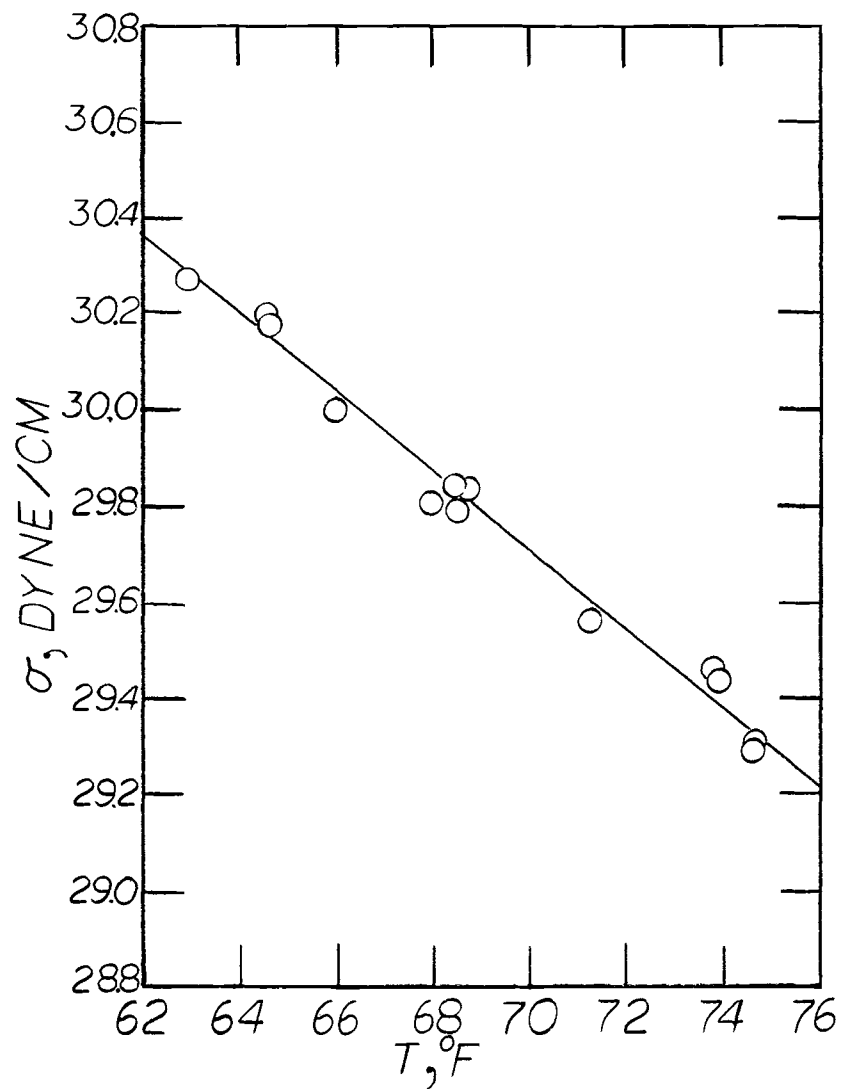


Figure I-11. Surface tension vs. temperature - light oil.

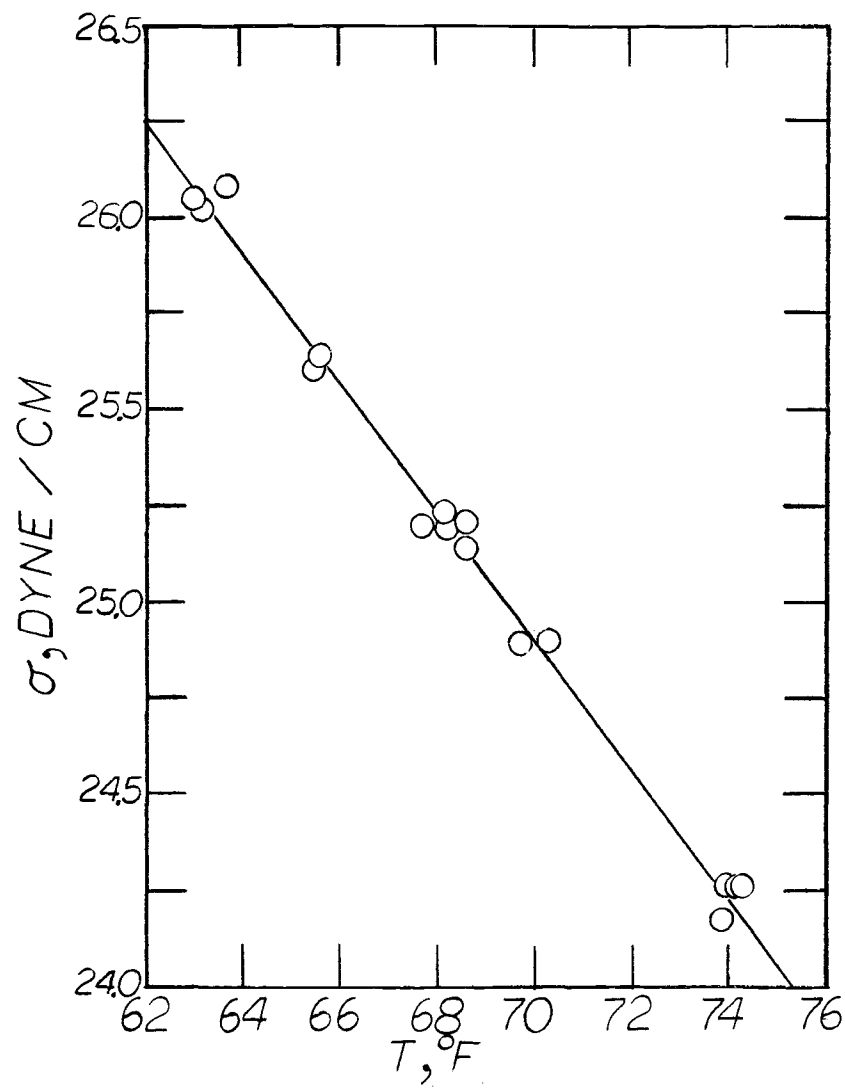


Figure I-12. Surface tension vs. temperature - iso-octyl alcohol.

APPENDIX II

Calibration of the Air Flow Orifice

CALIBRATION OF THE AIR FLOW ORIFICE

The orifice was originally calibrated using a Metric Orifice Flow Prover (Type CR, size 2) manufactured by the American Meter Company. Calibration had also been checked by integration of the velocity profiles, resulting in an accuracy of $\pm 1\%$ (Kim). The calibration was rechecked in the present work by removing the center rod on the annular test section and integrating the measured velocity profile; an accuracy of $\pm 2\%$ was realized. The calibration curve was found for air (at 68 °F and 1 atm) and had to be corrected for operating conditions.

Considering only one orifice and only one gas, and assuming that the pressure drop across the orifice is small compared to the total pressure in the tube, Whitwell (1938) showed that the well-established expression for an orifice can be written in the form

$$Q_A = C \sqrt{R} \sqrt{\frac{T_A}{P_A}} \quad (\text{II-1})$$

where Q_A is volumetric flow rate at T_A and P_A , T_A and P_A represent the system temperature and pressure, R is the reading from a differential manometer, and C is a constant. Rearranging Equation (II-1), one gets

$$Q_A \sqrt{\frac{P_A}{T_A}} = C \sqrt{R} \quad (\text{II-2})$$

If Equation (II-2) is used to plot $Q_A \sqrt{P_A/T_A}$ vs. \sqrt{R} , a universal curve is obtained that is valid for all T_A and P_A . The orifice plate calibration curve has been presented in this form in Figure II-1.

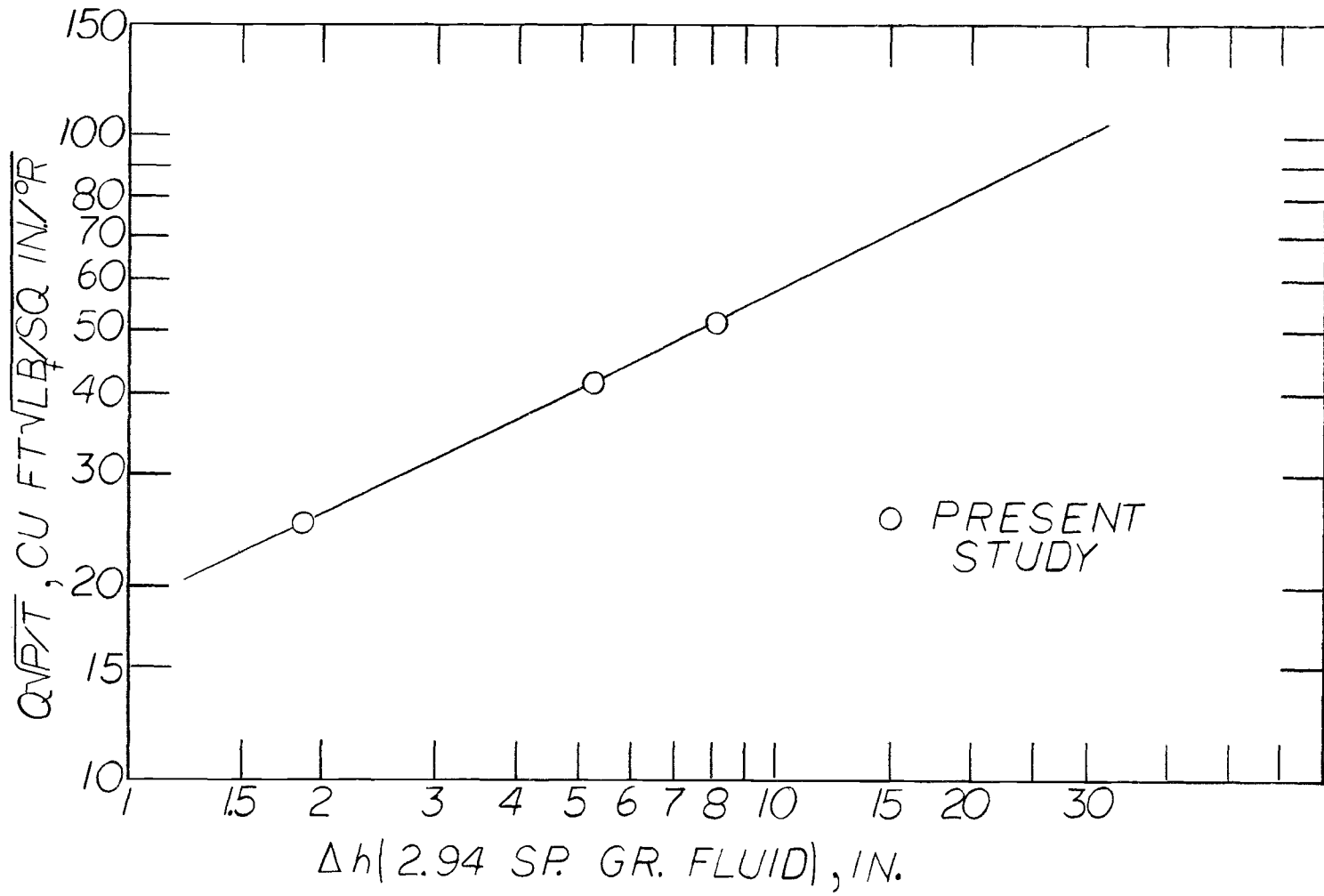


Figure II-1. Air flow orifice calibration curve.

APPENDIX III

Shear Stress at the Outer Wall

SHEAR STRESS AT THE OUTER WALL

Ludwig (1950) showed that at a smooth wall, in turbulent flow, the velocity profile next to the wall is dependent only upon the physical properties of the flowing medium and the shear stress at the wall. He described a heating element that could directly measure the skin friction. Although the method was fairly satisfactory, it required a tedious calibration.

Ludwig and Tillmann (1950) utilized the method of Ludwig and established that in a limited region near the surface, independent of pressure gradient and upstream disturbances, the following relation holds:

$$\frac{u}{\sqrt{\tau_w/\rho}} = f\left(\sqrt{\tau_w/\rho} \frac{y}{\nu}\right) \quad (\text{III-1})$$

where u is the velocity at a distance y from the wall and τ_w is the wall shear stress. If this relation is true, then there exists a region near the surface in which conditions are functions only of the skin friction, the relative physical properties, and a suitable length.

Preston (1954) adopted this idea and attempted to find a more convenient form for Equation (III-1). Since the velocity is related to the difference in kinetic and static pressure readings at a point, Preston developed the relation

$$(P_k - P_s) \frac{d^2}{2\rho\nu} = F\left(\frac{\tau_w d^2}{2\rho\nu}\right) \quad (\text{III-2})$$

where P_k is the kinetic pressure recorded by a pitot tube on the wall, P_s is the static pressure at the wall, and d is the diameter of the pitot tube. Calibration entails finding the function F , and Preston arrived at the following expression for a pipe:

$$\log_{10} \frac{\tau_w d^2}{4\rho\nu} = 2.604 + \frac{7}{8} \log_{10} \frac{(P_k - P_s)}{2\rho\nu} d^2 \quad (\text{III-3})$$

where τ_w was calculated from experimental pressure gradient measurements.

Calibration in the present system was carried out in the annulus with air flow alone. The wall shear stress was determined experimentally from the pressure gradient and the point of maximum velocity using Equation (82)

$$\tau_2 = \frac{r_2^2 - r_m^2}{2r_2} \frac{-dP_f}{dx} \quad (82)$$

The values of τ_2 were then plotted against the manometer readings resulting from the difference of the kinetic pressure (the Preston tube on the wall) and the static pressure (the upper static pressure tap).

The calibration curve can be seen in Figure III-1.

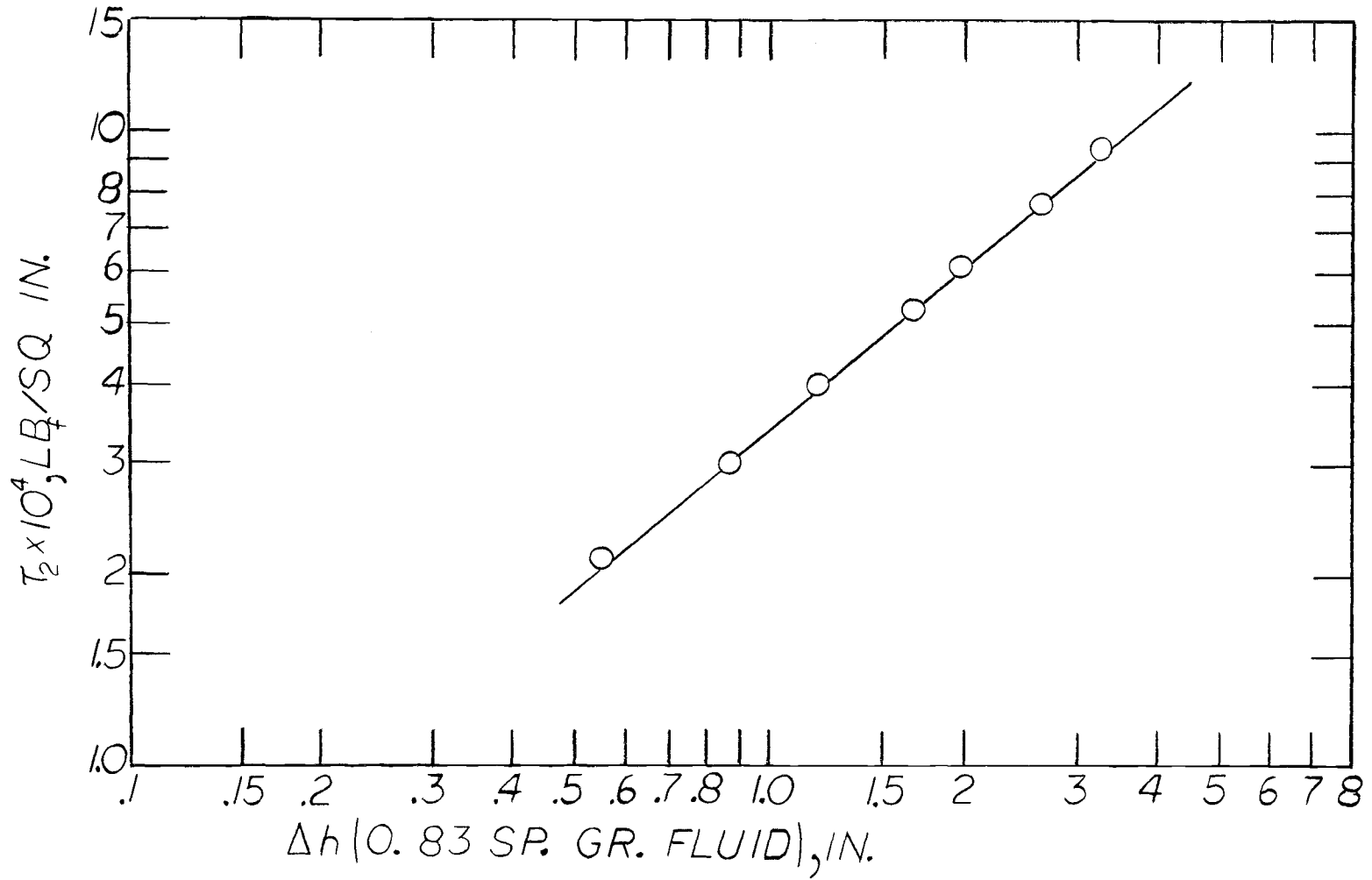


Figure III-1. Preston tube calibration.

APPENDIX IV

Photographic Methods and Data

PHOTOGRAPHIC METHODS AND DATA

Cooper, Hewitt and Pinchin described the ways in which photographic methods have been used by the United Kingdom Atomic Energy Authority research group at Harwell, England. Most of the photographic problems discussed therein are related to the use of a circular tube in the film flow studies. Light refracted through liquid on the tube wall presented a considerable number of obstacles which the present system avoids because the outer annular wall remains dry.

Hyzer (1962) presented an excellent discussion of high-speed photography in engineering and science. He enumerated the relations needed to predict the required camera settings and the necessary frame speeds (to sufficiently stop the subject). The photographic procedure used in the present work is given below:

1. The maximum speed of the waves to be photographed was estimated from theoretical predictions; the estimated speed, S , was found in ft/min.
2. The width, W , of the viewing field to be captured on the film was estimated in inches.
3. Allowing for an image blur of .0002 in., the minimum number of frames per sec required was derived using the expression

$$F_{\min} = \frac{12S}{W}$$

4. The optimum film speed, as recommended by Hyzer, will therefore be three to six times F_{\min} . For this study, three times was used.
5. With a Yashica (model YEM55) light meter, readings were taken of the waves (which were backlighted by a 150 watt photo flood lamp). Readings were taken at ASA 40 and ASA 160, and diaphragm settings, f vs. exposure time, t_e were recorded.
6. Knowing F (from step 4), the exposure time was found using the relation $1/t_e = 3F$, which is characteristic of the WF14S model.
7. Once the exposure time was calculated, the diaphragm setting was determined by using the light meter readings and the relation

$$\frac{f_1}{f_2} = \sqrt{\frac{t_{e1}}{t_{e2}}}$$
8. The camera was then placed in position and focused on the reference wires using the parallax method. The camera was clamped in place once the focus was realized.
9. The film was loaded and voltage to the camera was set on the "Goose" control unit.
10. With only air flowing in the tube, the camera was turned on briefly and then turned off. By taking this preliminary step

the distance from the reference wires to the wall could later be determined. The liquid was then allowed to flow and, once steady state was attained, the remainder of the roll was exposed.

A total of 18 rolls of film were taken: six rolls depicted the water film, six rolls the Shellsolv 345, four rolls the iso-octyl alcohol, and two rolls the light oil. Each roll of film was analyzed in the following manner:

1. The total number of timing marks and frames were counted, the first and last frame having been marked.
2. The total number of time marks was multiplied by $1/120$ to give the total duration of the film, θ (sec), and the number of frames were multiplied by the exact film width, W , to give the film length between time marks. W was determined by measuring the projected size of the reference wires and the projected frame size. Since the actual reference wire size was known, W was easily obtained.
3. Since the total time of the film θ was known, the film could be run at low speed and the number of waves could be counted between the first and last marked frames, N_W .
4. The wave frequency, f , which suggests how often the cycle repeats itself in a unit of time, was calculated using the relation $f = N_W/\theta$. By measuring the number of peaks in a

known distance of film, the wave number, k , was found.

The wavelength, λ , was calculated by taking the reciprocal of the wave number.

5. The average wave speed, or celerity, c , was then calculated using the expression $c = f\lambda$.
6. The initial section of the photographic film, in which only air flowed in the tube, was projected onto the screen and the distance from the reference wires to the inner wall was determined.
7. Twenty-five frames were projected at random on the screen and traced on paper. The tracings were cut out and weighed to determine average film thicknesses.

The photographic data can be found in Table IV-1.

Table IV-1. Photographic settings.

| Liquid | Liquid Flow Rate lb _m /min | Air Flow Rate lb _m /hr | Film | Voltage Applied | Diaphragm f |
|----------------|--|--------------------------------------|--------|-----------------|----------------|
| Water | .305 | 875.51 | Plus-X | 40 | 2.0 |
| Water | .305 | 1354.99 | Plus-X | 70 | 2.0 |
| Water | .305 | 2069.48 | Tri-X | 100 | 2.8 |
| Water | .59 | 893.44 | Plus-X | 70 | 2.0 |
| Water | .59 | 1364.66 | Plus-X | 70 | 2.0 |
| Water | .59 | 2091.02 | Tri-X | 135 | 2.4 |
| Shellsohv | .305 | 982.05 | Plus-X | 40 | 5.6 |
| Shellsohv | .305 | 1398.25 | Tri-X | 70 | 5.6 |
| Shellsohv | .305 | 1997.37 | Tri-X | 100 | 4.0 |
| Shellsohv | .59 | 991.61 | Plus-X | 70 | 5.6 |
| Shellsohv | .59 | 1411.64 | Tri-X | 80 | 5.6 |
| Shellsohv | .59 | 2091.62 | Tri-X | 135 | 4.0 |
| Iso-octyl Alc. | .10 | 1270.29 | Tri-X | 45 | 8.0 |
| Iso-octyl Alc. | .10 | 1948.36 | Tri-X | 80 | 4.0 |
| Iso-octyl Alc. | .305 | 1357.67 | Tri-X | 60 | 7.0 |
| Iso-octyl Alc. | .305 | 1943.79 | Tri-X | 100 | 4.0 |
| Light Oil | .10 | 1331.35 | Plus-X | 45 | 5.6 |
| Light Oil | .10 | 1954.89 | Plus-X | 75 | 5.2 |

APPENDIX V

Entrainment

ENTRAINMENT

The annular region of two-phase flow can be described as that region in which the gas and liquid flow parallel to each other as totally separate phases with a single interface between them. In any duct, the liquid flows on the duct wall as a film, and the gas occupies the remainder of the duct.

In annular flow, if the liquid flow rate is held constant and the gas velocity is reduced, the liquid film will break up and become entrained in the gas phase. In pipe flow, the liquid will form bridges across the gas core. When one wall remains dry as in the present experimental system, the liquid will simply break away from the liquid film and impinge upon the dry wall. If only small numbers of liquid droplets impinge upon the outer wall, they will immediately be re-entrained into the gas phase. However, as the number of liquid droplets impinging on the outer wall increases, the liquid will begin to flow on the outer wall as a film. Further reduction of the gas flow will result in down flow of the liquid film, flooding, and subsequently, commencement of the churn flow regime.

In another case of annular flow, if the liquid flow rate is again held constant, but the gas velocity increased rather than decreased, the liquid film will become thinner and the wave frequency on the surface will increase. Further air velocity increase will force liquid

to be blown off the tops of the waves and become entrained in the gas phase. If the gas velocity is increased, the liquid film will ultimately be broken up and the liquid will become entrained, resulting in a homogeneous mist which will flow in the duct.

Collier and Hewitt (1961) studied air-water climbing film flow. The film thicknesses in their study were of the same order of magnitude as in the present study. From their results it can be deduced that significant entrainment of the liquid does not occur until a certain pressure drop is achieved. This two-phase pressure drop, at which appreciable entrainment starts to occur, is approximately twice the pressure drop which would have occurred had the gas been flowing alone in the test section.

Van Rossum used water, aqueous solutions and oils to investigate entrainment in horizontal film flow. His method of observing the onset of entrainment was a visual one: he looked through the end of the tube while increasing the air velocity. The mean air velocity at which he first observed liquid droplets coming from the entire liquid surface he designated as the critical velocity V_{CR} . For each liquid there was a V_{CR} below which no entrainment occurred. He also found that V_{CR} was a hyperbolic function of the liquid film thickness with entrainment being higher for thick films. He concluded that V_{CR} was only a function of surface tension and gave the approximate

expression

$$V_{CR} \cong 0.82\sigma \quad (V-1)$$

where V_{CR} is measured in ft/sec and σ in dyne/cm. His data deviated as much as 100% from this relation.

Van Rossum also presented plots showing that, for each gas velocity, there is a minimum liquid flow rate per unit width required for the onset of entrainment. Furthermore, he showed that this threshold liquid flowrate decreases as the viscosity of the liquid increases.

Hall-Taylor and Hewitt observed roll waves inside a circular tube and noted that liquid droplets were impinging upon the water surface preceding the roll waves. Since the initial appearance of these roll waves closely corresponded to the onset of entrainment, they suggested the possibility that roll waves are responsible for entrainment and that liquid entrainment coincides with the first occurrence of roll waves.

Zhivaikin (1962) did experimental work on film flow and upward and downward co-current gas-film flow using water and aqueous glycerine solutions. Data were obtained which showed the onset of entrainment. It was found that the critical gas velocity depends upon both the liquid flow rate and the liquid physical properties, that is,

$$V_{CR} = f(Q_L, \mu_L, \rho_L, \sigma) \quad (V-2)$$

where Q_L is a liquid flow rate per unit width. Using Equation (V-2), dimensional analysis yields

$$\frac{V CR^{\mu} L}{\sigma} = A Re^n \quad (V-3)$$

where $Re = 4Q_L / \nu_L$. The breakup and entrainment of the liquid film in upward flow follows the relation

$$Re = 164 \left(\frac{V CR^{\mu} L}{\sigma} \right)^{-.2} \quad (V-4)$$

With a set of experiments, Wallis and Steen (1964) tried to determine the point of transition from annular to annular-mist flow. A sampling probe in the gas phase was used to measure entrained liquid droplets. The experimenters noted that droplets entrained by the air stream came from the tops of the large roll waves. They found no proof that the appearance of roll waves coincided with the onset of entrainment as was reported by Hall-Taylor and Hewitt. The percent entrainment increased with increasing liquid flow rate or air velocity. The percent entrainment is defined as

$$E = \frac{j_{LCL}}{j_L} \quad (V-5)$$

where j_{LCL} is the superficial liquid velocity at the tube centerline (as measured with a sampling probe) and j_L is the total superficial

liquid velocity. Note that for pure annular flow $E = 0$ and for pure mist or homogeneous flow $E = 1$.

In addition, they agreed with Van Rossum that V_{CR} is approximately proportional to surface tension. They arrived at the expression

$$V_{CR} \cong 1.25\sigma \quad (V-6)$$

For thick films (on the order of 1 cm and larger), Wallis and Steen suggested the following criterion for the onset of entrainment:

$$\frac{j_G \mu_G}{\sigma} \left(\frac{\rho_G}{\rho_L} \right)^{\frac{1}{2}} > 2.46 \times 10^{-4} \quad (V-7)$$

This relation is valid only when viscous forces in the film are not significant. For very thin films, the liquid layer will be much more stable; hence, a lower amount of entrainment will result.

Wallis and Steen reviewed the work of several investigators and noted that, qualitatively, the onset of entrainment can be detected by the appearance of drops in the gas stream or by the appearance of droplets which strike the unwetted wall of the duct. Sampling probes or other experimental apparatus are necessary to obtain quantitative measurements.

In the present study, the only entrainment that was detected occurred at low air flow rates. For all liquids and all liquid flow rates, there existed an air velocity below which liquid was entrained.

At low air velocity the surface was extremely irregular and exhibited waves of a very large amplitude slowly climbing. The tops of these waves could be seen to break away from the liquid film and become entrained, ultimately striking the liquid-free outer tube. At the onset of entrainment, the liquid droplets striking the outer wall were extremely small and struck at a rather low frequency. The drop impingement on the outer wall was actually detected by observing the streaks of liquid striking the outer wall at high speeds.

For the low viscosity liquids (water and Shellsolv), the droplets remained on the wall only a fraction of a second, whereupon they were re-entrained into the airstream. As the gas flow was reduced, the liquid struck the outer wall in larger drops. A further decrease in air velocity would cause the film to climb on both walls.

The high viscosity liquids (iso-octyl alcohol and light oil) were far more susceptible to low air velocity entrainment. That the higher viscosity liquids flow in thicker films and do not flow as rapidly as the low viscosity liquids probably explains this susceptibility. The larger relative velocity between the air stream and the liquid film caused the liquid to be entrained more readily. The high viscosity liquids, especially the light oil, also tended to stick to the outer wall and were therefore not re-entrained. At the low flow rates, the outer wall would take on a very foggy appearance, thus presenting some experimental problems. If the outer wall became covered with a mist,

resulting in a rough wall condition, the shear stress at the outer wall would become larger than in a smooth wall condition; the rough wall would thus displace the velocity profile toward the center tube.

Once the outer wall was fogged with liquid droplets, the only way to clean the wall was to flush the column with a solvent. Shellsolv was therefore used to rinse the column after each run with the light oil. After the Shellsolv, air was blown through the column in order to dry it. Data were then taken for air alone and checked to insure that the walls were completely clean. In more cases than not, several rinses were necessary. It should be noted that the oil sticking to the outer wall during a run may have rendered some of the data for light oil questionable.

At the highest gas velocities used, entrainment was not detected. In the work of Kim, Sutey (1967) and B. Scott, the centering screw arrangement disturbed the liquid film to such a degree that the minimum entrainment realized was larger than that which occurred at any time in the present experiment.

In this study the effect of surface tension on the low air velocity entrainment did not seem to be as significant a variable as did the viscosity. It would seem that the transition from annular to churn flow is dependent upon viscosity and the transition from annular flow to mist dependent upon surface tension.

Quantitative description of entrainment is not a possibility of the present study. However, it was generally observed that liquid entrainment was significant at a gas Reynolds number of 8×10^4 and below. This is a very rough estimate.

All of the previous studies cited in this section are concerned with thick film flow; therefore, the correlations presented underpredict the critical gas velocity for the present work. It is useful, however, to compare the agreement among the correlations. The comparisons are given in Table V-1.

The critical velocity predicted by Equations (V-1), (V-6) and (V-7) are all of the same order of magnitude. In every case they predict that entrainment should occur in the present study. Equation (V-4) given by Zhivaikin is extremely erratic in predicting V_{CR} . In this expression the term v_L/Q_L is raised to the fifth power causing large variations in the value of V_{CR} .

Table V-1. Prediction of V_{CR} .

| Liquid | Liquid Flow Rate lb/min | V_{CR} ; ft/sec | | | |
|----------------|-------------------------------|-------------------|-----------|-----------|-----------|
| | | Eq. (V-1) | Eq. (V-4) | Eq. (V-6) | Eq. (V-7) |
| Water | .305 | 59.65 | 1397.54 | 90.94 | 91.37 |
| Water | .590 | 59.65 | 51.59 | 90.94 | 91.37 |
| Water | .755 | 59.65 | 15.04 | 90.94 | 91.37 |
| Shellsolv | .305 | 20.01 | 971.97 | 30.5 | 27.35 |
| Shellsolv | .590 | 20.01 | 35.88 | 30.5 | 27.35 |
| Shellsolv | .755 | 20.01 | 10.45 | 30.5 | 27.35 |
| Iso-octyl Alc. | .10 | 20.75 | $> 10^7$ | 31.62 | 29.01 |
| Iso-octyl Alc. | .305 | 20.75 | $> 10^6$ | 31.62 | 29.01 |
| Light Oil | .10 | 24.52 | $> 10^8$ | 37.38 | 34.60 |

APPENDIX VI

Freely Falling Liquid Film

FREELY FALLING LIQUID FILM

Of all the film flow systems, freely falling liquid film has received the most attention. Many of the more important studies have been mentioned elsewhere in this paper. It is proposed that, using the ideas of several of these investigations, it is possible to arrive at a falling film solution that matches the experimental data for wave celerity as well as, or perhaps better than, any solutions given in the literature.

Equation (45) given in the theoretical development for a climbing film is rewritten below:

$$\frac{\partial u}{\partial t} + u \frac{\partial u}{\partial x} + v \frac{\partial u}{\partial y} = \nu \frac{\partial^2 u}{\partial y^2} + 3\nu \frac{\partial^2 u}{\partial x^2} - \frac{1}{\rho} \frac{dP_G}{dx} + \gamma \frac{\partial^3 h}{\partial x^3} - g \quad (45)$$

For a falling film in the presence of a stagnant gas, the gas pressure can be neglected. Changing the sign on the gravity term,

$$\frac{\partial u}{\partial t} + u \frac{\partial u}{\partial x} + v \frac{\partial u}{\partial y} = \nu \frac{\partial^2 u}{\partial y^2} + 3\nu \frac{\partial^2 u}{\partial x^2} + \gamma \frac{\partial^3 h}{\partial x^3} + g \quad (VI-1)$$

As pointed out by Semenov, for very thin falling films in the low liquid Reynolds number region, the viscous effects in the film should be considerably larger than the inertia terms. Making this assumption,

(VI-1) becomes

$$\frac{\partial u}{\partial t} = \nu \frac{\partial^2 u}{\partial y^2} + 3\nu \frac{\partial^2 u}{\partial x^2} + \gamma \frac{\partial^3 h}{\partial x^3} + g \quad (VI-2)$$

The boundary conditions for this system are

$$\text{at } y = 0 \quad u = v = 0$$

$$\text{at } y = h(x, t) \quad \frac{\partial u}{\partial y} = 0$$

From this point, the solution is identical to that used in the climbing film solution. The final differential equation is

$$\frac{h_o^2}{We} \frac{d^3 \phi}{dz^3} + \frac{9}{2} (\alpha-1) \frac{\nu}{u_o} \frac{d^2 \phi}{dz^2} + \frac{3}{2} \alpha(\alpha-1) \frac{d\phi}{dz} + (3-\alpha) \frac{3\nu}{h_o u_o} \phi + \frac{g}{u_o} - \frac{3\nu}{h_o u_o} = 0 \quad (\text{VI-3})$$

For a periodic solution to exist, the constant term must vanish; thus,

$$\frac{g}{u_o} - \frac{3\nu}{h_o u_o} = 0$$

or

$$h_o = \sqrt{\frac{3\nu u_o}{g}} \quad (\text{VI-4})$$

which is the Nusselt film thickness solution, Equation (33). The remainder of the equation will yield the appropriate periodic solution given by Equation (57) when

$$1 = \frac{\left(\frac{h_o^2}{We}\right) \left[(3-\alpha) \frac{3\nu}{h_o u_o}\right]}{\left[\frac{9}{2} (\alpha-1) \frac{\nu}{u_o}\right] \left[\frac{3}{2} \alpha(\alpha-1)\right]} \quad (\text{VI-5})$$

which, when rearranged, gives

$$We = \frac{4}{9} \frac{3-\alpha}{\alpha(\alpha-1)^2} \quad (VI-6)$$

The wave number is of the form

$$kh_o = \sqrt{\frac{3}{2} We \alpha(\alpha-1)} \quad (VI-7)$$

and the wavelength

$$\frac{\lambda}{h_o} = \frac{2\pi}{\sqrt{\frac{3}{2} We \alpha(\alpha-1)}} \quad (VI-8)$$

Several investigators have obtained data for We vs. α for the falling liquid film. The data gathered by a few experimenters and the models presently available in the literature are presented in Figure VI-1. It can be seen from Figure VI-1 that the present model approximates the data more closely than any of the other models. The theories of Yih, Hanratty and Hershmann, Kapitza, and Benjamin all predicted that α is constant and equal to three. All of these were solutions for low profile disturbances, and they presented a limiting solution to the falling film problem which has apparently been verified. The model of Massot, Irani, and Lightfoot was the first to predict the reduction of α with increasing We . Although the analysis was in error, the ideas presented by these three investigators aided Gollan and Sideman in finding their solution.

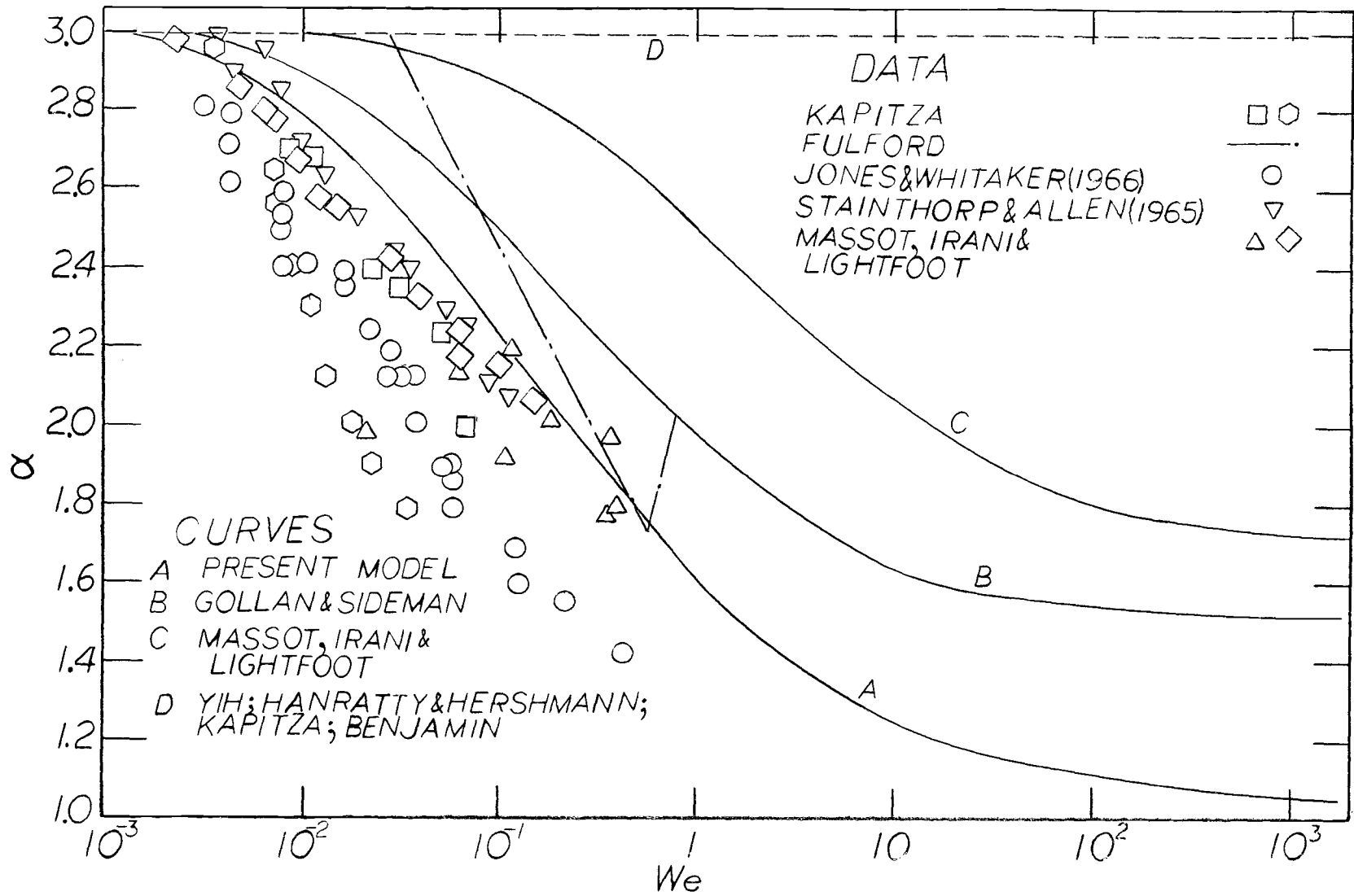


Figure VI-1. We vs. α - falling film.

It is interesting to examine the asymptotic limits of Equation (VI-8). As $We \rightarrow 0$, say as $\sigma \rightarrow \infty$, the wavelength $\lambda \rightarrow \infty$. This suggests that a surface displaced an infinitesimal distance from its equilibrium will be immediately restored to the minimum free energy state. For $\sigma \rightarrow \infty$, $We \rightarrow \infty$, the wavelength $\lambda \rightarrow 0$. This seems reasonable upon examination. Any point on the surface that is displaced from its equilibrium position will have no restoring force acting to return it to a "flat" surface. All such points on the surface will essentially form spikes, and, since no restoring forces exist to broaden the spikes and dissipate the energy, they will be directly adjacent to one another, giving rise to a wavelength of zero.

Since the present model and that of Gollan and Sideman both exhibit good agreement with experimental data, Yih's analysis regarding the controlling effect of surface waves and interfacial velocities on film characteristics would seem to be substantiated.

The author has examined several models for the cases of falling and climbing flow. In each model, assumptions were made concerning the significance of the various terms in the original differential equations and in the boundary conditions. Two solutions were obtained for each model, each solution being the result of one of the following techniques: (1) integrating the motion equation across the film as done by Kapitza, or (2) setting the terms in the motion equation equal to their interfacial values as done in the analyses of Gollan and Sideman

and by the author. Although the second solution technique will yield models which are closer to the experimental values, this does not give it an overwhelming advantage. The important thing, it is felt, is not the 10% or even 50% better accuracy obtained with one model compared to another, but the fact that the model predicts that the dimensionless wave celerity decreases as We is increased. Only models which include the term $\partial^2 u / \partial x^2$ in their analysis will show such a trend. Most of the solutions treating the liquid film as laminar will use boundary layer arguments to neglect this term, including the present climbing film solution. It appears to the author that, in light of the above findings, at least for the falling film, where data can be of a quantitative nature, the normal boundary layer assumptions employed may be incorrect.

APPENDIX VII

Tables of Data

Table VII-1. Air data.

| Run No. | Q_G ft ³ /min* | W_L lb _m /min | W_G lb _m /hr** | \bar{U}_G ft/sec | $\frac{dP_G}{dx} \times 10^3$ lb _f /in ³ | $\tau_2 \times 10^4$ lb _f /in ² | $\frac{y_m}{r_2 - r_1}$ |
|---------|--------------------------------|-------------------------------|--------------------------------|-----------------------|---|--|-------------------------|
| o-1 | 186.5 | 0 | 854.9 | 70.00 | .3969 | 2.183 | .391 |
| o-2 | 443.3 | 0 | 2152.5 | 156.37 | 1.897 | 9.397 | .392 |
| o-3 | 351.2 | 0 | 1684.0 | 126.87 | 1.230 | 6.053 | .415 |
| o-4 | 273.5 | 0 | 1287.5 | 100.36 | .779 | 4.007 | .393 |
| o-5 | 320.1 | 0 | 1527.6 | 116.39 | 1.044 | 5.298 | .370 |
| o-6 | 400.1 | 0 | 1949.2 | 142.63 | 1.557 | 7.794 | .412 |
| o-7 | 232.5 | 0 | 1089.3 | 86.13 | .5866 | 3.069 | .396 |
| o-8 | 428.1 | 0 | 2075.9 | 151.15 | 1.753 | 8.772 | .395 |
| o-9 | 378.2 | 0 | 1785.9 | 137.13 | 1.407 | 6.934 | .385 |
| o-10 | 288.2 | 0 | 1341.2 | 106.03 | .8598 | 4.314 | .390 |
| o-11 | 252.5 | 0 | 1166.7 | 93.56 | .6829 | 3.456 | .396 |
| o-12 | 214.3 | 0 | 984.9 | 79.83 | .5109 | 2.673 | .373 |

* At 68°F, 1 atm

** At column conditions

Table VII-2. Air-water data.

| Run No. | Q_G ft ³ /min* | W_L lb _m /min | W_G lb _m /hr** | U_G ft/sec | $\frac{dP_G}{dx} \times 10^3$ lb _f /in ³ | $\tau_2 \times 10^4$ lb _f /in ² | $\frac{y_m}{r_2 - r_1}$ |
|---------|--------------------------------|-------------------------------|--------------------------------|-----------------|---|--|-------------------------|
| W1 | 194.5 | .305 | 895.7 | 72.98 | .5158 | 2.635 | .460 |
| W2 | 202.0 | .305 | 921.1 | 75.82 | .5483 | 2.597 | .481 |
| W3 | 228.8 | .305 | 1058.9 | 85.32 | .6466 | 3.079 | .460 |
| W4 | 236.6 | .305 | 1097.2 | 88.15 | .6858 | 3.403 | .454 |
| W5 | 281.0 | .305 | 1290.5 | 104.71 | .9040 | 4.306 | .466 |
| W6 | 300.8 | .305 | 1407.8 | 110.92 | 1.036 | 4.901 | .454 |
| W7 | 332.3 | .305 | 1548.5 | 122.07 | 1.217 | 5.805 | .458 |
| W8 | 388.0 | .305 | 1822.1 | 141.40 | 1.618 | 7.597 | .462 |
| W9 | 413.2 | .305 | 1972.1 | 149.42 | 1.821 | 8.252 | .461 |
| W10 | 432.2 | .305 | 2052.4 | 155.81 | 1.962 | 9.178 | .464 |
| W11 | 219.8 | .305 | 1018.4 | 82.09 | .6200 | 2.928 | .459 |
| W12 | 190.7 | .305 | 880.5 | 71.46 | .5247 | 2.439 | .479 |
| W13 | 190.0 | .305 | 875.5 | 71.25 | .5070 | 2.469 | .457 |
| W14 | 293.6 | .305 | 1354.9 | 108.88 | .9836 | 4.720 | .463 |
| W15 | 435.6 | .305 | 2069.4 | 156.96 | 1.997 | 9.494 | .452 |
| W1 | 357.5 | .59 | 1685.4 | 130.57 | 1.506 | 6.814 | .496 |
| W2 | 212.7 | .59 | 977.4 | 79.48 | .6603 | 2.876 | .525 |
| W3 | 443.1 | .59 | 2113.7 | 159.50 | 2.216 | 10.02 | .488 |
| W4 | 294.2 | .59 | 1367.4 | 108.69 | 1.082 | 4.826 | .508 |
| W5 | 257.1 | .59 | 1228.3 | 92.69 | .8608 | 3.839 | .493 |
| W6 | 388.8 | .59 | 1842.1 | 141.34 | 1.725 | 7.770 | .506 |
| W7 | 332.7 | .59 | 1560.4 | 122.18 | 1.324 | 5.933 | .494 |
| W8 | 234.0 | .59 | 1085.6 | 87.14 | .7478 | 3.312 | .476 |
| W9 | 412.5 | .59 | 1970.1 | 149.23 | 1.923 | 8.689 | .497 |
| W10 | 189.8 | .59 | 876.3 | 71.12 | .5896 | 2.748 | .501 |
| W11 | 205.5 | .59 | 949.3 | 76.97 | .6338 | 2.800 | .512 |
| W12 | 196.5 | .59 | 906.7 | 73.68 | .6092 | 2.740 | .507 |
| W13 | 232.5 | .59 | 1079.7 | 86.62 | .7301 | 3.267 | .485 |
| W14 | 194.5 | .59 | 893.4 | 72.91 | .6023 | 2.740 | .488 |
| W15 | 293.6 | .59 | 1364.6 | 108.46 | 1.077 | 4.924 | .494 |
| W16 | 438.3 | .59 | 2091.0 | 157.76 | 2.166 | 9.780 | .502 |
| W1 | 376.4 | .755 | 1759.0 | 137.25 | 1.689 | 8.402 | .514 |
| W2 | 417.5 | .755 | 1969.8 | 150.79 | 2.026 | 10.13 | .518 |
| W3 | 454.2 | .755 | 2155.5 | 163.09 | 2.343 | 12.01 | .491 |
| W4 | 345.9 | .755 | 1609.6 | 126.66 | 1.459 | 7.205 | .509 |
| W5 | 296.3 | .755 | 1367.3 | 109.41 | 1.123 | 5.240 | .515 |
| W6 | 245.5 | .755 | 1128.3 | 91.21 | .8382 | 3.749 | .513 |
| W7 | 387.2 | .755 | 1818.8 | 140.75 | 1.763 | 8.787 | .516 |
| W8 | 266.5 | .755 | 1227.3 | 98.82 | .9364 | 4.208 | .500 |
| W9 | 256.5 | .755 | 1193.1 | 95.42 | .8912 | 4.073 | .530 |
| W10 | 189.0 | .755 | 872.5 | 70.83 | .6259 | 3.809 | .511 |
| W11 | 216.2 | .755 | 996.4 | 81.17 | .7075 | 3.885 | .512 |

Table VII-3. Air-shell solv data.

| Run No. | Q_G ft ³ /min* | W_L lb _m /min | W_G lb _m /hr** | \bar{U}_G ft/sec | $\frac{dP_G}{dx} \times 10^3$ lb _f /in ³ | $\tau_2 \times 10^4$ lb _f /in ² | $\frac{y_m}{r_2 - r_1}$ |
|---------|--------------------------------|-------------------------------|--------------------------------|-----------------------|---|--|-------------------------|
| S1 | 350.5 | .305 | 1667.8 | 127.21 | 1.448 | 6.475 | .468 |
| S2 | 442.6 | .305 | 2160.4 | 156.61 | 2.157 | 10.50 | .475 |
| S3 | 435.0 | .305 | 2115.2 | 153.53 | 2.076 | 10.74 | .461 |
| S4 | 414.2 | .305 | 1970.9 | 149.39 | 1.870 | 10.20 | .470 |
| S5 | 194.2 | .305 | 888.8 | 72.78 | .5267 | 2.484 | .490 |
| S6 | 360.0 | .305 | 1688.2 | 131.69 | 1.490 | 6.927 | .479 |
| S7 | 297.3 | .305 | 1379.1 | 109.94 | 1.068 | 4.696 | .446 |
| S8 | 229.9 | .305 | 1055.3 | 85.82 | .6927 | 3.214 | .469 |
| S9 | 258.2 | .305 | 1191.0 | 95.91 | .8391 | 3.952 | .496 |
| S10 | 237.8 | .305 | 1095.7 | 88.56 | .7399 | 3.358 | .472 |
| S11 | 213.9 | .305 | 982.0 | 79.92 | .6210 | 2.891 | .486 |
| S12 | 301.3 | .305 | 1398.2 | 111.38 | 1.088 | 5.044 | .467 |
| S13 | 419.5 | .305 | 1997.3 | 151.21 | 1.911 | 9.720 | .463 |
| S1 | 240.8 | .59 | 1112.3 | 89.50 | .8048 | 3.749 | .506 |
| S2 | 293.3 | .59 | 1374.5 | 108.42 | 1.102 | 5.187 | .524 |
| S3 | 364.5 | .59 | 1725.5 | 133.39 | 1.613 | 7.906 | .500 |
| S4 | 444.2 | .59 | 2131.6 | 160.36 | 2.286 | 11.19 | .499 |
| S5 | 189.2 | .59 | 871.9 | 71.20 | .5286 | 2.221 | .499 |
| S6 | 333.0 | .59 | 1551.1 | 122.42 | 1.383 | 6.708 | .482 |
| S7 | 445.2 | .59 | 2116.8 | 160.34 | 2.288 | 11.23 | .498 |
| S8 | 409.3 | .59 | 1950.6 | 148.79 | 1.972 | 9.743 | .493 |
| S9 | 219.3 | .59 | 1017.7 | 81.86 | .6839 | 3.011 | .490 |
| S10 | 213.9 | .59 | 991.6 | 79.94 | .6613 | 2.989 | .516 |
| S11 | 301.2 | .59 | 1411.6 | 111.34 | 1.162 | 5.526 | .513 |
| S12 | 436.6 | .59 | 2091.6 | 157.89 | 2.215 | 10.83 | .489 |
| S1 | 409.3 | .755 | 1950.6 | 148.79 | 1.989 | 10.00 | .516 |
| S2 | 219.3 | .755 | 1017.7 | 81.86 | .7035 | 3.132 | .543 |
| S3 | 240.8 | .755 | 1122.1 | 89.52 | .8156 | 3.696 | .520 |
| S4 | 444.8 | .755 | 2110.4 | 160.54 | 2.300 | 11.41 | .501 |
| S5 | 364.5 | .755 | 1725.5 | 133.39 | 1.624 | 7.973 | .515 |
| S6 | 189.3 | .755 | 871.9 | 71.20 | .5935 | 2.333 | .522 |
| S7 | 443.2 | .755 | 2124.2 | 160.20 | 2.295 | 11.34 | .520 |
| S8 | 293.3 | .755 | 1374.5 | 108.42 | 1.117 | 5.278 | .517 |
| S9 | 330.0 | .755 | 1569.2 | 122.42 | 1.398 | 6.794 | .532 |

Table VII-4. Air-light oil data.

| Run No. | Q_G ft ³ /min* | W_L lb _m /min | W_G lb _m /hr** | \bar{U}_G ft/sec | $\frac{dP_G}{dx} \times 10^3$ lb _f /in ³ | $\tau_2 \times 10^4$ lb _f /in ² | $\frac{y_m}{r_2 - r_1}$ |
|---------|--------------------------------|-------------------------------|--------------------------------|-----------------------|---|--|-------------------------|
| L1 | 284.0 | .10 | 1321.3 | 104.50 | 1.111 | 4.495 | .539 |
| L2 | 259.0 | .10 | 1192.1 | 96.33 | .9551 | 4.028 | .547 |
| L3 | 338.3 | .10 | 1569.0 | 124.87 | 1.504 | 6.309 | .499 |
| L4 | 267.9 | .10 | 1228.6 | 100.01 | 1.007 | 4.239 | .536 |
| L5 | 395.2 | .10 | 1855.0 | 144.14 | 1.965 | 8.229 | .529 |
| L6 | 423.1 | .10 | 1998.1 | 153.38 | 2.236 | 9.374 | .503 |
| L7 | 320.5 | .10 | 1488.6 | 118.22 | 1.408 | 5.729 | .533 |
| L8 | 371.8 | .10 | 1738.4 | 136.24 | 1.814 | 7.477 | .511 |
| L9 | 217.2 | .10 | 993.0 | 81.39 | .7389 | 3.056 | .551 |
| L10 | 288.2 | .10 | 1331.3 | 106.89 | 1.139 | 4.645 | .529 |
| L11 | 414.0 | .10 | 1954.8 | 150.22 | 2.157 | 8.945 | .499 |

Table VII-5. Air-iso-octyl alcohol data.

| Run No. | Q_G ft ³ /min* | W_L lb _m /min | W_G lb _m /hr** | \bar{U}_G ft/sec | $\frac{dP_G}{dx} \times 10^3$ lb _f /in ³ | $\tau_2 \times 10^4$ lb _f /in ² | $\frac{y_m}{r_2 - r_1}$ |
|---------|--------------------------------|-------------------------------|--------------------------------|-----------------------|---|--|-------------------------|
| I1 | 206.1 | .10 | 940.9 | 77.28 | .6279 | 2.687 | .523 |
| I2 | 263.2 | .10 | 1210.1 | 98.00 | .9453 | 3.922 | .510 |
| I3 | 300.8 | .10 | 1388.2 | 111.58 | 1.204 | 4.773 | .493 |
| I4 | 356.6 | .10 | 1659.2 | 131.21 | 1.624 | 7.190 | .505 |
| I5 | 380.9 | .10 | 1780.4 | 139.50 | 1.823 | 7.883 | .497 |
| I6 | 465.5 | .10 | 2220.2 | 167.09 | 2.594 | 11.43 | .508 |
| I7 | 275.8 | .10 | 1270.2 | 102.52 | 1.012 | 4.148 | .502 |
| I8 | 413.0 | .10 | 1948.3 | 149.88 | 2.107 | 9.329 | .480 |
| I1 | 206.2 | .305 | 941.2 | 77.22 | .7331 | 2.800 | .556 |
| I2 | 454.5 | .305 | 2163.3 | 163.24 | 2.682 | 11.42 | .509 |
| I3 | 271.8 | .305 | 1252.6 | 100.82 | 1.129 | 4.344 | .546 |
| I4 | 347.7 | .305 | 1616.6 | 127.84 | 1.690 | 6.897 | .527 |
| I5 | 314.0 | .305 | 1454.0 | 115.94 | 1.435 | 5.639 | .568 |
| I6 | 294.7 | .305 | 1357.6 | 109.36 | 1.292 | 5.067 | .535 |
| I7 | 412.7 | .305 | 1943.7 | 149.79 | 2.263 | 9.532 | .544 |

APPENDIX VIII

Nomenclature

NOMENCLATURE

The following fundamental dimensions are represented by the following symbols: F = force, L = length, M = mass, T = time.

Roman Symbols

| <u>Symbol</u> | <u>Definition</u> | <u>Dimensions</u> |
|---------------|--|-------------------|
| A | wave amplitude | L |
| B_m | dimensionless variable, $= \tau_{i0} h / \mu u_0$ | |
| C_1, C | constants | |
| c | wave celerity | L/T |
| d_1, d_2 | diameter of inner and outer tube of annulus, respectively | L |
| D | equivalent duct diameter | L |
| E | percent entrainment, Equation (V-5) | |
| f | friction factor defined by Equation (9) | |
| f_1, f_2 | friction factor at inner and outer wall of annulus; see Equation (1) | |
| f_k | friction factor defined by Equation (57) | |
| f_{TP} | two-phase friction factor defined by Orkiszewski | |
| \tilde{f} | wave frequency | T^{-1} |
| F | function defined by Equation (III-2) | |
| g | acceleration of gravity | L/T^2 |
| g_c | gravitational constant | ML/FT^2 |

| <u>Symbol</u> | <u>Definition</u> | <u>Dimensions</u> |
|--|--|-------------------|
| G | total mass flux | M/L^2 |
| h | local liquid film thickness | L |
| h_o | average liquid film thickness | L |
| j_L, j_G | superficial liquid and gas velocity, respectively | L/T |
| j_G^*, j_L^* | dimensionless liquid and gas velocities, respectively, as defined by Equations (25) and (26) | |
| k | wave number | L^{-1} |
| P | local pressure | F/L^2 |
| P_G | pressure in the gas phase | F/L^2 |
| P_σ | pressure induced by capillary forces | F/L^2 |
| P_k | kinetic pressure | F/L^2 |
| P_s | static pressure | F/L^2 |
| $(\frac{dP}{dx})_L, (\frac{dP}{dx})_G$ | pressure drop occurring if the liquid or gas flows alone in the tube, respectively | F/L^3 |
| $\frac{dP_f}{dx}$ | frictional pressure drop | F/L^3 |
| $(\frac{dP}{dx})_{TP}$ | two-phase pressure drop | F/L^3 |
| $\Delta P_G^*, \Delta P_L^*$ | dimensionless pressure drops defined by Equations (28) and (29) | |
| ΔP^* | two-phase dimensionless pressure drop defined by Equation (30) | |
| Q_G | gas volumetric flow rate | L^3/T |

| <u>Symbol</u> | <u>Definitions</u> | <u>Dimensions</u> |
|---------------|---|-------------------|
| r | radial coordinate | L |
| r_1, r_2 | radius of inner and outer tube of annulus, respectively | L |
| r_i | $r_1 + h_o$ | L |
| r_m | radius of maximum velocity | L |
| r^* | diameter ratio d_1/d_2 | |
| R_L | fraction of tube volume occupied by liquid | |
| Re | Reynolds number defined by Equation (8) | |
| Re_2 | Reynolds number defined by Equation (2) | |
| Re_B | Reynolds number defined by Equation (10) | |
| Re_k | Reynolds number defined by Equation (16) | |
| Re_L | Reynolds number defined by Equation (90) | |
| R | correlation coefficient | |
| t | time | T |
| u | local velocity in x-direction | L/T |
| U | average velocity in flow direction | L/T |
| U_{GS} | superficial gas velocity | L/T |
| \bar{u} | local average velocity in liquid film | L/T |
| u_o | average velocity in liquid film | L/T |
| V_{CR} | critical gas velocity at which entrainment begins | L/T |
| v | local velocity in the y-direction | L/T |

| <u>Symbol</u> | <u>Definition</u> | <u>Dimensions</u> |
|----------------------|---|-------------------|
| \bar{v} | average homogeneous mixture specific volume | L^3/M |
| We | Weber number, $= u_o^2 h_o / \gamma$ | |
| W_L, W_G | liquid and gas mass flow rate, respectively | M/T |
| x | coordinate in direction of main flow | L |
| y | coordinate in direction perpendicular to main flow | L |
| y_m | distance from inner wall to point of maximum velocity | L |
| y^* | dimensionless point of maximum velocity as defined by Equation (89) | |
| z | $x - ct$ | L |
| <u>Greek Symbols</u> | | |
| α | dimensionless wave celerity c/u_o | |
| γ | kinematic surface tension | FL^2/M |
| Γ_L | mass liquid flow rate per unit of wetted perimeter | M/LT |
| ϵ/D | relative roughness | |
| θ | angle from the horizontal | |
| λ | wavelength | L |
| μ | viscosity coefficient | M/LT |
| μ_L, μ_G | liquid and gas viscosity, respectively | M/LT |
| μ^* | dimensionless viscosity | |
| ν | kinematic viscosity | L^2/T |

| <u>Symbol</u> | <u>Definition</u> | <u>Dimensions</u> |
|------------------|---|-------------------|
| ρ | density | M/L^3 |
| ρ_L, ρ_G | liquid and gas density, respectively | M/L^3 |
| σ | coefficient of surface tension | F/L |
| τ_1, τ_2 | shear stress at inner and outer wall of annulus, respectively | F/L^2 |
| τ_i | shear stress at gas-liquid interface | F/L^2 |
| τ_w | shear stress at a wall | F/L^2 |
| τ_f | frictional pressure drop defined by Orkiszewski | F/L^2 |
| ϕ | defined by Equation (34) | |
| ϕ_* | correction factor defined in Equation (11) | |
| Φ_L, Φ_G | liquid and gas, Lockhart and Martinelli parameters | |
| χ | Φ_G/Φ_L | |